

UNCLASSIFIED

AD NUMBER

AD352834

CLASSIFICATION CHANGES

TO: UNCLASSIFIED

FROM: CONFIDENTIAL

LIMITATION CHANGES

TO:
Approved for public release; distribution is unlimited.

FROM:
Distribution authorized to U.S. Gov't. agencies and their contractors;
Administrative/Operational Use; 05 JUN 1964.
Other requests shall be referred to Naval Ordnance Laboratory, White Oak, MD.

AUTHORITY

30 Jun 1976, DoDD 5200.10 USNOL per ltr, 29 Aug 1974

THIS PAGE IS UNCLASSIFIED

CONFIDENTIAL

NOLTR 63-125

AD 352 834

**A STUDY OF UNDERWATER EXPLOSIONS IN
A HIGH GRAVITY TANK (U)**

NOL

5 JUNE 1964

UNITED STATES NAVAL ORDNANCE LABORATORY, WHITE OAK, MARYLAND

NOLTR 63-125

NOTICE: This material contains information affecting the national defense of the United States within the meaning of the Espionage Laws, Title 18, U.S.C. Sections 793 and 794, the transmission or revelation of which in any manner to an unauthorized person is prohibited by law.

*Downgraded at 3 Year Intervals
Declassified after 12 Years. DOD Dir 5200.10*

CONFIDENTIAL

DESTROY WHEN NO LONGER REQUIRED

CONFIDENTIAL

NOLTR 63-125

A STUDY OF UNDERWATER EXPLOSIONS IN A HIGH GRAVITY TANK (U)

by

R. S. Price

W. G. Zuke

C. Infosino

ABSTRACT: Model underwater explosion tests were conducted in a test tank accelerated at up to 190 gravities on the Sandia 35 ft radius centrifuge. High speed movies were made of the explosion phenomena. The effects of tank size, air pressure, acceleration, and charge depth on the explosion characteristics were determined and several methods of using the scaling laws were compared. Models of specific prototype explosions were fired. Results indicated that three criteria scaling provided scaled measurements closely approximating their full scale equivalents, i. e., sizes of successive bubble maxima, successive periods of oscillation, and migration.

UNDERWATER EXPLOSIONS DIVISION
EXPLOSIONS RESEARCH DEPARTMENT
U. S. NAVAL ORDNANCE LABORATORY
WHITE OAK, SILVER SPRING, MARYLAND

CONFIDENTIAL

NOLTR 63-125

5 June 1964

A STUDY OF UNDERWATER EXPLOSIONS IN A HIGH GRAVITY TANK (U)

This report describes the first extensive series of model underwater explosions conducted in an accelerated test tank. Several different programs were conducted to explore and evaluate the use of a centrifugally accelerated test tank and its effects on explosion phenomena. This study is part of a continuing investigation of techniques for modeling explosions of underwater weapons. The work was carried out under Tasks RRRE-51001-003, Nuclear Explosion Bubble Phenomena and NOL-440/DASA, High Gravity Tank.

R. E. ODENING
Captain USN
Commander



C. J. ARONSON
By direction

CONFIDENTIAL
NOLTR 63-125

ACKNOWLEDGEMENT

The authors wish to express appreciation for the excellent cooperation with the Sandia Corporation personnel concerned with the hydraulic centrifuge at Albuquerque, New Mexico. The contributions of the Hayes Aircraft Corporation (now Hayes International Corporation) personnel who participated in the design and initial installation of the test tank are also acknowledged.

CONTENTS

	Page
1. INTRODUCTION	1
2. EQUIPMENT AND INSTALLATION	2
2.1 Background	2
2.2 Optical Path.	9
2.3 Tank and Windows	9
2.4 Mirror.	14
2.5 Beam and Bonnet.	14
2.6 Fairing	14
2.7 Camera.	15
2.8 Camera Mounting.	15
2.9 Illumination.	15
2.10 Electrical Circuits	17
2.11 Explosives	18
2.12 Tank Fittings	18
2.13 Fluid Controls	18
2.14 Construction and Testing.	19
2.15 Equipment Performance.	22
3. MEASUREMENTS AND EXPERIMENTAL CONTROL	22
3.1 General	22
3.2 Bubble Period	23
3.3 Bubble Size	23
3.4 Above Surface Characteristics	23
3.5 Charge Depth.	25
3.6 Acceleration.	31
3.7 Air Pressure.	32
3.8 Water Temperature	33
3.9 Experimental Control	35
4. RESULTS AND DISCUSSION	39
4.1 General	39
4.2 General Information Programs	39
4.2.1 Effect of Tank Size.	40
4.2.2 Effects of d_m , a_m , and P_m on the Explosion Bubble.	43
4.3 Specific Scaling Programs	43
4.3.1 Comparison of Different Forms of Bubble Scaling	45
4.3.2 Scaling of High Explosives	49
4.3.3 Scaling Under-Ice Explosions.	67
4.3.4 Scaling Deep Nuclear Explosions.	69
4.3.5 Scaling Shallow Nuclear Shots	69
5. CONCLUSIONS.	73
APPENDIX A	A-1

CONTENTS Cont'd

Figure	Title	Page
1	General View of High Gravity Tank Assembled on the Sandia Centrifuge.	4
2	Tip End	5
3	Observation Opening	6
4	High Gravity Tank During Manufacture.	7
5	Window Frame Cross Section	8
6	Mirror Structure	10
7	Camera Installation	11
8	77 Lamp Bank.	12
9	Electrical System Block Diagram, 1960	13
10	Fluid Control Equipment	16
11	Testing Beam via Bonnet Loading of 364,000 Lbs	20
12	Loading Bottom of Tank to 206,000 Lbs	21
13	Calculation of Charge Depth and Optical Geometry.	24
14	Charge Depth Variation from the Nominal Levels for Various Systems of Control	34
15	Frequency Distribution of Acceleration Differences from their Nominal Levels	36
16	Air Pressure Variation Relative to Nominal Levels	37
17	Frequency Distribution of Water Temperatures	38
18	Effects of d_m , P_m and a_m on $A_{max m}$ and T_m	44
19	Displacement Histories for Shots Comparing Different Kinds of Bubble Scaling	46
20	Selected Frames from Films in the Comparison of Various Kinds of Bubble Scaling	47
21	Displacement Histories of Deep Water Shots.	55
22	Displacement Histories of Deep Water Shots.	56
23	Displacement Histories of Deep Water Shots.	57
24	Comparison of Surface Development of a Three Criteria Scaled Model with its Prototype for a Deep Water Shot.	58
25	Displacement Histories of Bottom Shots	64
26	Displacement Histories of Bottom Shots	65
27	Comparison of Surface Development of a Three Criteria Scaled Model with its Prototype for a Bottom Shot	66
28	Bubble and Surface Development of a Simplified Two Criteria Scaled Under-Ice Shot	68
29	Bubble and Surface Development of Two Criteria Scaled Deep Nuclear Explosion	71
30	Selected Frames of Shallow Shots Approximating Baker Plumes	74
31	Selected Frames of Shallow Shots Approximating Umbrella Plumes	75

TABLES

Table	Title	Page
1	Data from Accelerated Tank Underwater Explosion Experiments	27
2	Data from Corresponding Shots in Two Tank Sizes	42
3	Evaluation of Tank Effects	42

CONTENTS Cont'd

Table	Title	Page
4.	Prototype Conditions Determined by Various Kinds of Bubble Scaling	48
5.	Prototype Conditions for High Explosive Shots in Deep Water	50
6.	Comparison of Scaled Three Criteria Explosion Characteristics with Prototype Predictions of Reference 11	54
7.	Calculated Prototype Conditions for High Explosive Shots Fired on a Bottom	62
8.	Prototype Conditions for Deep Nuclear Explosions.	70
9.	λ_d for Shallow Shots	72

A STUDY OF UNDERWATER EXPLOSIONS IN A HIGH GRAVITY TANK (U)

1. INTRODUCTION

The evolution of methods of simulating underwater explosions on a laboratory scale has logically led to the development of a high gravity tank. In addition to the controlled variables used in the past for laboratory explosion scaling, the high gravity tank offers control of acceleration or gravity*.

In general the many phenomena produced by an underwater explosion are so complicated and interdependent as to make any single scaling procedure impossible. However, certain gross characteristics (such as the bubble size and period, shock wave peak pressure, plume heights, etc.) are amenable to more or less independent scaling. When more complete knowledge of the interrelated motions and effects from a full scale explosion is desired, model tests are made. In essence, these are calculations made by an analog process using real materials, times, and distances in the computation. The basic inputs are explosion characteristics found both on full scale and model. The outputs are measurements of other phenomena not usually measurable on the prototype.

The scaling laws applicable to these tests dictate certain relationships among the model characteristics. In the static tank, some control of these characteristics could be attained by controlling the atmospheric pressure, the depth of the explosion, the water temperature, and the nature of the explosive (e.g., spark, exploding wire, primary explosives). In an accelerated test tank the acceleration can be controlled in addition; this satisfied more of the scaling requirements so that the model experiment is a more exact replica of the prototype.

Previous work (Ref. 7) had indicated that a centrifuge could be used to accelerate a test tank without introducing gross distortions of the explosion bubble. The experiments described here were carried out primarily to check the

* Reports (Refs. 4, 10, and 15) concerned with simulation of large underwater explosions on a very small scale in the NOL vacuum tank, and studies preparatory to the experiments described in this report (Refs. 7, 14, and 16) explain the terminology used in this report and give some of the background of explosion scaling in a high gravity tank.

practicability of using a large centrifuge to accelerate the test tank. Other purposes were (1) to determine whether systems of explosion scaling which had been previously developed can be used in the high gravity tank and for how wide a range of conditions, (2) to determine how well model simulations agree with their prototypes, and (3) assuming applicability and good simulation, to obtain data on certain nuclear and chemical prototype explosions.

Seven series of shots, or programs, were fired. These may be resolved into two categories, as follows:

1. General Information Programs
 - a. Effect of tank size or "wall effect".
 - b. Effect of charge depth, tank acceleration, and air pressure on the explosion bubble.
2. Programs for Scaling Specific Prototypes
 - a. Comparison of different forms of bubble scaling.
 - b. Scaling high explosive prototype shots, in deep water and on the bottom.
 - c. Scaling under-ice explosions.
 - d. Scaling shallow underwater nuclear explosions.
 - e. Scaling deep underwater nuclear explosions.

In Section 2 the equipment and instrumentation used in these tests is described and discussed. Section 3 presents information about the experimental control which was obtained. The specific planning, experimental results, analysis, and conclusions for each of the seven programs are presented in Section 4. In Section 5, general conclusions arising from this series and recommendations for future efforts are presented.

The data contained in this report were obtained at the Sandia Corporation centrifuge during a two week period during August and September of 1960 and a two week period during May of 1961. This report contains all the data except for a calibration program (31 shots) fired in 1961. That program is presented in a separate report (Ref. 18).

2. EQUIPMENT AND INSTALLATION

2.1 BACKGROUND

A tank diameter of 2 feet, a water depth of 2 feet, and acceleration to 109 g had been postulated in reference (14). The diameter had probably been selected to maintain a bubble diameter to tank diameter ratio less than about 0.3 when using 0.2 gm charges, which gives rough similarity to the shots fired in the 4 foot diameter stationary vacuum tank at NOL. The water depth of 2 feet had been selected to permit scaling of a 250-lb charge in 240 feet of water.

CONFIDENTIAL

NOLTR 63-125

Preliminary work on a small NOL centrifuge indicated the practicability of centrifugal acceleration (Ref. 7). The Sandia Corporation hydraulic centrifuge at Albuquerque, N. M. was found to be available and it seemed advisable to tailor the proposed tank to the capabilities of the Sandia machine so that tests could be run using a tank of the desired size for 0.2 gm charges. If centrifugal acceleration with this size of system was shown to be unsuitable through testing at Sandia, another type of accelerator should be considered for the NOL facility. If centrifugal acceleration was found to be acceptable, a centrifuge could be built at NOL for use with the tank.

Assuming a 2 foot diameter tank containing water 2 feet deep and use of the Sandia machine, further studies were made (Ref. 16) to guide design and operation of the tank. These studies showed that very little might be gained by exceeding 200 g, but that accelerations to that level should be useful. The acceleration limit of the Sandia machine (without an arm extension) was about 220-230 g. At 200 g, the Sandia centrifuge's limitations did not allow any increase in the tank diameter and water depth. The limitations at Sandia were imposed by the strength and location of bolts for attaching equipment to the arm, and strength of the arm, and the rotational speed allowed.

The engineering problem, then, was to design a tank and fittings, with appropriate instrumentation, to fit the Sandia centrifuge. Design proceeded as follows:

1. A general optical and mechanical plan of the tank, windows, Sandia centrifuge arm, and camera location. (Figures 1, 2, and 3.)
2. A tank capable of withstanding the hydrostatic and explosion forces (Figure 4).
3. Suitable windows, window supporting structure, and access ports (Figures 4 and 5).
4. A mirror with a backing structure rigid enough to permit reasonable undistorted photography (Figure 6).
5. A beam between the prongs of the Sandia centrifuge arm to support the tank, mirror, and accessories; a bonnet structure to attach the tank to the beam; and attachment plates to connect the beam to the prongs (Figure 4).
6. A fairing structure capable of withstanding aerodynamic and acceleration forces (Figures 1, 2 and 3).
7. A camera and mounting (Figures 1 and 7).
8. Other equipment, including illumination, control circuitry, fluid control and charges.

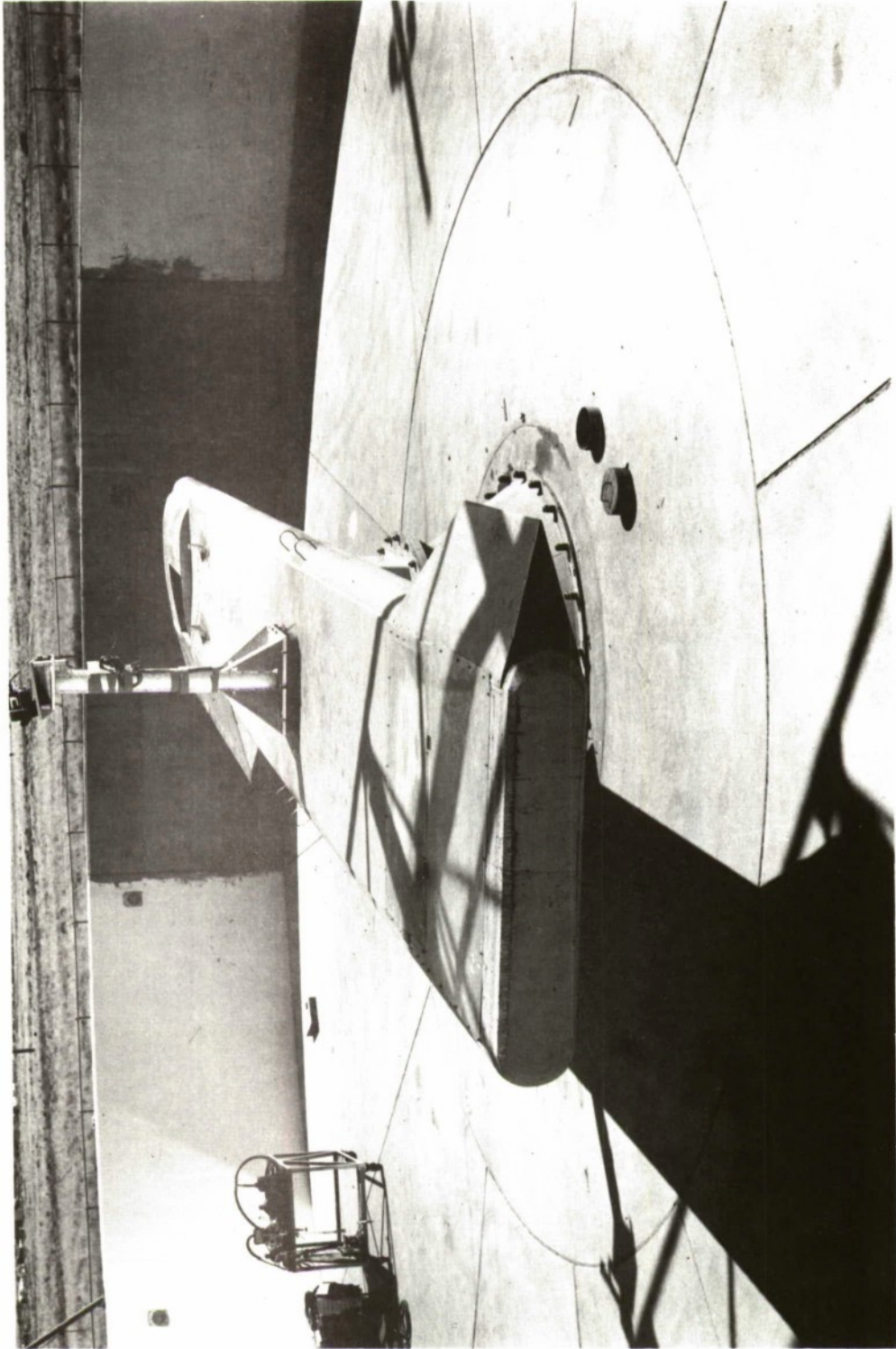


FIG.1 GENERAL VIEW OF
HIGH GRAVITY TANK ASSEMBLED ON THE SANDIA CENTRIFUGE

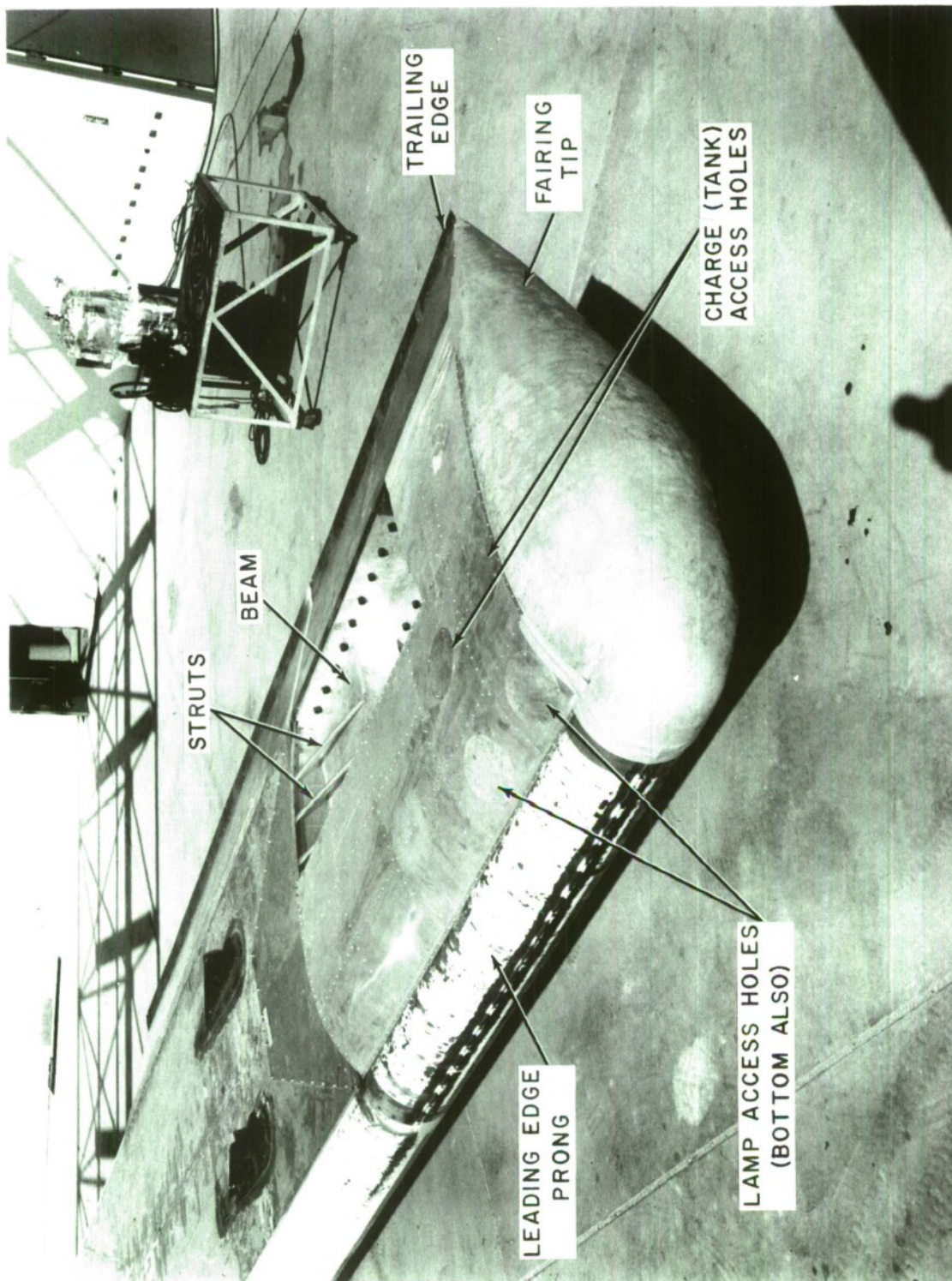


FIG.2 TIP END

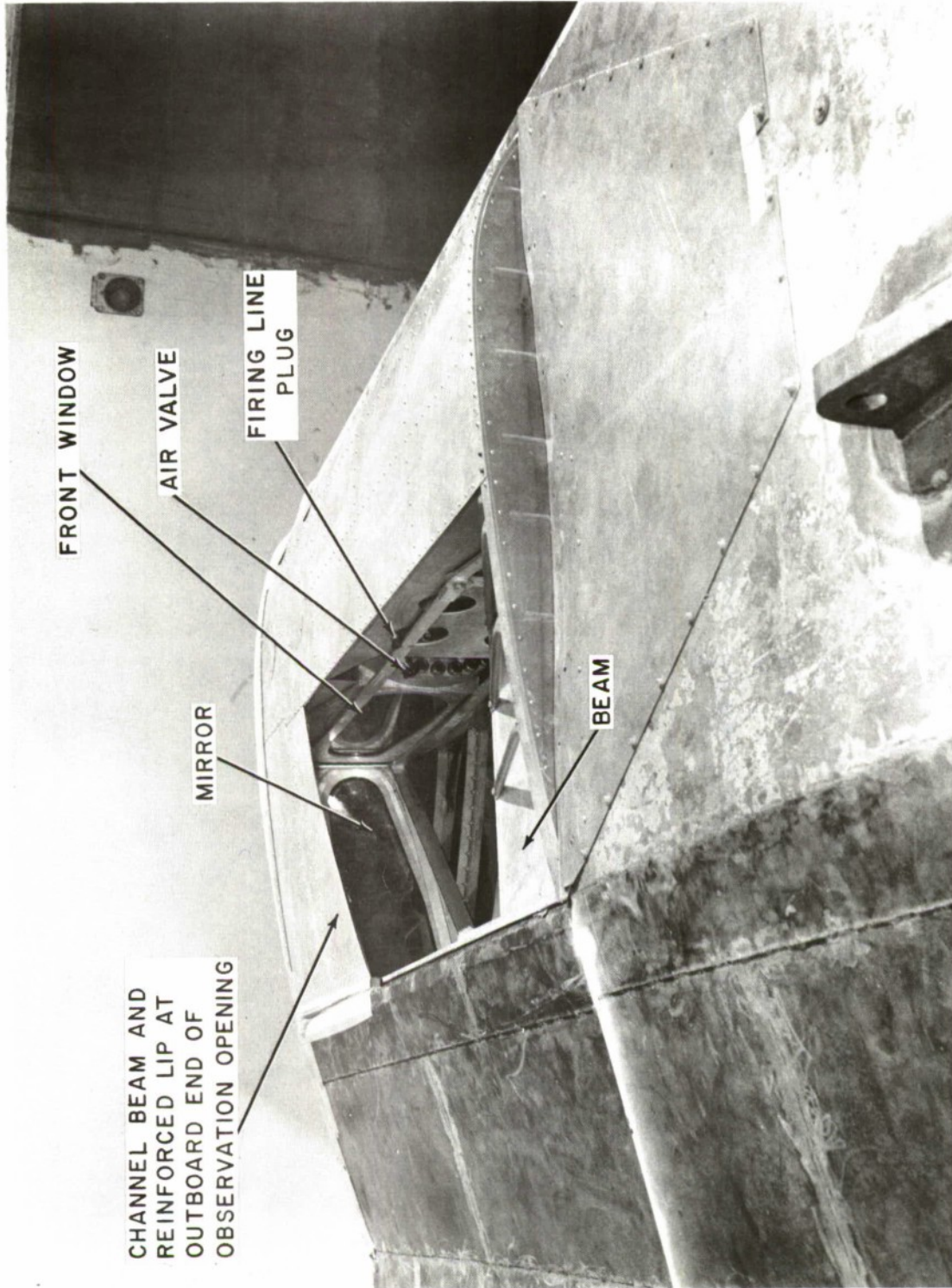
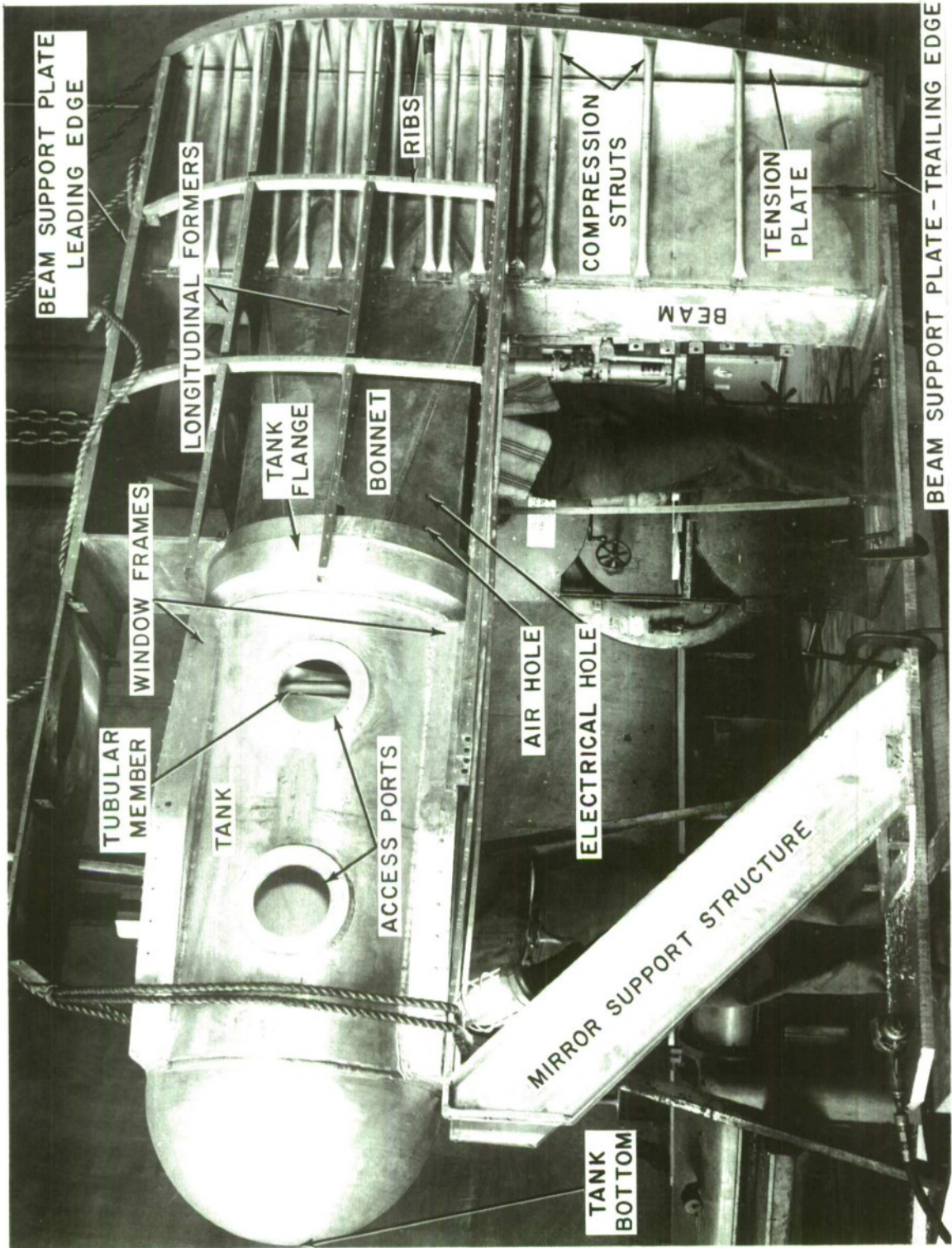


FIG.3 OBSERVATION OPENING



BEAM SUPPORT PLATE - TRAILING EDGE
PHOTO SUPPLIED BY HAYES CORPORATION

FIG. 4 HIGH GRAVITY TANK DURING MANUFACTURE

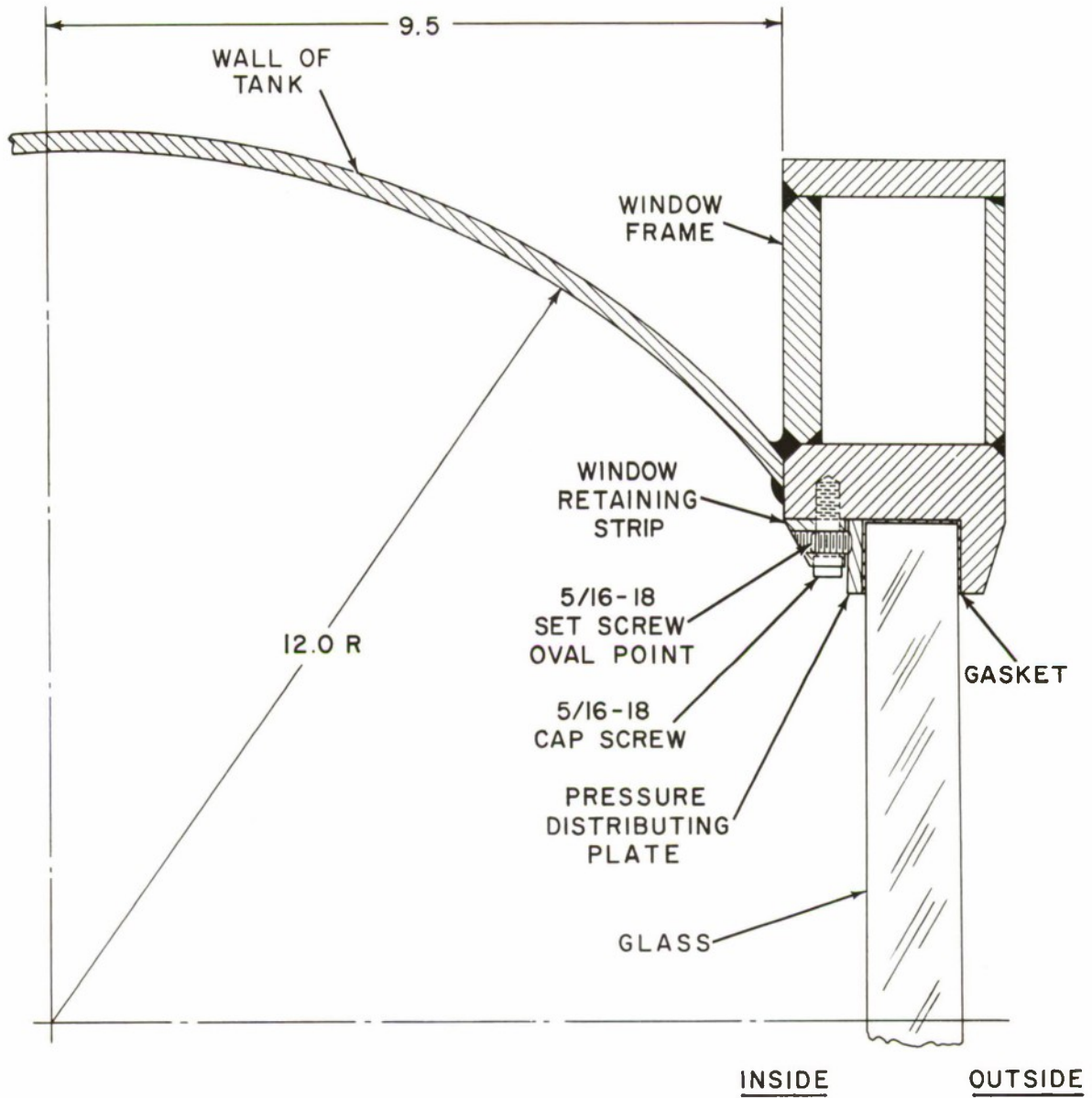


FIG.5 WINDOW FRAME CROSS SECTION

2.2 OPTICAL PATH

It was desired that the axis of the optical path pass through the tank perpendicular to the plane of the windows at the water surface. Failing this, the axis was to enter the tank between the charge and water surface. Fulfilling such conditions would simplify photographic measurements.

The optical path should also be unobstructed. The tank was located between the prongs of the centrifuge arm with just enough space on the trailing side (relative to arm motion) for a mirror. To clear the centrifuge structure and the beam supporting the tank, the optical axis was reflected not only sharply inward at the mirror, but slightly upward also toward the camera which was located at the center of the centrifuge on a high pedestal. On the other side of the tank, enough space was allowed between the tank and leading prong for the illumination equipment.

2.3 TANK AND WINDOWS

Aluminum alloy 6061 was selected for the basic structural material because of its weldability, high strength, and corrosion resistance. Parts were fabricated at the -T6 temper or, if welded, they were of -O or -T4 temper material restored to -T6 temper by heat treating.

The tank was designed with a hemispherical bottom to minimize weight; this incidentally increased the available water depth to 3 feet. An O-ring sealed flange at the top was provided for tank attachment to the bonnet with 36 1-1/8" bolts.

The window structure was somewhat unusual because the windows would be under non-uniform hydrostatic pressure. They extended uninterrupted from 13 inches above to 21 inches below the nominal water surface. The window width was 12 inches at and above the surface and tapered to a width of 8 inches near the bottom. Both top and bottom of the windows were semi-circular to reduce stress concentration. (See Figure 3) This shape was well fitted to the expected sizes of the phenomena to be observed in various parts of the tank. The maximum available thickness of heat treated plate glass was used (1-1/4 inches).

The window side frames were variable depth beams of box cross-section (See Figure 5) to resist twisting by the eccentric loading by the window glass and to resist the non-uniform hydrostatic loading by the tank walls. The windows destroyed the cylindrical symmetry of the tank walls causing forces tending to press the window frames together. These forces were resisted by four tubular members connecting the window frames inside the tank (Figure 4).

The windows seated on and were completely edged by flat rubber gaskets. The window retaining strips were on the inside of the tank so that hydrostatic pressure aided in sealing the windows against the solid external lip.

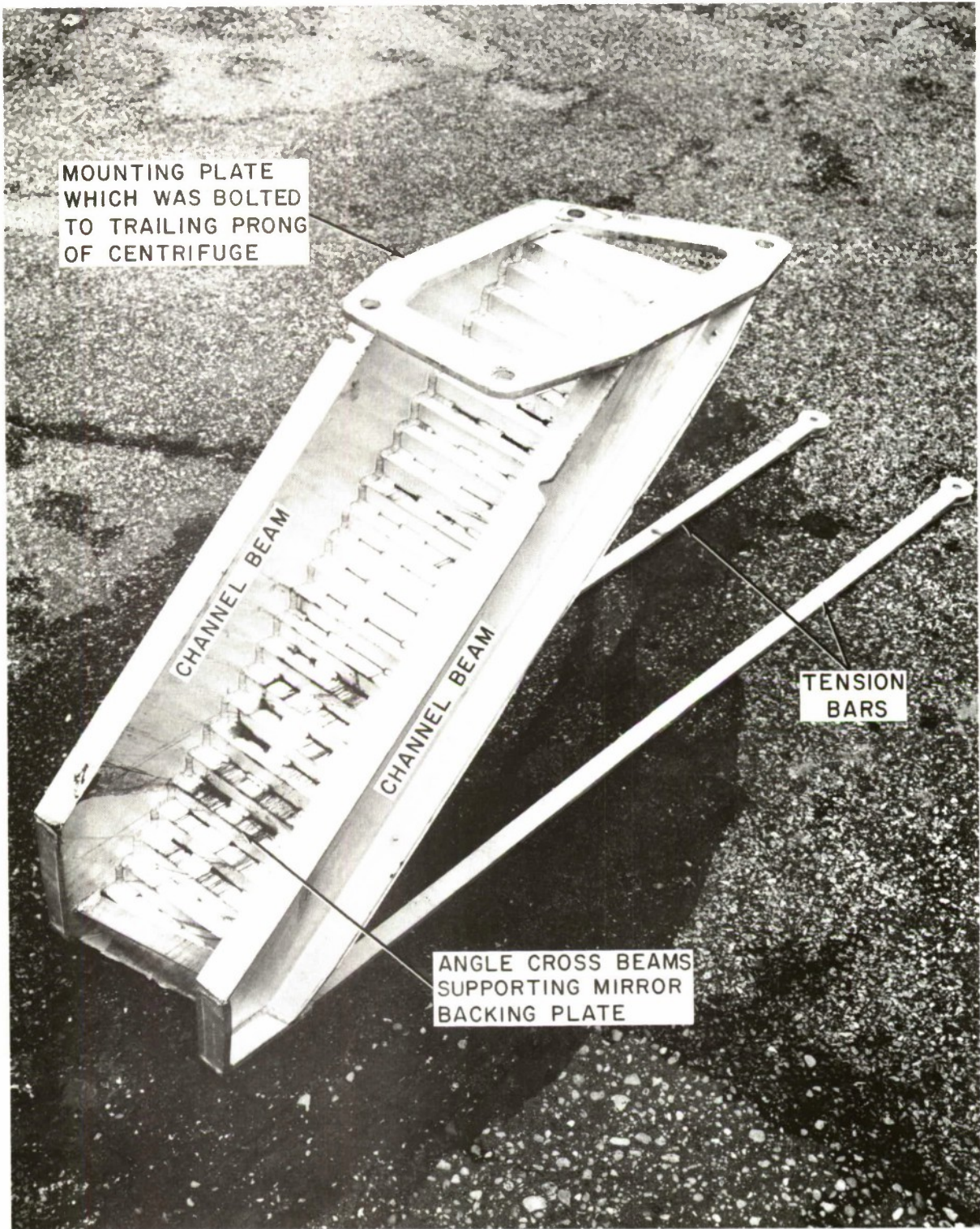


FIG.6 MIRROR STRUCTURE

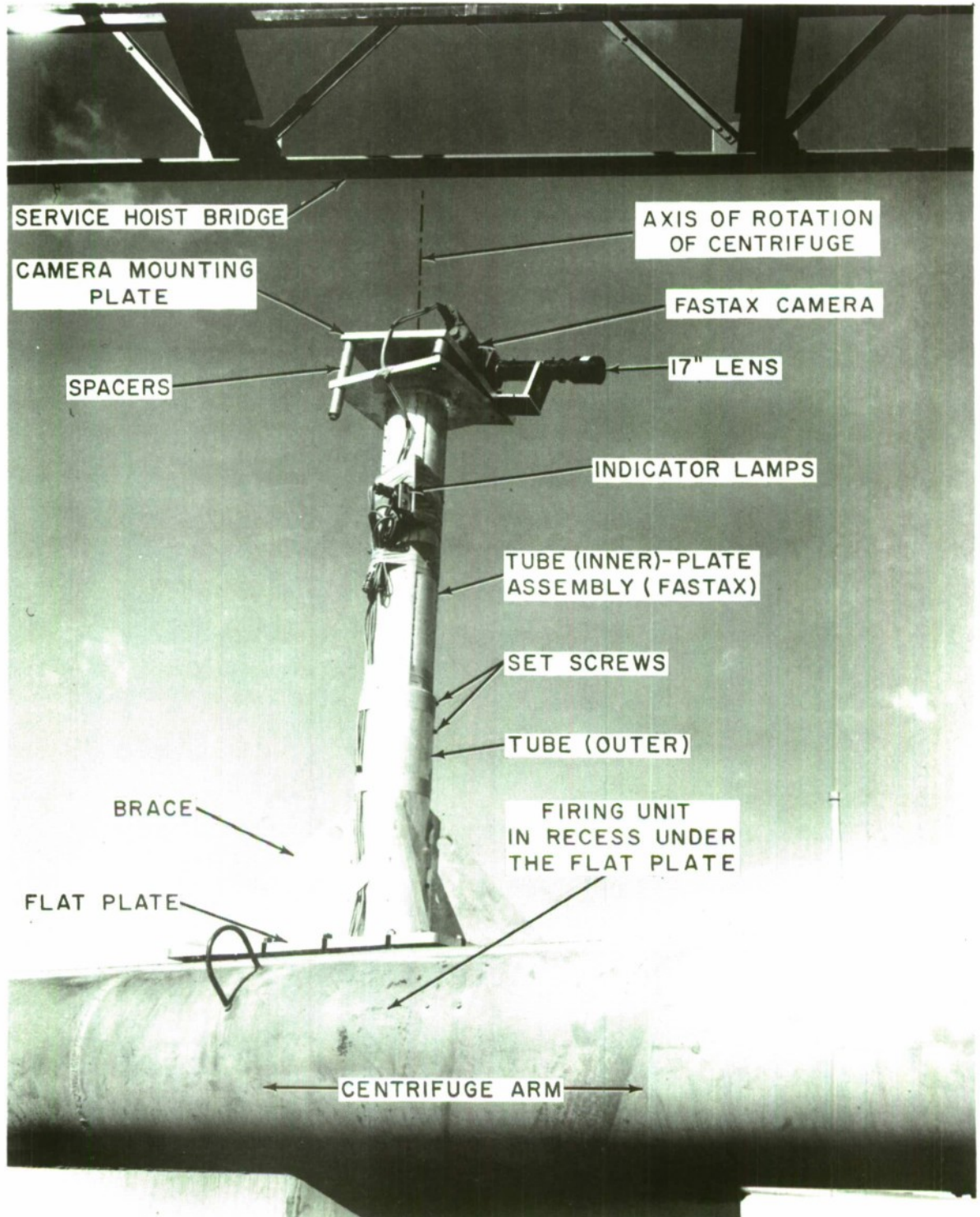


FIG. 7 CAMERA INSTALLATION

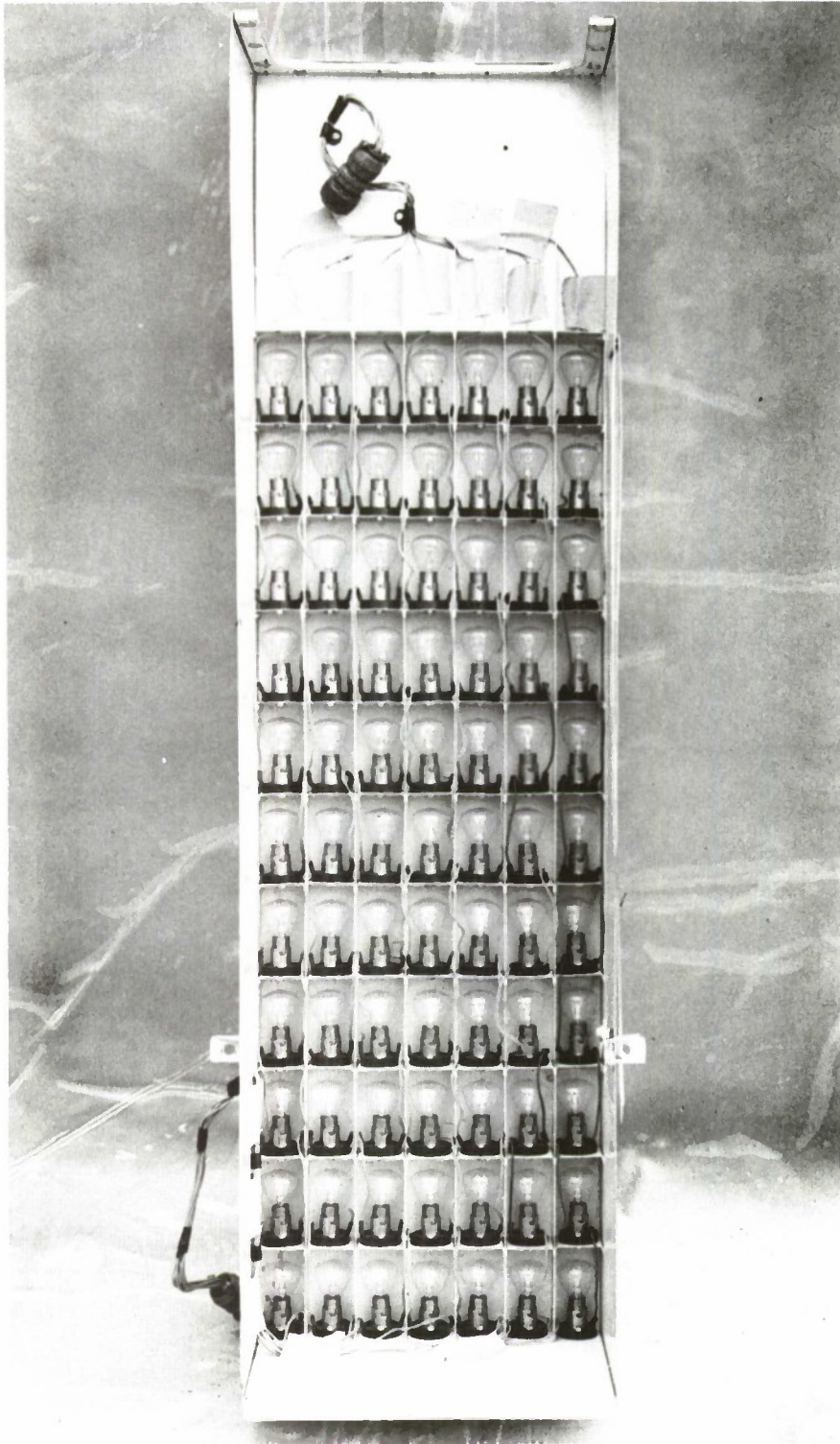


FIG. 8 77 LAMP BANK

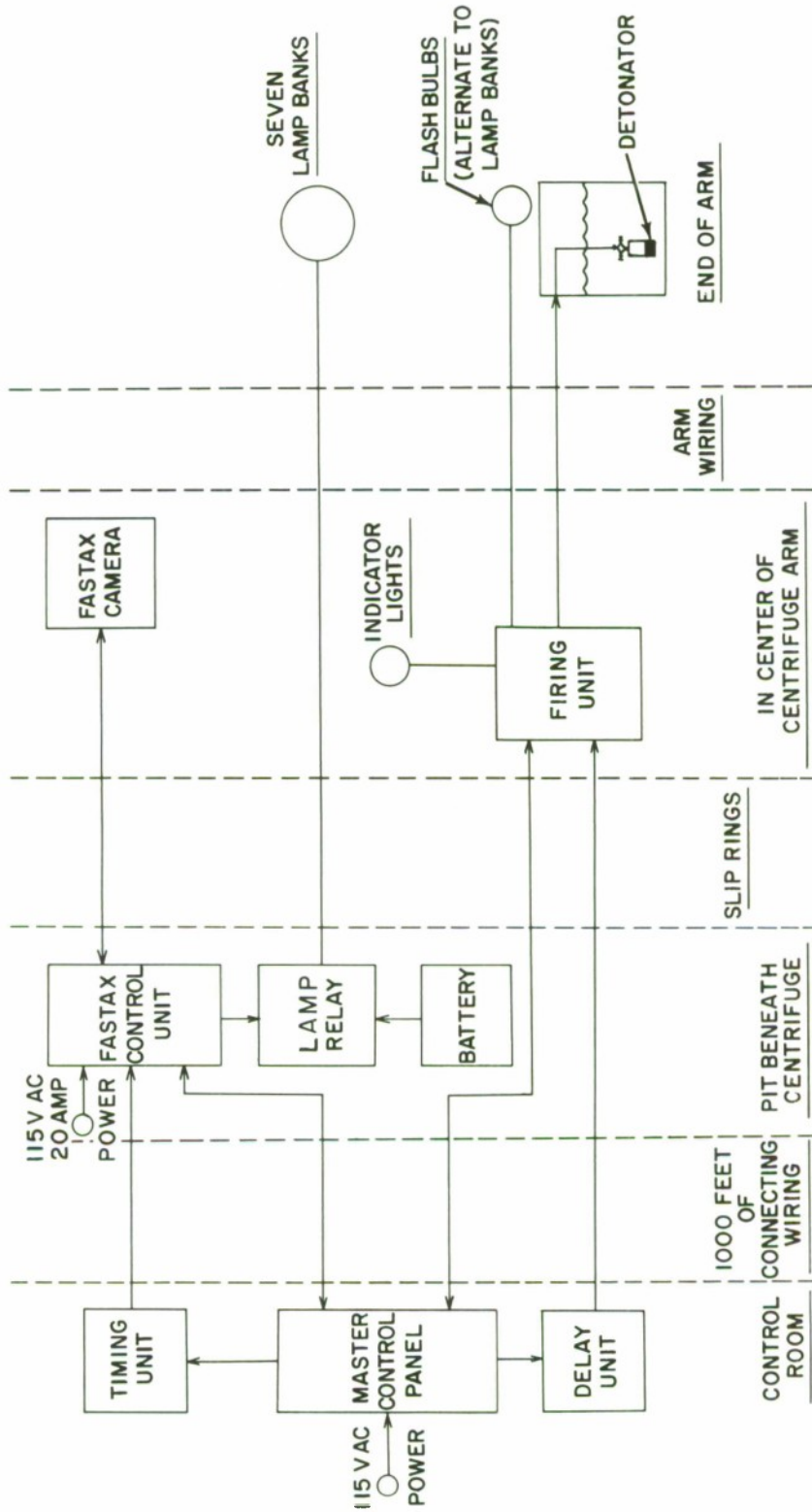


FIG.9 ELECTRICAL SYSTEM BLOCK DIAGRAM, 1960

CONFIDENTIAL
NOLTR 63-125

Two access ports 6 inches in diameter allowed the operator to get both hands into the tank. The port covers seated on O-rings from inside the tank; a securing bar on the outside provided only seating pressure and resistance to external air pressure when the tank was evacuated.

2.4 MIRROR

The mirror's shape, size, and angular position were calculated to provide the maximum undistorted field of view consistent with space limitations. The mirror support structure consisted of two 9-inch channel beams and a step-like arrangement of 24 angle cross beams which was designed to deflect less than 0.010 inch under 200 g loading. A flat plate over the angle beams provided a smooth backing to which the front surface plate glass mirror was adhesive bonded. One end of the mirror structure was bolted to the trailing prong of the centrifuge arm; the other end was supported by tension bars (on either side of the window) which were attached to the main tank support beam (Figures 4 and 6).

2.5 BEAM AND BONNET

The beam and bonnet (Figure 4) were designed as a unit. A box type welded beam provided the required support between the centrifuge prongs and also flat surfaces to which other parts could be readily attached. Plates pierced by holes for the bolts attaching the assembly to the centrifuge prongs were welded to the beam ends. The bonnet, which was welded to the beam, was left open to the tank so that the air volume over the water in the tank was relatively large. Air, water, and electrical connections were made through holes in the bonnet.

2.6 FAIRING

The fairing structure had to resist aerodynamic forces as well as centrifugal forces. The shape chosen to enclose the tank structure and fit the centrifuge arm was an approximation of an NACA wind section (Refs. 1 and 5). The assumption of this general shape permitted calculation of the pressure distribution (or skin aerodynamic loading) and assurance of fairly low drag forces. The large opening required for photographic observation on the upper surface (Figure 3) provided ready access of air to the interior to minimize aerodynamic skin loading but also introduced an unknown and presumably large amount of drag. The remaining aerodynamic skin loading was resisted by attachment of the skins to the tank or to each other by longitudinal (parallel to centrifuge arm axis) formers. Transverse ribs stiffened the air foil shape and broke the areas between longitudinals into short rectangular panels (Figure 4).

The centrifugal force made transverse sheet metal undesirable, so the skin sections were made longitudinally continuous where possible. This made the skin self supporting insofar as centrifugal loading was concerned except at the outer edge of the observation opening where a channel beam and welded lip carried the load of the upper rear skin panel and part of the end fairing. The end fairing was fabricated of fiberglass reinforced polyester plastic with aluminum reinforcement around the attachment rim. The centrifugal load of the skin was

transferred to the main tank support beam at the inboard end via a transverse tension plate braced by a series of diagonal compression struts.

2.7 CAMERA

A 35mm Fastax recently rebuilt by the manufacturer to provide good resolution and capable of taking 3,600 frames per second (Figure 7) was used. A 17-inch focal length lens was used, which, with a 1/2 normal frame height film format, provided a field of view that nearly covered the window of the tank.

2.8 CAMERA MOUNTING

Some variation of the optical axis from its planned position was expected because of manufacturing tolerance in the mirror structure (which was not adjustable) and because one centrifuge prong had been bent previously. In order to align the camera lens with the intended optical axis, a camera mount with a wide range of adjustment was required.

A flat plate was bolted to a hatch opening at the center of the centrifuge in place of the ordinary cover. A heavily braced vertical tube was welded to the plate. Into this tube telescoped a tube and plate assembly. The camera height was adjusted by the amount of telescoping of the tubes and the position locked with set screws through the outer tube. In the mount used for the 1960 tests (Fig. 7) the camera mounting plate was secured to the tube plate by long bolts and spacers to attain the desired tilt and aim of the camera. In the 1961 mount, metal arc segments were welded to the plates. The tilt of the camera plate was continuously adjustable within limits of the arc and could be locked in position with a bolt.

2.9 ILLUMINATION

To obtain high illumination efficiency the photographs were backlighted; i.e., the explosions appeared in silhouette against a bright background. Attached to the rear window frame was a translucent sheet of acrylic plastic. A grid was drawn on the plastic to provide a length scale in the photographs. Light was furnished by either incandescent or photo flash lamps placed between the plastic and the leading prong of the centrifuge.

In the 1960 tests, illumination was usually provided by 77 General Electric No. 1184, 6-8 volts, 50 candle-power lamps wired in 7 parallel strings, each containing 11 lamps in series. Automobile storage batteries provided 84 volts and ample current capacity. A light weight, white painted, aluminum alloy structure (Fig. 8) provided a small shelf for each receptacle and a reflecting background for each lamp. This arrangement provided ample light for an f/8 camera aperture at 3,600 frames per second, using Kodak Tri-X film in the Fastax camera.

For the 1961 tests it was felt desirable to reduce the aperture in an effort to increase photographic resolution. The light intensity was increased to permit this. A 224 lamp bank operating on 108 volts DC was used. The No. 1184 lamps were arranged in 16 parallel strings, each with 14 bulbs in series.

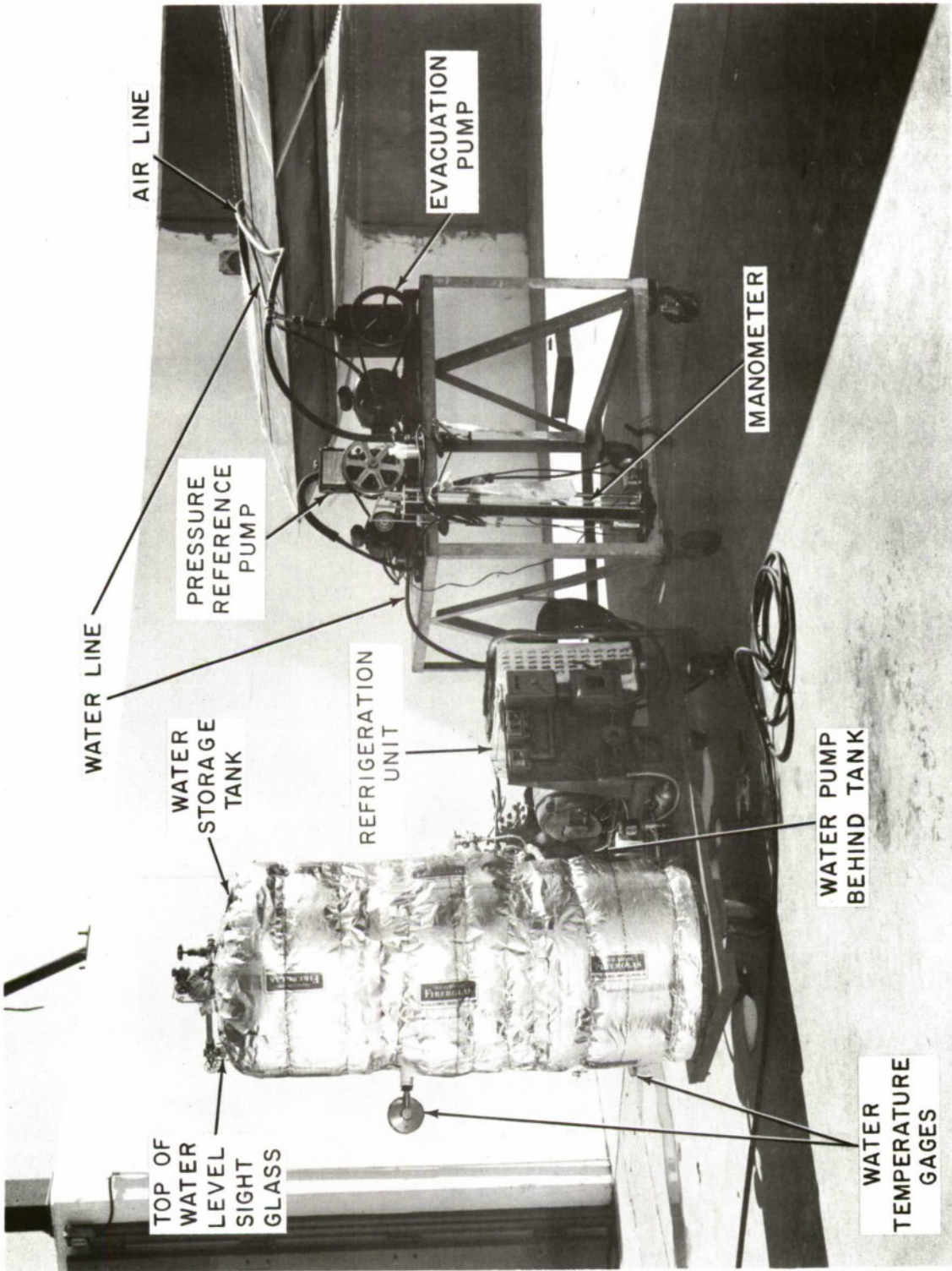


FIG.10 FLUID CONTROL EQUIPMENT

The lamp sockets were arranged hexagonally on a 1/4 inch sheet of laminated Micarta. With this arrangement the aperture was reduced to $f/11$.

As an alternate 3 speed-midget photoflash lamps could be used inserted in sockets screwed to the long beam support plate. These gave ample illumination for the Fastax with its aperture at $f/11$.

Both types of lamp were selected on the basis of breakage resistance to high acceleration; the GE 1184 had an extremely strong filament structure, and the photoflash lamps had a solid, pellet-type flash element (rather than shredded metal).

2.10 ELECTRICAL CIRCUITS

Figure 9 is a block diagram of the instrumentation used on the centrifuge. The diagram shows the physical relationship between the various electrical units. The master control panel transmitted power and control signals to all other units as required except for the camera and lamps, which obtained power from other sources.

The timing unit, containing a 1000 cycles per second tuning fork, provided electrical pulses for lighting an argon timing lamp in the camera. The delay unit triggered the firing unit flash bulb output 0.4 seconds after the camera power was applied and also triggered the firing unit detonator output about 3 milliseconds later. The firing unit, located near the center of rotation of the arm, was a Strobotron controlled condenser discharge unit featuring rapid charging and remote control. Its orientation was such that centrifugal force pressed the tubes into their sockets. It was in the arm to avoid passing heavy currents and high voltages through the centrifuge slip rings.

The Fastax control unit consisted of a Variac (to adjust camera speed) and a heavy duty relay to turn power on and off. The camera contained a cut-off switch which was connected to the control circuit, so that unless there was a roll of film in the camera none of the circuits could be activated. Moreover, when the 100 foot roll of film had passed through the camera, all power to lights, camera, etc., was turned off.

The lamp relays were heavy duty units. To avoid overheating the plastic diffusing screen, and to avoid running down the batteries, the power was on the lamps only while the film was running through the camera.

Small indicator lamps were located near the camera (Fig. 7) so that the camera operator and especially the charge armer could have visual indication of the condition of the firing unit.

If flash bulbs were used in place of a lamp bank, the delay unit supplied enough time delay so that the charge would not fire until the lamps had reached operating brightness.

One innovation for the 1961 test was the introduction of a water level control circuit which permitted water to flow through a slip joint on the centrifuge axis and into the test tank during a centrifuge run. A solenoid valve was activated from the master control panel until the rising water level opened an adjustable float switch in the test tank, thereupon deactivating the solenoid valve. This equipment was used for shots in which the charge position was fixed in the test tank, i. e., for shots with a simulated bottom (see Section 2.12).

2.11 EXPLOSIVES

Most of the explosive charges contained 0.2 grams of lead azide in a thin walled aluminum cup (Ref. 8). Two of the charges used in the "wall effects" program (see Section 4.2) contained 0.05 grams of lead azide and were similar to those used in the earlier high gravity tank tests (Ref. 7).

2.12 TANK FITTINGS

A false bottom which mounted at window level was provided to simulate shallow water conditions. Charges could be mounted either with half of the charge recessed in the bottom or on metal rod stand-offs.

The bottom was an aluminum plate which was made in sections which could be passed through the hand ports and assembled in the tank.

For deep shots, in the 1960 tests, a system of four copper toilet floats supported each corner of an "X" shaped beam, via tension rods. At the center of the "X" was a metal block into which a 1/8 inch diameter aluminum alloy rod could be inserted. The charge was supported on and taped to the upper end of the rod. The depth of the charge, relative to the floats, and hence the surface, could be adjusted by changing the length of the aluminum rod or by changing in increments of 2 inches the points where the "X" beam attached to the tension rods. The maximum aluminum rod design length was 8 inches, determined by its resistance to bending by the charge and rigging weight at 200 g. (Failure to comply with this design criterion leads to structural failure (see Section 2.15)).

The copper toilet floats leaked and were deformed by the combined action of the explosion and acceleration loading. In the 1961 float suspension, seamless stainless steel floats replaced the toilet floats.

2.13 FLUID CONTROLS

In the 1960 tests, auxiliary equipment for tank evacuation and tank pressure measurements was mounted on a movable work table. Equipment for water temperature control, storage of water, and for filling and emptying the tank was mounted on a separate hand cart (Fig. 10). For the 1961 tests, all the equipment was mounted on a single larger hand cart, thus simplifying the test tank servicing operation between runs.

CONFIDENTIAL

NOLTR 63-125

Stored water, circulated by a small centrifugal pump, was chilled by a 10 horsepower refrigeration unit. A filter was in the circulation loop to remove coarse impurities. The temperature of the water at the storage tank was measured with industrial stem type dial thermometers.

The same pump was used to transfer water to and from the test tank through a garden hose. The amount of water pumped in or out of the storage tank was measured with a sight glass and steel tape. In the 1960 tests, for shots in which the charges were mounted on or close to the simulated bottom, the amount of water admitted into the test tank was critical. Because of inaccuracies of water volume calibrations and resulting generally discouraging results for shallow shots, a water level control circuit was introduced for the 1961 tests (see Section 2.10).

A laboratory vacuum pump was used to evacuate the test tank. In the 1960 tests, the tank pressure was measured, after pumping had stopped, with a manometer system previously used with the NOL vacuum tank (Ref. 15). With this manometer, the tank pressure readings were referenced to (approximately) zero pressure provided by a second vacuum pump. In the 1961 tests a Wallace-Tiernan Type FA 173 manometer, set up as a barometer, was used. This eliminated the need for a second vacuum pump.

The water connection was near the bottom of the bonnet and the air-vacuum connection was near the top (Figure 3). Both openings were controlled by globe type aluminum angle valves with resilient seats.

2.14 CONSTRUCTION AND TESTING

Testing of the tank-beam assembly was required by the Sandia Corporation before it could be used on their centrifuge. Static testing at 120% of full load was requested for basic structural parts to be used or appropriate derating from the failure point of duplicate units. Since the time schedule had little allowance for rectification of failures, two beam-bonnet-tank-mirror assemblies were made so that if one failed catastrophically during test, the second could be used during the time scheduled on the centrifuge in August and September 1960.

The assemblies were fabricated and tested by the Hayes Aircraft Corporation (now Hayes International Corporation), Birmingham, Alabama. Testing was in five steps. First, the beam was loaded hydraulically via the bonnet to a load of 364,000 pounds (see Figure 11). Deflection measurements on the beam indicated performance as expected. Second, using a sand cushion and hanging it from a substitute bonnet, the bottom of the tank was loaded to 206,000 pounds. This was a severe test of the tank shell welds. Third, the mirror support brackets were loaded to 6,000 pounds. The fourth step was evacuation of the tank to check for leaks, and the final step was to pressurize the tank-bonnet assembly to 77 psi to check the window strength. Some leakage at a window was noted and repaired with a sealing compound.

After testing, further calculations based on actual component weights showed that if the tank were to be used at 200 g, the beam should have been



FIG.II TESTING BEAM VIA BONNET LOADING OF 364,000 LBS.

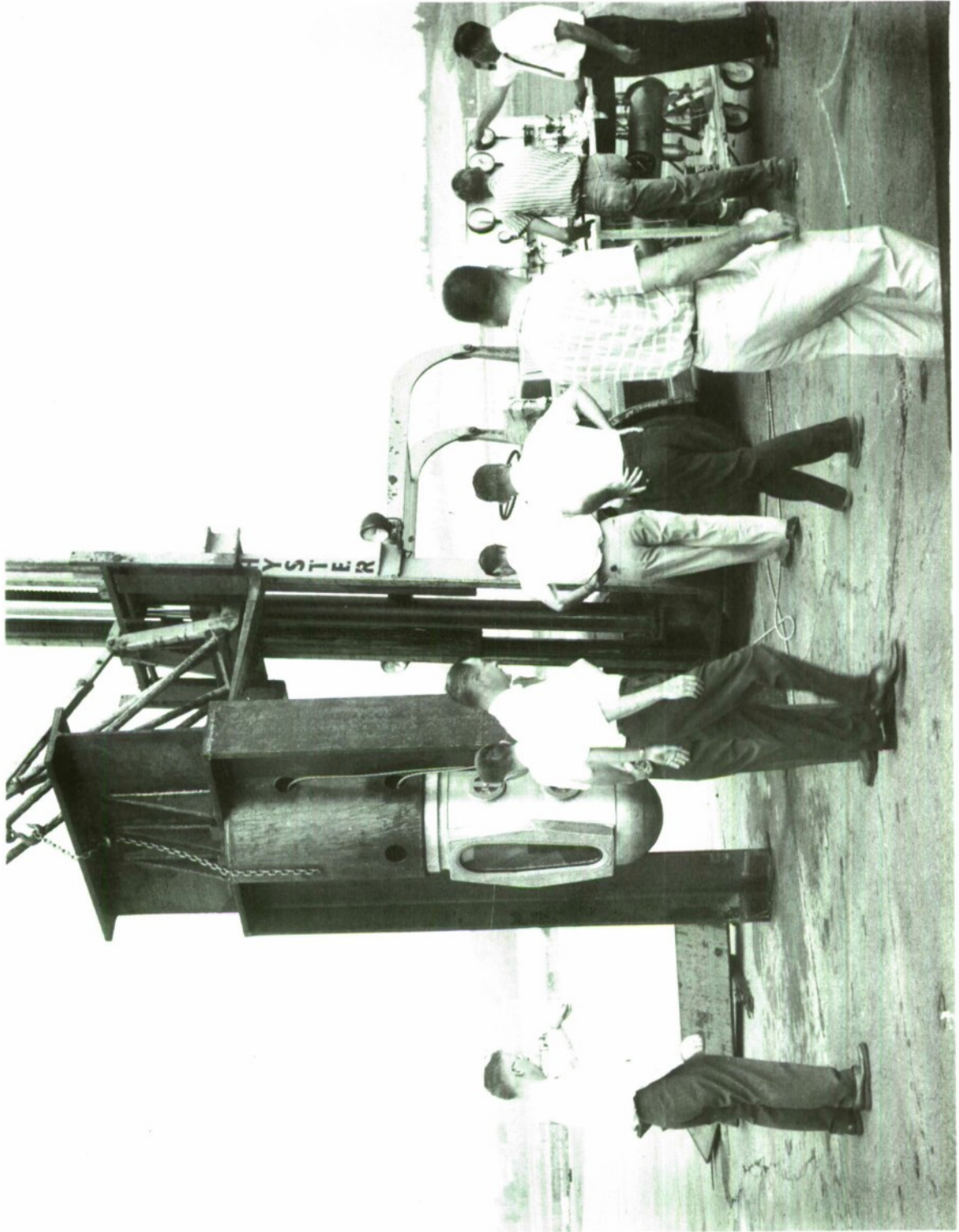


FIG.12 LOADING BOTTOM OF TANK TO 206,000 LBS.

tested to 380,000 pounds. The assemblies were subsequently derated for use at up to 191.6 g (or 190 g) with a 20% margin of safety.

Both units were tested as described.

2.15 EQUIPMENT PERFORMANCE

Few failures of test tank equipment could be attributed to high accelerations alone. A number of small fairing screws along the trailing edges were sheared off because of spreading of the centrifuge arm prongs under load, but this did not affect operation. The only serious failure was the rupturing of the rear (illumination) window on shot PR 1320 by an explosive charge that had been placed on a support rod over one foot in length. The rod, far too long (see Section 2.12), bent over until the charge was in contact, or nearly in contact, with the window. Pictures showed the bent rod and window failure at the time of detonation. The water and broken glass swept out most of the lamps and sockets from the lamp housing and then burst out through the fiberglass end fairing. Only the leading end of the fairing was carried away.

The window was replaced without dismantling the tank. Flash bulb illumination was used until a second lamp housing was completed and installed. A sheet aluminum patch closed the gaping hole in the end fairing. For the 1961 tests, a spare lamp housing and end fairing were on hand but were not needed.

Most other deficiencies in the equipment were in control functions and are discussed in detail in Section 3.

3. MEASUREMENTS AND EXPERIMENTAL CONTROL

3.1 GENERAL

For most of the deep shots fired in these tests, the maximum explosion bubble radius, A_{\max} , and its first period, T , are the primary measurements of interest. Secondary characteristics of interest are the growth of the water mound at the surface and plume development. For shallow shots the general surface characteristics are of primary importance. Measurements of these dynamic explosion characteristics were obtained from high speed movie films.

In addition to explosion characteristics, the initial experimental conditions must be taken into account. The charge depth was measured on the films; acceleration at the tank was computed from the RPM and radius arm of the centrifuge; the pressure was determined from manometer readings; and the water temperature from thermometer readings. A comparison of the conditions attained with the intended values indicates the degree of experimental control.

In the following paragraphs the methods of measurement are discussed.

3.2 BUBBLE PERIOD

The first bubble period is defined here as the time span from the initiation of the charge to the time when the curve of the upper bubble surface location versus time experiences an inflection. Successive bubble periods are defined as the time span between successive inflections of this curve. This method of measuring the periods has been found (Ref. 17) to be comparable to the use of pressure-time records.

The time of initiation and inflection of the bubble top motion were determined from plots of bubble vertical displacement histories (Figure 19 shows examples). This time was measured as the number of frames between events and then multiplied by the reciprocal of the framing rate, which had been determined from the 1000 cps timing marks appearing at the edge of the film strip, to obtain units of seconds. Since there was only a slight variation in framing rate during the recording time, the average framing rate during the first period of bubble oscillation was used for all conversions.

The periods thus determined are listed in Table 1 under T_m .

3.3 BUBBLE SIZE

The maximum bubble size was determined from frame by frame projections. Tracings of the bubble circumference were made and compared until the largest one was identified. The reference grid at the rear illumination window was also traced. The bubble radius was found by superimposing graduated circles of known radii over it and selecting the one which came closest to having the same area. The projected bubble radius thus determined was multiplied by a scale factor which was determined from reference grid measurements and corrected for parallax to the plane of the explosion. The projections were nearly full size in all cases and the scale factor near unity.

The measured maximum bubble radii are listed in Table 1 under $A_{max m}$.

3.4 ABOVE SURFACE CHARACTERISTICS

Other characteristics which are of interest are the growth of the water mound and plume development. The above surface events are of particular interest in scaled shots for which there is surface photography of prototype explosions. A comparison of the model and prototype surface development can give a direct evaluation of scaling effectiveness. Where comparisons were made, they were of the maximum vertical displacement histories of surface development; this comparison was chosen because surface displacement histories of prototype shots were readily available. In the comparisons, a scale factor is used to convert model measurements into prototype units.

Because of the optical geometry (see Section 3.5), there is a zone just above the water surface over the charge which is hidden from view. This region is schematically illustrated in Figure 13. As a result, the very early surface development is not visible.

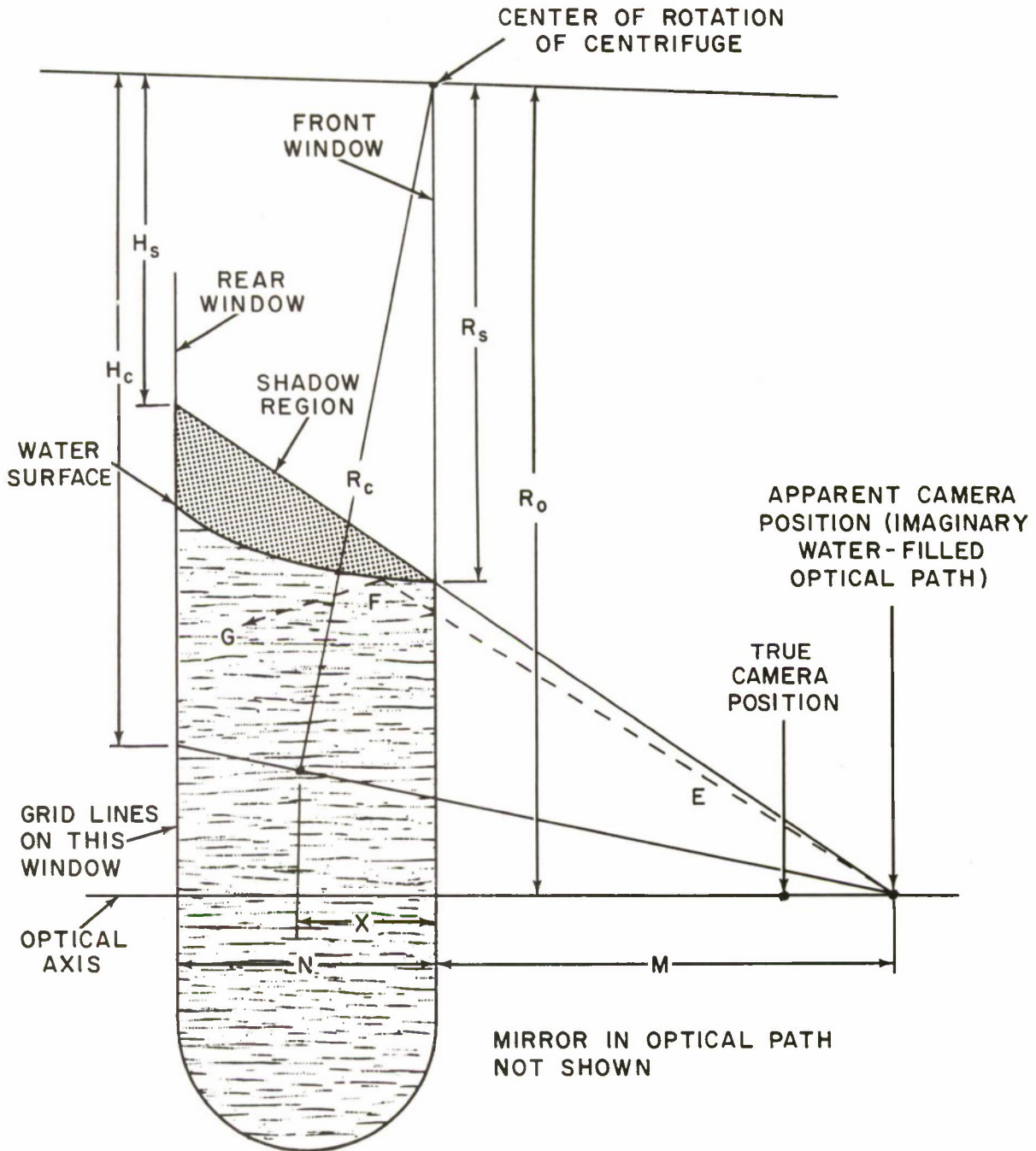


FIG.13 CALCULATION OF CHARGE DEPTH AND OPTICAL GEOMETRY

3.5 CHARGE DEPTH

Unfortunately, the charge depths could not be measured directly from the photographs as had originally been thought. The position of the surface directly over the charge could not be seen. The water line most apparent on the pictures was that at the front window. The water surface is approximately cylindrical with an axis coinciding with the centrifuge axis. In addition, though the test tank, mirror, and camera arrangement had been carefully designed to provide an optical axis passing perpendicularly through the center of the window (34.48 feet radius from the axis of rotation of the centrifuge), this geometry was not attained.

Studies of the grid photographed through water and air indicate that the optical axis pierced the tank at a radius of 35.80 feet in the 1960 tests and 34.54 feet in the 1961 tests; and was about 0.30 feet below the horizontal (relative to the ground) or long axis of the window. A grid line passing perpendicularly behind the water surface and through the optical axis would appear as a straight line. Lines not passing through the optical axis would appear offset because of differences in refraction. The amount of offset was proportional to the distance the lines were displaced from the axial position. A plot of the measured offset vs nominal line position indicated the position of the optical axis (where the offset became zero). Measurements of the offsets observed in perpendicular sets of lines when the water surface is vertical (centrifuge running) or horizontal (centrifuge stopped) provided the optical axis location relative to the known grid lines.

The optical axis could have been raised to pass through the horizontal axis of the tank by raising the camera, but at the time of the experiments this error in position was undetected. Attempts were made to correct the error in radial distance but the mirror angle could not be changed and the camera could not be moved sideways enough on its mount to place it where needed. It was not desirable to move the camera too far sideways, i.e., off the centrifuge axis, since the increased centrifugal force could cause camera malfunction.

Upon establishing certain dimensions in the test configuration, an expression for determining the radius from the centrifuge axis to the water surface, R_s , and to the charge, R_c , can be developed. The difference between the two will be the charge depth.

The position of the camera relative to the mirror and front window of the tank was known well enough to permit calculation of the length of the optical axis (36.2 feet). The distance between the front window and rear window (or reference grid) was determined from tank dimensions (2.0 feet). It was assumed that the charge was located on the tank centerline although this was known to be slightly in error on shots where the float charge support system was used. The float system did not fit closely in the tank and was free to drift a few inches from the centerline. In addition, on shots prior to PR 1320 (where the rear window was blown out) the long support rods that were used could have bent away from the centerline.

The positions of the reference grids (three were used) were determined in several ways. One grid was located with reference to the simulated bottom whose position was known. The other grids were located with reference to a corner of the tank window frame which appeared in some photographs.

The water surface was viewed more or less from the edge and the line of intersection with the front window was expected to be very sharp since meniscus effects were reduced in proportion to the acceleration. The front edge of the water surface was indeed readily distinguishable while the other manifestations of the surface (the rear edge, the cylindrical water surface over the charge) were either out of focus or invisible because of reflection. Since the front window was exactly radial to the axis of rotation, measurements on it (as to the water surface) were actual radial distances. The rear window grid and the axis of the tank were not radial but were parallel to the front window. Dimensions in these planes were transferred to the front window plane by rectilinear projections. The actual radial distances to points on the projected planes were greater than they appeared to be at the front window (see Figure 13).

From the geometric properties shown in Figure 13, measurements of distance on the film relative to the grid lines could be converted to radial distances, thus:

$$R_c = \sqrt{\left[\frac{R_o N - R_o X + H_c X + H_c M}{N + M} \right]^2 + X^2} \quad (1)$$

and

$$R_s = R_o - \frac{M(R_o - H_s)}{M + N} \quad (2)$$

Where:

- R_c = radial distance from centrifuge axis of rotation to charge.
- R_s = radial distance from centrifuge axis of rotation to the surface.
- R_o = distance from centrifuge axis of rotation to the optical axis.
- H_c = apparent position of charge relative to rear grid lines.
- H_s = apparent position of intersection of water surface with front window relative to the underwater grid lines.
- N = thickness of water-glass medium.
- M = apparent distance to camera from front window if the entire optical path were through water (approx $4/3$ of the air path).
- X = distance of charge from front window.

TABLE 1 DATA FROM ACCELERATED TANK UNDERWATER EXPLOSION EXPERIMENTS

Shot Number	A _{max m} (ft)	T _m (ms)	d _m (ft)		a _m (g)		a _z (g)		P _m (ft H ₂ O)		τ (°F)	I _A	I _T
			Nom	Meas	Nom	Meas	Nom	Meas	Nom	Meas			
EFFECT OF TANK SIZE													
PR 1337	.112	5.94	.271	.295	20	20.7	20.6	34	27.5	47.0	0.765	0.751	1/
PR 1338	.104	4.91	.271	.281	60	60.9	60.7	34	27.5	48.0	0.780	0.786	1/
EFFECTS OF d _m , a _m , AND P _m ON THE EXPLOSION BUBBLE													
PR 1304	.198	9.45	.5	.546	70	69.9	69.3	10	10.57	52.0	0.988	0.980	
PR 1305	.141	5.26	1.0	1.021	70	70.3	69.3	10	28.	50.0	0.917	0.967	2/
PR 1306	.193	9.26	.5	.653	70	69.6	69.0	3	3.35	45.0	0.974	0.948	
PR 1307	.148	6.66	1.0	1.132	70	70.4	69.2	3	3.25	48.0	0.905	1.040	
PR 1315	.166	6.14	.5	.514	140	138.5	137.4	10	10.55	50.0	0.982	0.986	
PR 1316	.133	3.55	1.0	.978	140	140.4	138.4	10	10.36	48.0	0.982	0.905	
PR 1317	.171	6.79	.5	.476	140	140.5	139.5	3	3.34	49.0	0.968	0.966	
PR 1318	.133	3.90	1.0	.979	140	140.3	138.4	3	3.35	50.0	0.966	0.955	
PR 1359	.158	6.77	1.0	.992	70	70.2	69.2	10	10.26	48.0	0.951	1.029	
COMPARISON OF DIFFERENT FORMS OF BUBBLE SCALING													
PR 1302	.259	15.52	.333	.343	35	35.1	35.0	12	12.30	53.0	1.012	0.958	
PR 1308	.180	6.74	.400	.593	75	76.2	75.6	33	27.5	47.0	1.025	0.972	
PR 1312	.173	6.43	.417	.420	109	109.6	108.9	33	27.5	49.0	0.976	0.963	
PR 1315	.175	6.48	.396	.400	112	112.5	111.9	33	27.5	48.0	0.981	0.964	
PR 1314	.190	7.10	.333	.329	135	136.3	135.7	33	27.5	51.0	1.058	1.080	

1/ .05 gm charge, non. water depth = .60 ft.

2/ Leaked air.

TABLE 1. DATA FROM ACCELERATED TANK UNDERWATER EXPLOSION EXPERIMENTS Continued

Shot Number	A _{max} (ft)	T _m (ms)	d _m (ft)		a _m (g)		a _z (g)		P _m (ft H ₂ O)	τ (°F)	I _A	I _T
			Nom	Meas	Nom	Meas	Nom	Meas				
SCALING HIGH EXPLOSIVES - DEEP WATER SHOTS												
PR 1322	.149	4.80	.458	.425	190	190.5	189.4	189.4	27	27.3	51.0	0.989
PR 1323	.153	4.72	.458	.408	190	190.5	189.4	189.4	27	27.5	48.0	0.953
PR 1324	.153	4.62	.458	.425	190	190.5	189.3	189.3	27	27.1	51.0	0.951 ^{3/}
PR 1325	.143	4.49	.500	.504	190	190.2	188.8	188.8	27	27.1	47.0	1.016
PR 1326	.142	4.25	.542	.533	190	190.6	189.1	189.1	27	27.3	51.0	0.996
PR 1327	.140	4.13	.542	.519	190	190.6	189.1	189.1	27	27.4	48.0	0.954 ^{3/}
PR 1328	.143	4.30	.542	.537	190	190.9	189.4	189.4	27	27.5	49.0	1.015
PR 1329	.138	4.01	.583	.604	190	190.6	190.0	190.0	27	27.5	50.0	1.016
PR 1331	.136	3.80	.625	.609	190	190.4	188.7	188.7	27	27.3	47.0	0.966
PR 1332	.136	3.75	.667	.652	190	190.4	188.6	188.6	27	27.4	52.0	0.995
PR 1333	.131	3.60	.667	.663	190	190.9	189.1	189.1	27	26.9	50.0	0.965
PR 1334	.135	3.47	.667	.667	190	190.9	189.1	189.1	27	27.5	49.0	0.933
PR 1360	.154	4.95	.437	.405	190	189.5	188.3	188.3	27	27.2	46.0	0.974
PR 1373	.154	5.62	.850	.837	112.5	112.1	110.8	110.8	27	5.75	51.5	1.035
PR 1377	.132	3.46	1.01	.984	127	127.3	125.5	125.5	33	33.1	48.0	0.937
PR 1380	.139	4.53	.850	.836	112.5	112.8	111.4	111.4	27	26.8	50.0	0.986
PR 1382	.167	5.69	.465	.467	141	141.1	140.2	140.2	27	27.0	50.0	1.025
PR 1386	.141	3.72	.640	.639	177	177.3	175.7	175.7	33	33.0	47.5	0.960
PR 1387	.143	4.33	.720	.713	141	140.7	139.2	139.2	27	27.1	49.0	0.989
PR 1388	.143	4.17	.740	.720	138	137.9	136.5	136.5	33	32.75	45.5	1.002
PR 1389	.175	5.90	.370	.408	144	143.5	142.7	142.7	27	26.9	47.0	1.004

^{3/} With ship model.

TABLE 1 DATA FROM ACCELERATED TANK UNDERWATER EXPLOSION EXPERIMENTS Continued

Shot Number	A _{max} (ft)	T _m (ms)	d _m (ft)		a _m (g)		a _z Meas (g)	P (ft H ₂ O)		T (°F)	I _A	I _T
			Nom	Meas	Nom	Meas		Nom	Meas			
SCALING HIGH EXPLOSIVES - BOTTOM SHOTS												
PR 1342	.176	5.69	.437	.428	190	191.0	189.8	27	27.6	52.0	1.134	1.183
PR 1344	.187	5.97	.437	.352	190	190.9	189.9	27	27.3	47.0	1.141	1.124
PR 1345	.176	5.61	.500	.415	190	190.9	189.7	27	27.5	49.0	1.124	1.147
PR 1346	.172	5.06	.542	.478	190	190.9	189.6	27	27.5	49.0	1.143	1.116
PR 1347	.170	4.93	.542	.506	190	190.9	189.5	27	27.3	49.0	1.149	1.121
PR 1348	.170	5.23	.542	.495	190	190.9	189.5	27	27.5	50.0	1.142	1.177
PR 1349	.160	4.73	.583	.556	190	190.9	189.4	27	27.5	48.0	1.113	1.139
PR 1350	.159	4.51	.625	.583	190	190.9	189.3	27	27.5	50.0	1.122	1.117
PR 1351	.153	4.20	.667	.636	190	190.9	189.1	27	27.5	47.0	1.109	1.098
PR 1352	.147	4.76	.667	.548	190	190.9	189.4	27	27.3	47.0	1.017	1.135
PR 1353	.157	4.75	.667	.554	190	190.9	189.4	27	27.5	47.0	1.091	1.141
PR 1358	.176	5.85	.437	.403	190	190.9	189.8	27	26.3	48.0	1.111	1.166
SCALING UNDER ICE EXPLOSIONS												
PR 1330	.216	5.70	.062	.042	62.5	65.2	65.2	33	27.5	48.0	.877	2.847
SCALING DEEP NUCLEAR EXPLOSIONS												
PR 1301	.316	26.6	.437	.403	25	25.1	24.9	3	3.38	48.0	1.029	0.976
PR 1303	.191	11.8	1.000	.915	40	37.2	36.7	6	6.45	54.0	0.914	1.014
PR 1319	.154	5.40	.500	.510	175	175.7	174.4	6	7.19	50.0	0.966	0.999
PR 1372	.220	13.3	.800	.787	40	40.0	39.6	6	5.93	42.0	1.020	1.073
PR 1374	.204	12.2	.900	.891	40	39.9	39.4	6	5.73	51.0	0.982	1.064
PR 1375	.197	11.3	1.000	.981	40	40.1	39.6	6	5.90	47.5	0.981	1.060
PR 1376	.195	11.3	1.000	.984	40	40.1	39.6	6	5.97	48.5	0.972	1.064
PR 1378	.192	11.2	1.100	1.072	40	40.1	39.5	6	4.67	49.0	0.975	1.093
PR 1379	.188	10.6	1.200	1.085	40	40.1	39.5	6	5.94	52.0	0.968	1.067

TABLE 1 DATA FROM ACCELERATED TANK UNDERWATER EXPLOSION EXPERIMENTS Continued

Shot Number	A _{max m} (ft)	T _m (ms)	d _m Nom (ft)	d _m Meas (ft)	a _m Nom (g)	a _m Meas (g)	a _z Meas (g)	P _m Nom (ft H ₂ O)	P _m Meas (ft H ₂ O)	τ (°F)	I _A	I _T
SCALING DEEP NUCLEAR EXPLOSIONS (Cont'd)												
PR 1381	.343	28.3	.437	.385	25	24.9	24.8	3	2.86	49.5	1.089	0.980
PR 1383	.325	27.6	.437	.429	25	25.0	24.9	3	2.98	50.5	1.066	1.014
PR 1384	.335	28.5	.447	.400	25	24.9	24.8	3	2.93	49.0	1.076	1.008
PR 1385	.322	27.6	.457	.456	25	25.0	24.8	3	2.92	48.5	1.073	1.040
PR 1390	.317	26.3	.417	.453	25	25.0	24.8	3	3.03	49.0	1.057	0.995
PR 1391	.320	26.2	.427	.432	25	25.0	24.8	3	3.04	49.0	1.053	0.969
SCALING SHALLOW NUCLEAR SHOTS												
PR 1310			.017	.014	80	80.3	80.2	34	27.5	44.0	1.012	1.055
PR 1311	.189	7.88	.396	.381	80	94.2	93.7	34	27.5	48.0	0.966	1.003
PR 1321	.153	5.02	.396	.400	190	190.4	189.3	34	27.5	53.0	0.977	0.923
PR 1335	.195	6.20	.017	.140	190	197.9	197.5	34	27.5	51.0	0.952	0.886
PR 1336	.189	6.00	0	.144	190	198.0	197.6	34	27.5	50.0	1.132	1.015 ^{4/}
PR 1339	.221	8.28	.396	.349	80	81.6	81.2	34	27.5	47.0	1.165	1.172 ^{4/}
PR 1354	.194	6.38	.396	.331	190	190.9	190.0	34	27.5	48.0	1.165	1.172 ^{4/}
PR 1368			.036	.020	90	86.4	86.4	34	27.7	53.0	1.165	1.172 ^{4/}
PR 1369			.036	.023	180	180.2	180.1	34	27.7	49.0	1.165	1.172 ^{4/}
PR 1370			.015	.028	90	86.4	86.4	34	27.7	40.0	1.165	1.172 ^{4/}
PR 1371			.015	.024	180	180.1	180.1	34	27.7	45.0	1.165	1.172 ^{4/}

^{4/} Bottom shot.
^{5/} Nom. Mid-depth.

The charge depth, d_m , can now be evaluated by:

$$d_m = R_c - R_s \quad (3)$$

Values thus determined are listed in Table 1.

Three other characteristics of the optical geometry may be noted. In the photographs it is seen that the rectangular reference grid is distorted, i.e., the horizontal and vertical lines are not at right angles. This is explained by the fact that the camera axis was not perpendicular to the plane of the windows since the camera was necessarily pointed to cover the required field of view. In general, the effect on measurements is believed to be negligible.

Because of hydrostatic loading on the windows during acceleration, the windows bulged slightly and acted like large magnifying lenses. Measurements of the distances between grid lines indicated that the effect was more noticeable, but small, below the water surface. By relating measurements to grid lines in the immediate vicinity of the measurement, cumulative errors from this source were avoided.

The third characteristic to be noted has significance for the observation of early surface development, as mentioned previously. There is a region just above the surface (the shadow region) in which events are not observable because the underside of the water surface acts as a mirror which diverts the light paths. This effect is shown schematically in Figure 13 at E-F-G.

3.6 ACCELERATION

The acceleration a , in g 's, at any point along the centrifuge arm can be computed from

$$a = 34.1 \times 10^{-5} r n^2 \quad (4)$$

where:

r is the radius from the centrifuge axis in feet

n is the revolutions per minute.

Experimental plans called for accelerations at the charges varying from 25 to 190g. Prior to the shots, estimates of n which would give the desired acceleration were required. They were obtained from the above equation by using an estimated radius to the charge, R_c . After the shots, the accelerations attained were determined with measurements^c of R_c , as described in the preceding paragraphs, and of n . The revolutions per minute at about the time of the shot were read from an electronic counter which measured the number of pulses in a

second that were produced by a generator geared to the centrifuge. Values of acceleration thus determined are listed in Table 1 under a_m .

The total hydrostatic head at the charge, Z_m , in feet of water, is defined by:

$$Z_m = d_m a_z + P_m \quad (5)$$

where:

- P_m is the air pressure in feet of water.
- d_m is the charge depth, in feet.
- a_z is the average acceleration acting on the water layer over the charge.

This acceleration may be computed from Equation 4 where the radius used is that to mid-depth above the charge:

$$r = R_s + [R_c - R_s] / 2 = [R_c + R_s] / 2 \quad (6)$$

and by inserting into Equation 5:

$$Z_m = 17.05 \times 10^{-5} d_m [R_c + R_s] n^2 + P_m \quad (7)$$

The radii, R_c and R_s , were determined from Equations 1 and 2.

3.7 AIR PRESSURE

Just before and immediately after each shot run, a period of from 20 to 60 minutes, the time and air pressure were recorded for all shots at reduced pressures. The time at which the shot was fired was also recorded. The air pressure at the time of firing was estimated by linear interpolation as indicated by the expression:

$$P_m = \frac{P_a - P_b}{t_a - t_b} [t_x - t_b] + P_b \quad (7)$$

where:

- P_m = air pressure at the time of firing.
 P_b = air pressure before the run.
 P_a = air pressure after the run.
 t_b = time of pressure reading before the run.
 t_a = time of pressure reading after the run.
 t_x = time of firing.

The air pressure was adjusted to the nominal or desired level before the shot.

The manometer used in the 1960 tests was sensitive to changes in atmospheric pressure. Since atmospheric pressure was not determined before and after each shot, it was assumed that it did not change significantly during the 20 to 60 minute interval between the pressure readings.

For shots which were fired at atmospheric pressure, the pressure in the test tank was not measured. Unfortunately, in the 1960 tests, the air valve on the test tank was left open during these runs; the aerodynamic properties of the fairing could have reduced the pressure at the air valve, and therefore in the tank, by several feet of water.

The Wallace-Tiernan manometer used in the 1961 tests was set up as a barometer, so that tank pressure readings were independent of atmospheric pressure changes.

3.8 WATER TEMPERATURE

Variation in water temperature is known to have an effect on explosion bubble behavior in the vacuum tank. The accelerated tank conditions predicted for the bubble scaling shots were based primarily on vacuum tank measurements in water at 48° F. Since the influence of water temperature in the accelerated tank was not known at the time of the experiments, a nominal water temperature of 48° was specified.

The water temperatures attained were determined from temperature readings made before and after the test similarly to the air pressure determination, thus:

$$\tau_m = \frac{\tau_a - \tau_b}{t_a - t_b} [t_x - t_b] + \tau_b \quad (8)$$

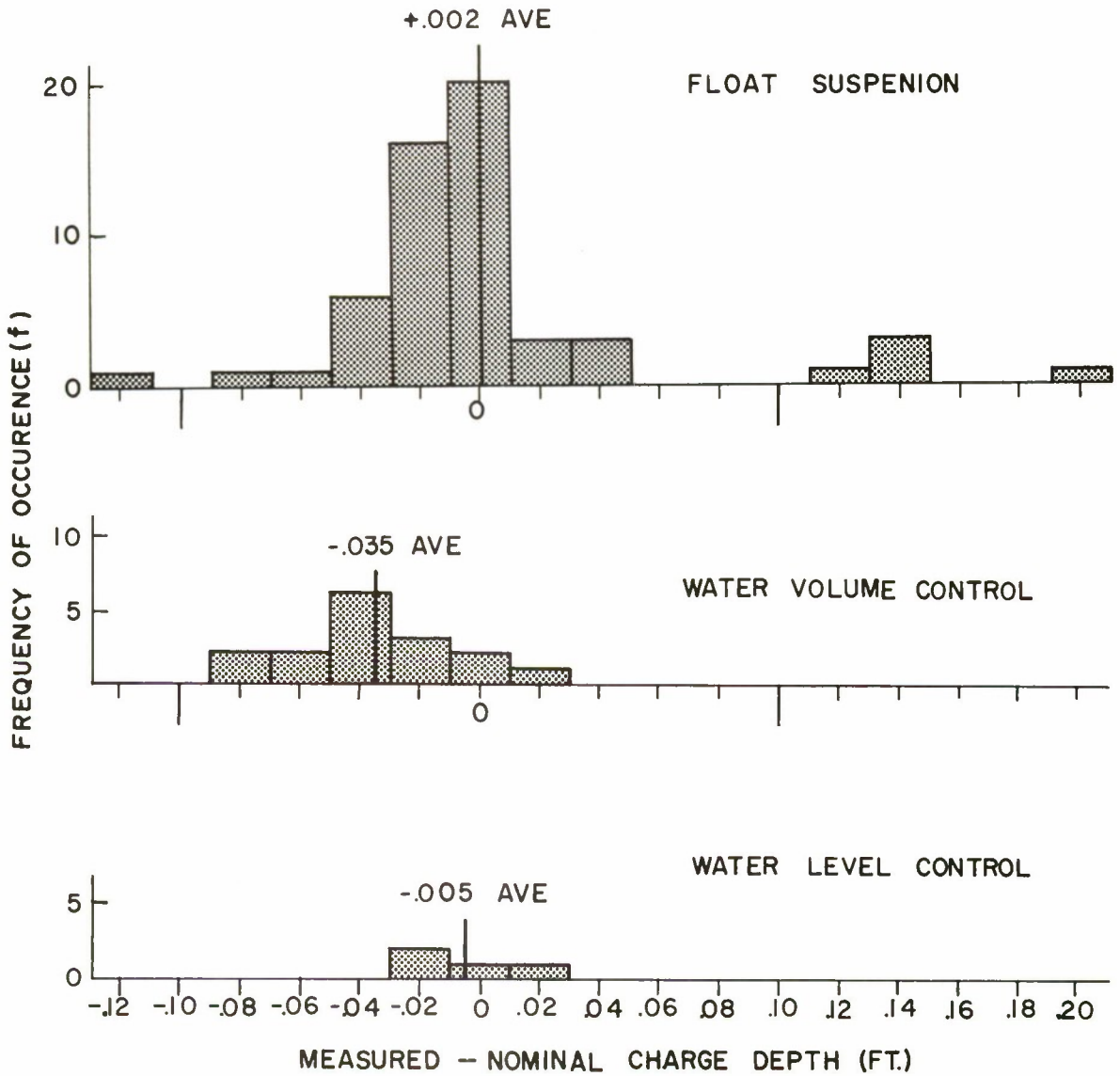


FIG.14 CHARGE DEPTH VARIATION FROM THE NOMINAL
LEVELS FOR VARIOUS SYSTEMS OF CONTROL

where:

$$\begin{aligned} \tau_m &= \text{temperature at time of firing.} \\ \tau_b &= \text{temperature at time of filling.} \\ \tau_a &= \text{temperature at time of draining.} \\ \left. \begin{array}{l} t_b \\ t_a \\ t_x \end{array} \right\} & \text{are the same as in Equation 7.} \end{aligned}$$

Water temperatures thus determined are listed in Table 1.

3.9 EXPERIMENTAL CONTROL

The degree of control of the conditions may best be shown by frequency distributions of the variables from their nominal or intended levels.

Figure 14 shows the charge depth variation from nominal levels for the three systems of depth control. Average values, calculated from the frequency distributions, are indicated. The float suspension system used in the 1960 and 1961 tests (56 shots) shows the least average variation from nominal levels. It is believed that variations beyond 0.1 foot resulted from either leaking floats or use of a charge suspension rod of the wrong length.

The water volume control method used in the 1960 tests when the charge was fired at a fixed position in the tank yielded the poorest results. From the shots plotted, the water depth was 0.035 feet too shallow on the average.

In the water level control system used in the 1961 tests on four shots with the charges in a fixed position in the tank, the water level was 0.005 feet too shallow on the average (0.002 if computed from data in Table 1). Although the number of shots using this method is quite limited, the figure does tend to indicate that the water level control system is an improvement over the water volume control system, especially for surface or shallow shots, where the depth control is critical.

Figure 15 shows the variation of accelerations from their nominal levels. In general, acceleration control was quite good with 68 of 76 shots falling within 1.5 g of their intended values. (Variations beyond 4 g are felt to result from errors in computation for desired RPM rather than control errors.) Excluding the variations beyond 4 g, the average difference from nominal was 0.26 g.

In Figure 16 the pressure variation is plotted relative to the nominal pressure level for 58 shots (18 shots at atmospheric pressure were not measured).

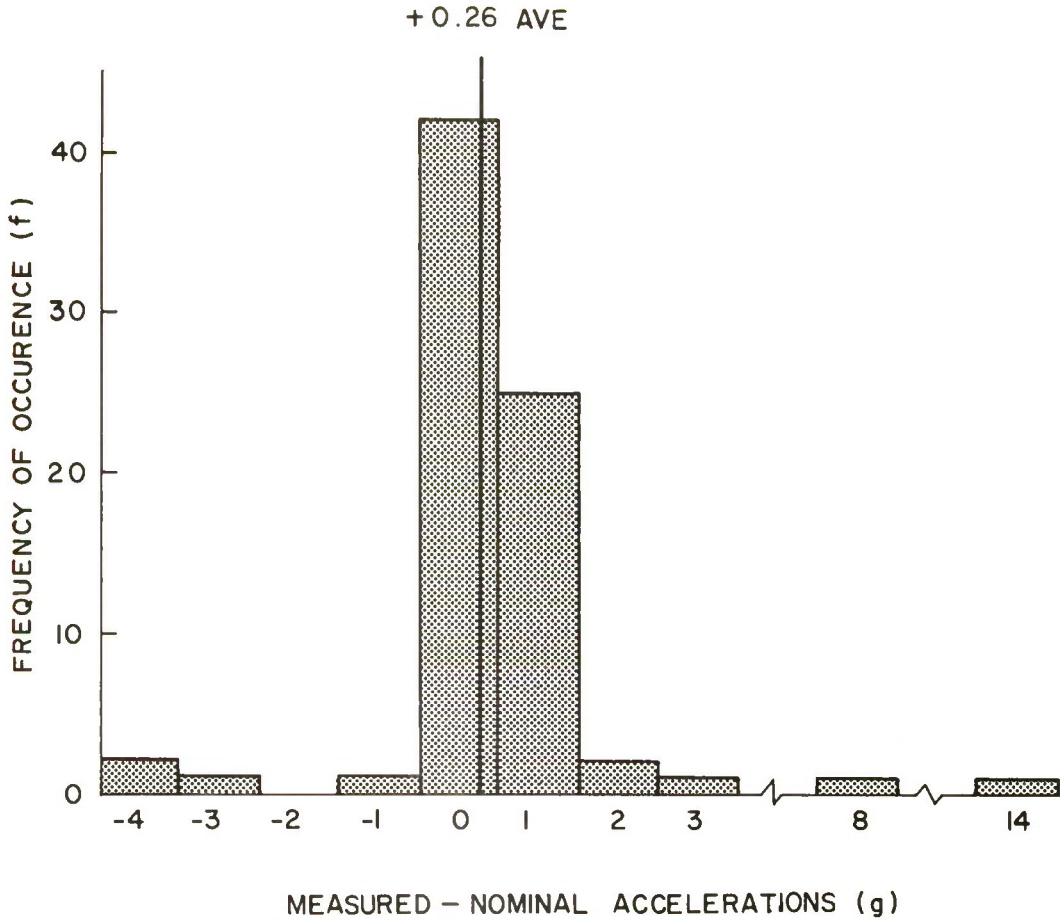


FIG.15 FREQUENCY DISTRIBUTION OF ACCELERATION
DIFFERENCES FROM THEIR NOMINAL LEVELS

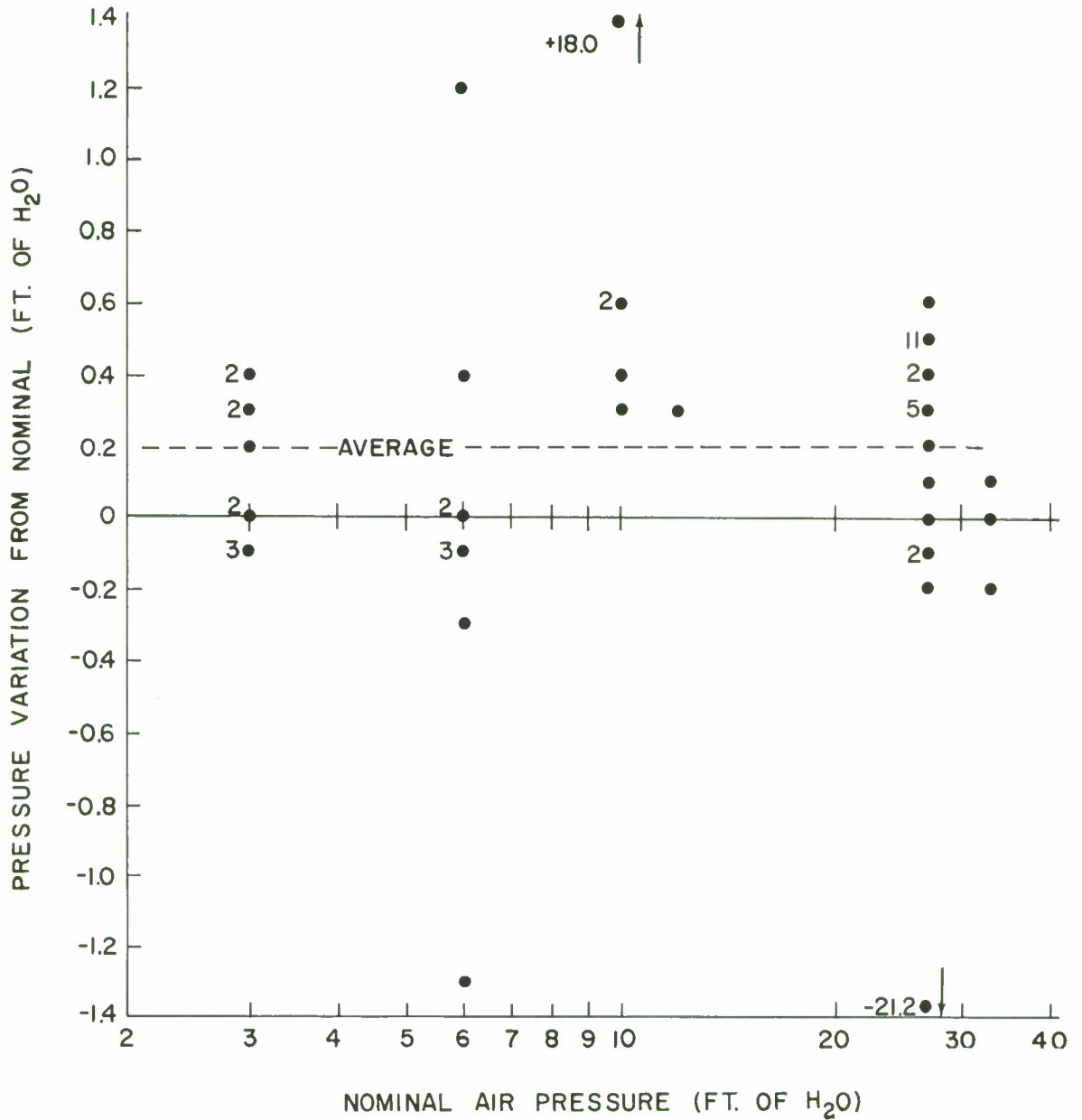


FIG.16 AIR PRESSURE VARIATION RELATIVE TO NOMINAL LEVELS

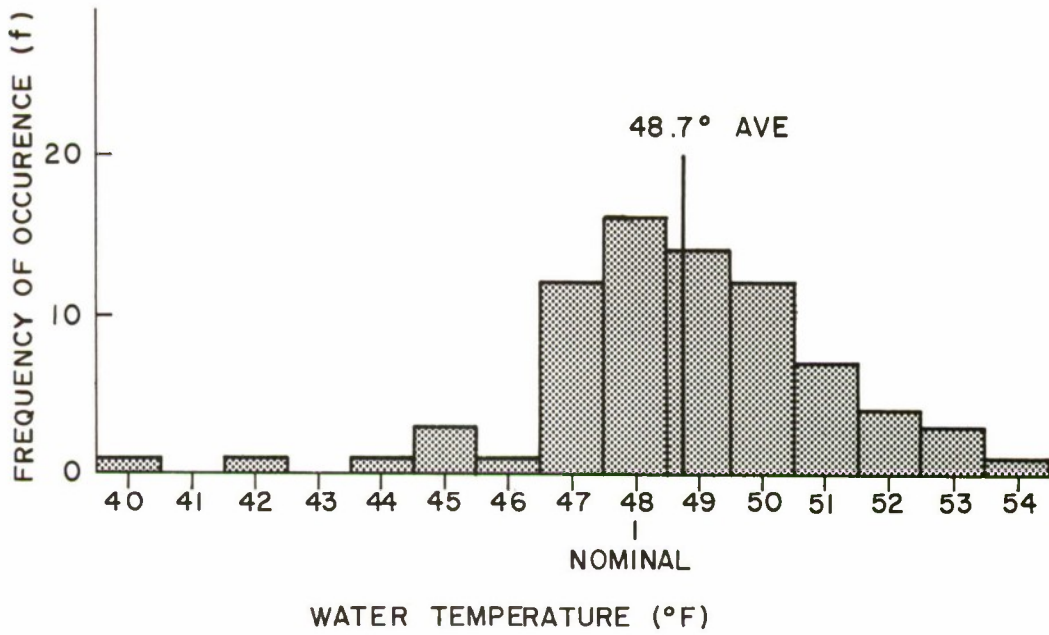


FIG.17 FREQUENCY DISTRIBUTION OF WATER TEMPERATURES

On the average the air pressure increased by 0.2 feet of water.* If the tank had an air leak, it would be expected that pressure variations would be greatest at low nominal pressures where the pressure differential from the atmosphere is greatest. This was not the case.

The cause of this pressure increase may have been heating of the air in the tank by the sun or admission of atmospheric air into the tank prior to the "after shot" pressure reading, although specific precautions against this possibility were taken in the 1961 tests. Explosion gas products and release of dissolved air from the water may also be contributing factors.

Figure 17 shows the distribution of water temperatures about the nominal 48° F level. Because of the water heating observed on early tests, the temperature was reduced 4° to 10° below nominal before each test. Control of water temperature was thus a trial and error process. The amount of heating varied with the time of day and cloud cover and the length of time taken for each shot run. On the average the temperature was 0.7° F too high.

For an initial series of experiments in a new and unique facility the control of variables was generally adequate. Water temperature and centrifuge speed were under good control. The control of charge depth, water depth (which with centrifuge speed affected accelerations attained), and air pressure were in many cases inadequate. Better control of and monitoring of the air pressure while the centrifuge is rotating is highly desirable; this was the only important variable that could not be measured either at shot time or on the film record. Improvement in charge and water depth control is also desirable.

4. RESULTS AND DISCUSSION

4.1 GENERAL

In the following paragraphs each of the programs undertaken is discussed. Table 1 lists the basic data grouped according to program. Shots numbered PR 1301 to PR 1360 were fired in 1960; those numbered PR 1368 to PR 1391 in 1961.

One program fired in the 1961 tests was intended for scaling a prototype series of 10,000 pound HBX-1 charges, but upon preliminary analysis it was found that 1,000 pound charges had been scaled instead. As a result, instead of being listed as an independent program, these data are grouped with the high explosive shots in deep water to which they correspond. Many other shots of the 1961 tests were a duplication and extension of the 1960 programs.

4.2 GENERAL INFORMATION PROGRAMS

Two programs were fired in an attempt to gain some estimate of tank wall

*

Excluding two maximum variations which resulted in one case from a known tank leak and in the other case from an erroneous manometer setting.

effects in accelerated test tanks and to observe the general effects of the experimental conditions on the explosion bubble characteristics. These programs differ from the remainder in that specific prototype scaling is not involved.

4.2.1 Effect of Tank Size. During evaluation of a centrifugal acceleration system for modeling underwater explosions, several shots were fired in a small test tank at NOL (Ref. 7). The test tank was approximately 7 1/2 inches square in the plane perpendicular to the centrifuge arm axis, by 12 inches deep. The radius to the charge from the centrifuge axis was 115 inches. Because the anticipated bubble size from a 0.2 gram charge would have been too large to observe through the tank windows, a smaller charge, 0.05 grams of lead azide, was used. These small tank experiments were repeated at Sandia with the only changes being the diameter and shape of the test tank and the radius of the centrifuge. The water depth was about 0.604 feet in both cases, and the charge weight was the same.

Table 2 compares the data for the most nearly equivalent shots in the small NOL and Sandia test tanks. The total hydrostatic pressure at the charge, Z_m , was computed from Equation 5.

The general expressions used for the calculation of A_{\max} and T are:

$$A_{\max} = J \left[W/Z \right]^{1/3} \quad (9)^*$$

and

$$T = K \left[1 - \alpha A_{\max} / d \right] W^{1/3} / Z^{5/6} \quad (10)^*$$

where J and K are explosion bubble coefficients. From static vacuum tank calibrations, these coefficients are found to be functions of air pressure and charge depth, and since the differences of these variables for comparable NOL and Sandia tank shots is relatively small, the coefficients may be considered the same. The charge weights, W, are presumed the same. The coefficient α , appearing in a surface correction term for T will be the same in the two size tanks, thus this term is neglected for comparison purposes. For comparable shots, A_{\max} and T are inversely proportional to the 1/3 and 5/6 power of the total hydrostatic pressure respectively, and:

* When the subscripts are not used, the expression has general application for field and tank relationships; subscript m indicates model or tank relationships; subscript p indicates prototype or field relationships; other subscripts are described as used.

$$\frac{A'_{\max m}}{A''_{\max m}} = \left[\frac{Z''_m}{Z'_m} \right]^{1/3} \quad (11)$$

$$\frac{T'_m}{T''_m} = \left[\frac{Z''_m}{Z'_m} \right]^{5/6} \quad (12)$$

where the single primes refer to the small NOL test tank and the double primes to the Sandia tank. These equalities should be valid if no other effects are acting. If these ratios are not equal, it is presumed to be because of other effects, most probably caused by the difference in tank size and shape.

Table 3 shows the evaluation of these ratios for each set of comparisons. It is obvious that the ratios are not equal. The correction coefficients which must be appended to the ratios of $A'_{\max m}$ and T'_m to make both sides of Equations (11) and (12) equal are also shown. By subtracting this coefficient from one we get an estimate of the percentage change of the Sandia measurement of $A'_{\max m}$ and T'_m , which can be attributed to tank effects; thus $A'_{\max m}$ in the small tank is about 14.5% (average of 18 and 11%) smaller than $A''_{\max m}$ and T'_m about 14.0% (average of 12 and 16%) greater than T''_m .

The result that T'_m is larger than would be expected is consistent with previous work. A tank correction term evaluated from static vacuum tank and field data (Ref. 16) is of the form:

$$\left[1 + .216 A_{\max m} / R_m + .783 (A_{\max m} / R_m)^2 \right]$$

where R_m is the radius of a cylindrical test tank. This term is appended to Equation (10) for T'_m . As R_m is reduced, all other parameters remaining constant, T'_m increases.

The result shows that $A'_{\max m}$ is smaller in the small tank; however, in previous static vacuum tank work it was assumed that there is no tank size correction to $A_{\max m}$. The results here indicate that there is such an effect; its magnitude is about equivalent to that for T'_m and its variation is in the opposite direction.

It is apparent that for a quantitative understanding of tank effects on bubble characteristics, additional studies must be inaugurated in both static and accelerated test tanks.

CONFIDENTIAL
NOLTR 63-125

TABLE 2 DATA FROM CORRESPONDING SHOTS IN TWO TANK SIZES

	NOL TANK	SANDIA TANK
Shot Number	5	PR 1337
d_m (ft)	.256	.295
a_m (g)	20.9	20.7
P_m (ft of H ₂ O)	34	27.5
Z_m (ft of H ₂ O)	39.3	33.6
$A_{max\ m}$ (ft)	.090	.112
T_m (ms)	5.9	5.94
Shot Number	4	PR 1338
d_m	.267	.281
a_m	59.5	60.9
P_m	34	27.5
Z_m	49.9	44.5
$A_{max\ m}$.090	.104
T_m	5.3	4.91

TABLE 3 EVALUATION OF TANK EFFECTS

	$\frac{A'_{max\ m}}{A''_{max\ m}}$	$\left[\frac{Z''_m}{Z'_m} \right]^{1/3}$	Required Correction Coefficient	$\frac{T'_m}{T''_m}$	$\left[\frac{Z''_m}{Z'_m} \right]^{5/6}$	Required Correction Coefficient
1st Set	.804	.949	1.18	.993	.878	.88
2nd Set	.865	.963	1.11	1.079	.909	.84

4.2.2 Effects of d_m , a_m , and P_m on the Explosion Bubble. The primary variables which are controlled in accelerated tank tests are the charge depth, d_m ; acceleration, a_m ; and air pressure, P_m . As discussed above, charge weight and water temperature were held constant.

Two levels of each controlled variable were arbitrarily chosen and an experiment planned to produce data allowing four paired comparisons of the effects of each variable. Table 1 shows the planned (nominal) values and actual measured values of each parameter. These shots were fired in a water depth of about 34 inches to reduce bottom influence on the bubble as much as possible. The results of one of the shots, PR 1305, was discarded because the tank leaked air. A repeat shot was fired.

The data are plotted in Figure 18. Also shown in these figures are prediction curves (based on Equations (13) and (9) for A_{\max} and (14) and (10) for T). When the controlled variables are changed to effect an increased hydrostatic pressure, A_{\max} and T become smaller. In addition, the data fall reasonably close to the predictions.

4.3 SPECIFIC SCALING PROGRAMS

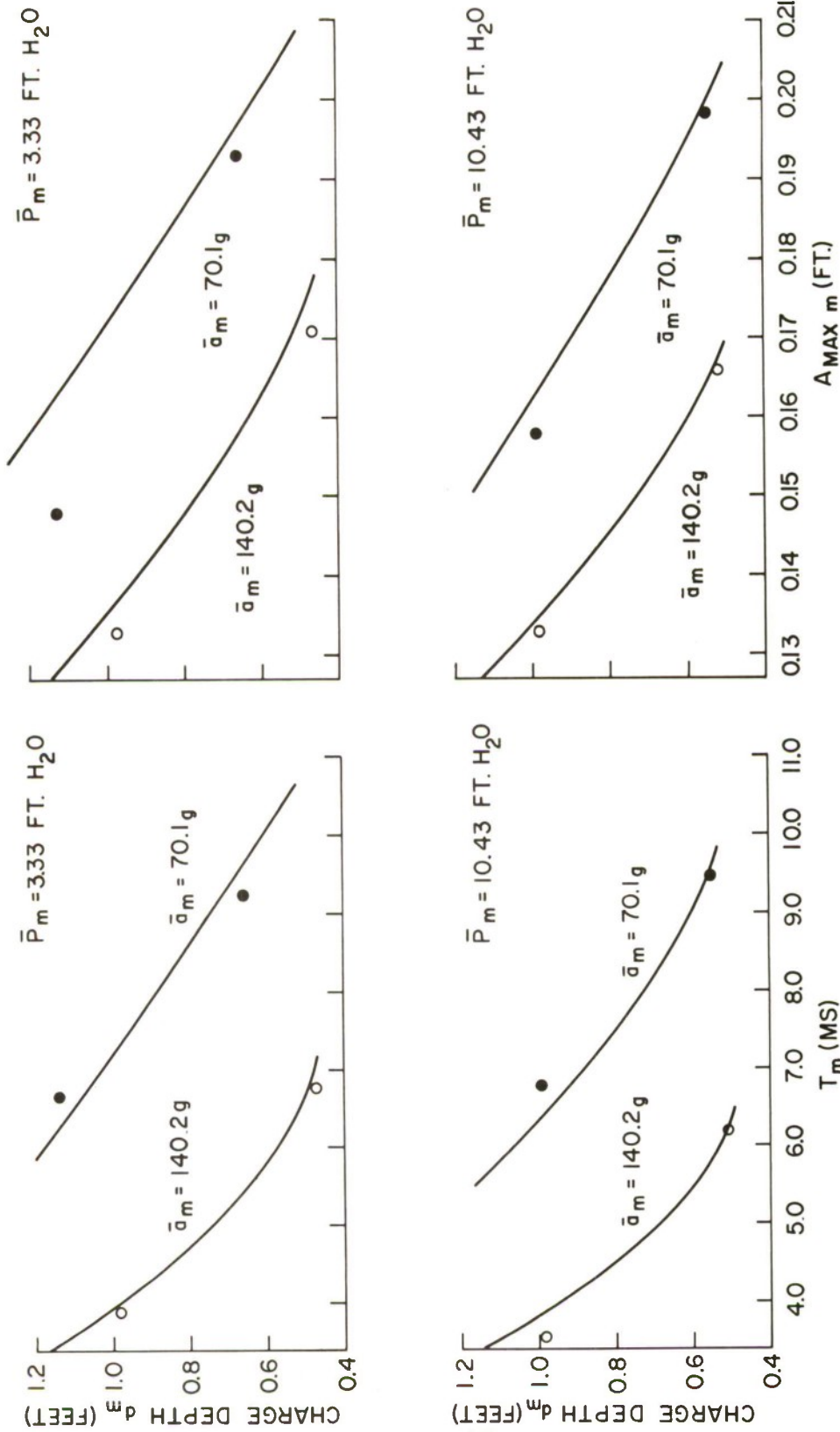
The five programs described in this section were attempts at explosion scaling or modeling of certain characteristics of prototype explosions. In most instances it is the explosion bubble characteristics which are of primary importance; thus to scale a prototype, the basic requirement is to achieve a specific $A_{\max m}$ and T_m and sometimes $A_{\min m}$ (minimum bubble radius). In order to do this it is necessary to find the proper set of variables, d_m , a_m , and P_m . These must be predicted from known data.

Since these tests represent the initial extensive explosion experiments in an accelerated test tank, direct empirical data was not available for predictions. Relationships were therefore developed from a combination of static vacuum tank "calibration" data and small scale field data (Ref. 16) for the bubble coefficients J_m and K_m which could be used in Equations (9) and (10) for predictions of $A_{\max m}$ and T_m . These empirical relationships were:

$$J_m = \left[.17 d_m^2 - .65 d_m + .46 \right] \frac{\log \left[\frac{P_m}{2} \right]}{\log 17} + .053 d_m^2 - .38 d_m + 9.7 \quad (13)$$

and

$$K_m = K_\infty \left(1 - .2 \frac{A_{\max m}}{d_m} \right) \left[.783 \left(\frac{A_{\max m}}{R_m} \right)^2 + .216 \frac{A_{\max m}}{R_m} + 1 \right] \quad (14)$$



NOTE: LINES SHOWN ARE PREDICTIONS BASED ON EQUATIONS 13 AND 9 FOR A_{MAX} AND 14 AND 10 FOR T . POINTS ARE MEASURED DATA.

FIG. 18 EFFECTS OF d_m , P_m AND a_m ON $A_{MAX\ m}$ AND T_m

where:

K_{∞} is a constant for a particular kind of explosive (3.23 for lead azide).

R_m is the radius of the test tank, and

the other terms are as previously indicated.

To aid in evaluating the accuracy of predictions, two scaling indexes are defined as:

$$I_A = \frac{A_{\max m} \text{ measured}}{A_{\max m} \text{ calculated}} \quad (14)$$

$$I_T = \frac{T_m \text{ measured}}{T_m \text{ calculated}} \quad (16)$$

The measured values are obtained as indicated in Sections 3.2 and 3.3; the calculated values as indicated above. These indexes are listed for most shots in Table 1. A value of unity indicates perfect agreement of prediction with measurement. Of the 76 tabulated shots, 54 were fired under conditions where the equations could be legitimately applied, i.e., the water was deep (nominally 34 inches) and the shots were sufficiently deep that there were measurable bubble characteristics. (Indexes listed in Table 1 for bottom shots are defined somewhat differently; see Section 4.3.2. They are not included in the analysis of this section). For these 54 shots, the average I_a was 0.990 with a standard deviation of $\pm .039$ while I_t was $0.994 \pm .045$.

Since the indexes were very near unity the standard deviation may be expressed as a percentage, thus 68% of the $A_{\max m}$'s were within about $\pm 4\%$ of their expected values and 68% of the T_m 's within about $\pm 4.5\%$.

Since the calculated $A_{\max m}$'s and T_m 's of Equations 15 and 16 are based on measured tank variables, the indexes indicate the reliability of the relationships used for bubble scaling (Equations 13 and 14) in the high gravity tank. They do not reflect the degree of experimental control (Section 3.9) which was often inadequate; nor do they reflect errors of interpolation (and sometimes extrapolation) from charts used to determine the nominal levels of d_m , a_m , and P_m .

Scaling of specific prototypes was often poor because of inadequate experimental control and inaccurate determination of the tank variables required.

4.3.1 Comparison of Different Forms of Bubble Scaling. This program was an attempt to scale the explosion of 250 pounds of HBX-1 at a 50 ft. depth

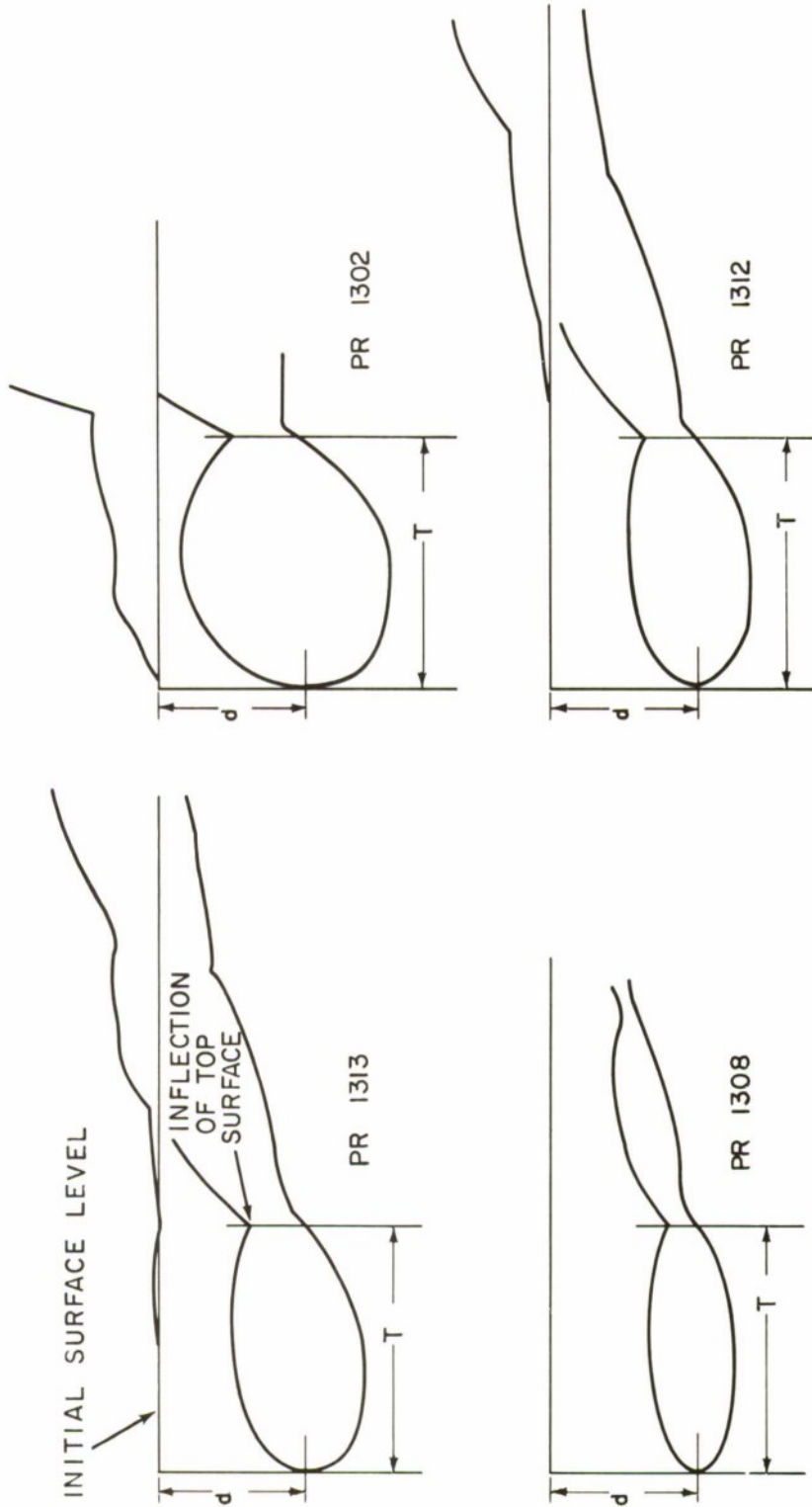


FIG. 19 DISPLACEMENT HISTORIES FOR SHOTS COMPARING DIFFERENT KINDS OF BUBBLE SCALING

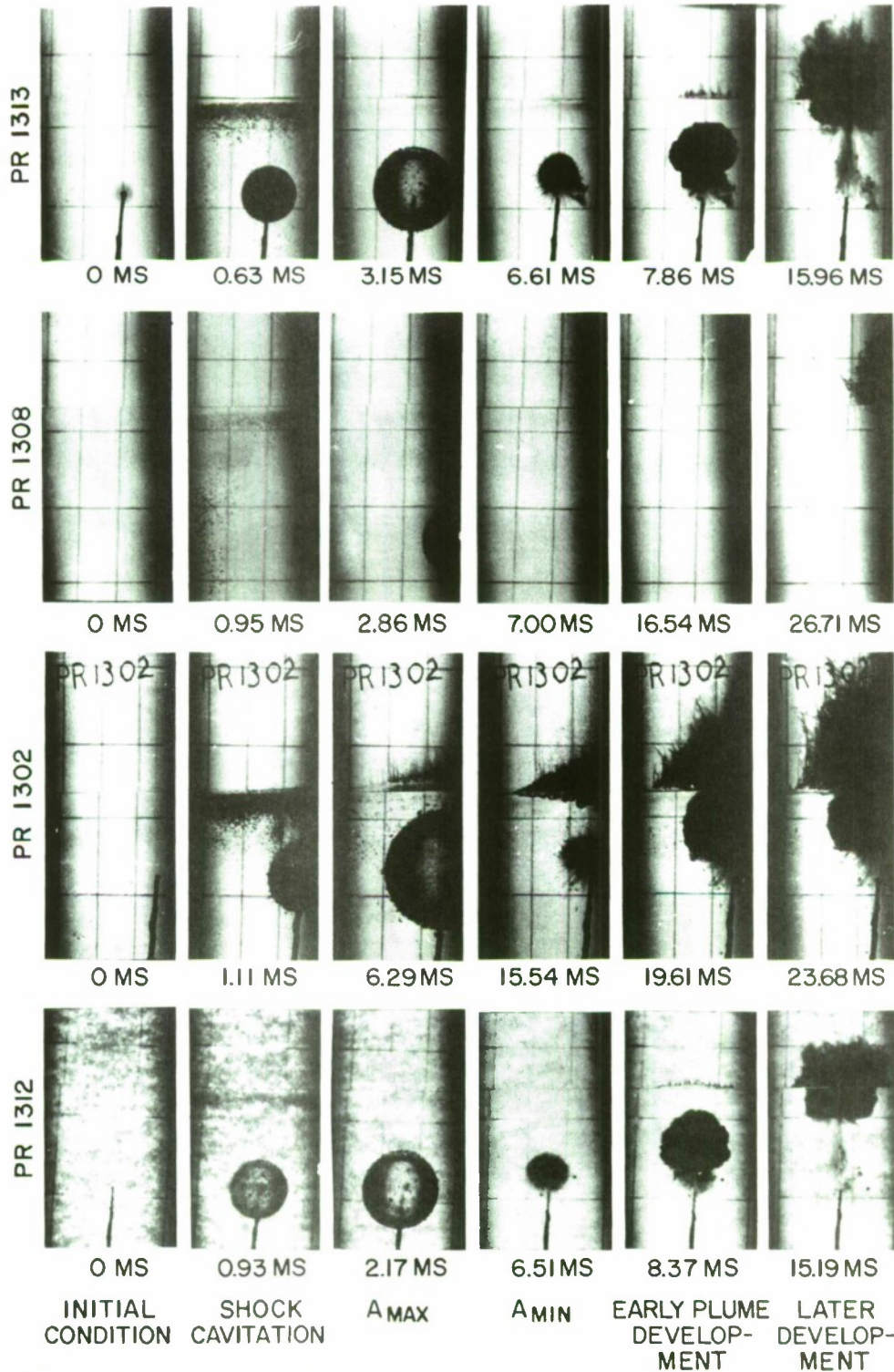


FIG.20 SELECTED FRAMES FROM FILMS IN THE COMPARISON OF VARIOUS KINDS OF BUBBLE SCALING

CONFIDENTIAL
 NOLTR 63-125

TABLE 4 PROTOTYPE CONDITIONS DETERMINED BY VARIOUS KINDS OF BUBBLE SCALING

Shot No.	Scaling	d_p (ft)	W_p (lb HBX-1)	T_p (sec)
FR 1302	3 C	-	-	-
	S 3 C	-	-	-
	2 C	30.4	266	.866
	S 2 C	30	214	.817
FR 1308	3 C	43.6	62.0	.504
	S 3 C	-	-	-
	2 C	44.1	64.1	.507
	S 2 C	49	78.7	.519
FR 1312	3 C	-	-	-
	S 3 C	-	-	-
	2 C	49.7	245	.732
	S 2 C	49.6	229	.718
FR 1313	3 C	-	-	-
	S 3 C	-	-	-
	2 C	47.5	250	.749
	S 2 C	48.6	250	.742
FR 1314	3 C	-	-	-
	S 3 C	-	-	-
	2 C	57.8	1160	1.10
	S 2 C	48.4	441	.882

using five variations of bubble scaling. This prototype condition was selected because it was used by the Washington Technological Associates (WTA) in their accelerated test tank feasibility studies (Ref. 14). The conditions determined by WTA for scaling this prototype are the nominal levels shown for Shot PR 1312 in Table 1. Three and two criteria bubble scaling, as described in reference (16), were used to calculate the conditions for shots PR 1313 and PR 1308 respectively. Simplified three and two criteria bubble scaling (see Appendix A) were used for shots PR 1314 and PR 1302, respectively.

In the originally planned analysis, the five shots scaling the same prototype by these five kinds of bubble scaling were to be compared. If all these scaling methods were equally valid, all the explosion characteristics would be similar; if not, as was expected, the differences between the explosions would have been of interest. This type of analysis could not be undertaken since the calculated conditions were not attained so all the shots did not scale the given prototype. In addition to errors in scaling mentioned in 4.3, on two of these shots, PR 1308 and PR 1314, there were gross errors committed in the computations of the tank parameters required (nominal levels). Also, for shot PR 1314, measurements of d_m , $A_{max m}$, and T_m represent only reasonable approximations since the charge support rod was bent away from the tank center so that less than 1/8 of the bubble was visible at its maximum (see Sections 2.14 and 2.15).

Although comparisons for the same scaled prototype could not be made as intended, it is possible to determine, for each shot, the prototypes scaled by four methods of bubble scaling (see Table 4). Since three criteria (3C) and simplified three criteria (S 3C) scaling are very restrictive, quite often no prototype solution was found. Two criteria (2C) and simplified two criteria (S 2C) scaling are less restrictive and a prototype solution may be evaluated for most model shots. Figure 19 shows the vertical bubble and surface displacement histories for four of these shots (PR 1314 excluded).* The scales are in prototype units which may be evaluated from the prototype depths and periods in Table 4. Figure 20 shows some selected frames of these shots.

4.3.2 Scaling of High Explosives. For this program, the prototypes considered are 1100-pound charges of HBX-1 fired over a range of charge depths from 85 feet to 140 feet. Two extensive field programs have been conducted by NOL with this size charge and range of depths. These were the series fired in June, July, and August of 1956, off Charleston, South Carolina and the series fired in June and July 1957 on Chesapeake Bay. Surface development was thoroughly documented by high speed photography. In addition, underwater pressure instrumentation was extensively employed on several shots.

*

In all vertical displacement histories contained in this report, the horizontal reference line is at the level of the water surface as observed at the front window of the tank. The water surface over the charge is slightly below this line. See Section 3.5

CONFIDENTIAL
NOLTR 63-125

TABLE 5 PROTOTYPE CONDITIONS FOR HIGH EXPLOSIVE SHOTS IN DEEP WATER

Shot No.	Scaling	d _p (ft)	W _p (lb HBX-1)	T _p (sec)
PR 1322	3 C	-	-	-
	S 3 C	81.7	934	.885
	2 C	111	2840	1.07
	S 2 C	83	986	.892
PR 1323	3 C	78.4	941	.904
	S 3 C	78.4	934	.902
	2 C	72.1	718	.866
	S 2 C	79.5	978	.909
PR 1324	3 C	-	-	-
	S 3 C	81.4	929	.885
	2 C	70.2	576	.820
	S 2 C	83.5	1010	.896
PR 1325	3 C	-	-	-
	S 3 C	97.2	937	.809
	2 C	172.0	8250	1.15
	S 2 C	97	929	.808
PR 1326	3 C	-	-	-
	S 3 C	103	949	.785
	2 C	134	2640	.932
	S 2 C	101	885	.776
PR 1327	3 C	101	940	.794
	S 3 C	101	949	.796
	2 C	105	1090	.812
	S 2 C	98.7	886	.788
PR 1328	3 C	-	-	-
	S 3 C	105	957	.782
	2 C	148	3800	.986
	S 2 C	102	864	.770
PR 1329	3 C	-	-	-
	S 3 C	118	959	.730
	2 C	178	4840	.949
	S 2 C	112	810	.712

CONFIDENTIAL
NOLTR 63-125

TABLE 5 PROTOTYPE CONDITIONS FOR HIGH EXPLOSIVE SHOTS IN DEEP WATER (Cont'd)

Shot No.	Scaling	d _p (ft)	W _p (lb HBX-1)	T _p (sec)
PR 1331	3 C	119	975	.732
	S 3 C	119	953	.726
	2 C	120	1030	.737
	S 2 C	114	823	.711
PR 1332	3 C	127	1070	.723
	S 3 C	127	957	.697
	2 C	143	1610	.767
	S 2 C	120	784	.677
PR 1333	3 C	129	976	.695
	S 3 C	129	960	.691
	2 C	150	1620	.747
	S 2 C	124	830	.677
PR 1334	3 C	-	-	-
	S 3 C	130	967	.691
	2 C	85.1	212	.543
	S 2 C	122	772	.668
PR 1360	3 C	77	1030	.938
	S 3 C	77	910	.903
	2 C	91.7	1820	1.02
	S 2 C	79.3	1000	.917
PR 1373	3 C	-	-	-
	S 3 C	-	-	-
	2 C	-	-	-
	S 2 C	306	20,500	1.05
PR 1377	3 C	-	-	-
	S 3 C	-	-	-
	2 C	85.1	60.5	.363
	S 2 C	105	131.	.413
PR 1380	3 C	-	-	-
	S 3 C	94.7	193	.496
	2 C	182	2040	.710
	S 2 C	97.9	215	.505
PR 1382	3 C	-	-	-
	S 3 C	65.2	369	.739
	2 C	78.5	851	.876
	S 2 C	70	462	.767

CONFIDENTIAL
NOLTR 63-125

TABLE 5 PROTOTYPE CONDITIONS FOR HIGH EXPLOSIVE SHOTS IN DEEP WATER (Cont'd)

Shot No.	Scaling	d_p (ft)	W_p (lb HBX-1)	T_p (sec)
FR 1386	3 C	-	-	-
	S 3 C	-	-	-
	2 C	71.8	144	.525
	S 2 C	95.1	356	.603
FR 1387	3 C	-	-	-
	S 3 C	102	378	.592
	2 C	118	827	.677
	S 2 C	102	380	.592
FR 1388	3 C	-	-	-
	S 3 C	-	-	-
	2 C	87.4	218	.540
	S 2 C	85.6	187	.520
FR 1389	3 C	57.3	463	.838
	S 3 C	-	-	-
	2 C	56.9	453	.835
	S 2 C	63.1	513	.830

The available pressure-time records were interpreted to give information about the bubble periods and migration. These results were compared with theoretical relationships for successive bubble periods and migration (Ref. 11) which had empirically evaluated coefficients. The author states that these equations predict "with fair accuracy most HE data available" (which includes the two series mentioned above). Also included in reference (11) is an equation for predicting successive maximum bubble radii; however, this characteristic cannot be checked against the prototype. With these relationships to describe the bubble phenomena and high speed photography to document surface development, there is a reasonably thorough description of the prototype explosion.

Since the prototype shots were fired both in deep water and on the bottom, the tank program included models of both conditions. Three criteria bubble scaling (Ref. 16) was employed to determine experimental conditions. The discussion and analysis of this program is divided into two parts: the deep water shots and the bottom shots.

Because of errors in the interpolation of experimental conditions and experimental control difficulties, the prototypes attained were not those intended. Table 5 lists the prototype conditions attained for the deep water shots using the four kinds of bubble scaling as done in Section 4.3.1. Figures 21, 22, and 23 show the vertical displacement histories. The scales of displacement and of time may be obtained from d_p and T_p in Table 5, and depend on the kind of bubble scaling considered.

The main interest in this program is the comparison with three criteria scaling. There were five model shots which had a three criteria prototype solution in the range of prototype data. For these shots, the depth to the center of the bubble at its maximum size, the successive $A_{\max p}$'s and successive T_p 's (as determined from the relationships in reference (11) and from scaled measurements of the model shots) are listed in Table 6. The scaled measurements were obtained from the displacement histories; the periods from inflections of the bubble top; the bubble maxima from the difference between the bubble top and bottom midway between bubble pulses. This one dimensional measurement of successive A_{\max} 's (in contrast to the first A_{\max}) is a crude approximation necessitated by the irregularity and turbulence usually associated with the bubble after its first oscillation.

By definition, A_1 and T_1 (A_{\max} and T_p for the first bubble period) are identical for the prototype and the 3C scaled case in Table 6. In the prediction of reference (11), it is assumed that there is no migration up to the time of the first bubble maximum; thus, the bubble depth at the first maximum, D_1 , is the same as the charge depth.

Considering first a comparison of the migration characteristics (D 's in Table 6 indicates the bubble depth at successive A_{\max} 's) it is noted that the

TABLE 6 COMPARISON OF SCALED THREE CRITERIA EXPLOSION CHARACTERISTICS WITH PROTOTYPE PREDICTIONS OF REF. 11

Shot No.	PR 1323		PR 1327		PR 1331		PR 1332		PR 1333		Average Difference	Standard Deviation of Difference
	3C	Ref 11										
W_p (1b HBX-1)	941	940	940	975	976	976	976	976	976	976	976	976
d_p (ft)	78.4	101	101	119	127	127	127	127	127	129	129	129
D_1 (ft)	74.5	78.4	98.5	101	114.5	119	125.2	127	126.5	129	-3.04	1.114*
A_1 (ft)	29.0	29.0	27.3	27.3	26.5	26.5	26.9	26.9	25.9	25.9	0	-
T_1 (sec)	.904	.904	.794	.794	.732	.732	.723	.723	.695	.695	0	-
D_2	35.8	32.3	59.4	61.1	80.4	82.5	93.0	90.5	92.2	94.7	-0.06	2.83
A_2	26.3	30.0	23.1	27.1	17.9	25.6	20.0	26.9	20.0	24.6	-5.38	1.81*
T_2	1.070	1.070	.908	.905	.730	.794	.676	.774	.683	.732	-.052	.042
D_3	-11.4	-11.4	17.5	17.5	44.7	44.2	58.0	52.8	53.5	59.8	-0.20	5.77
A_3					24.3	21.7	25.0	24.5	26.0	21.3	+2.60	2.1
T_3					.734	.789	.767	.766	.734	.727	-.016	.034
D_4					11.4	11.4	19.6	19.6	28.3	28.3		

* Statistically significant at 5% level.

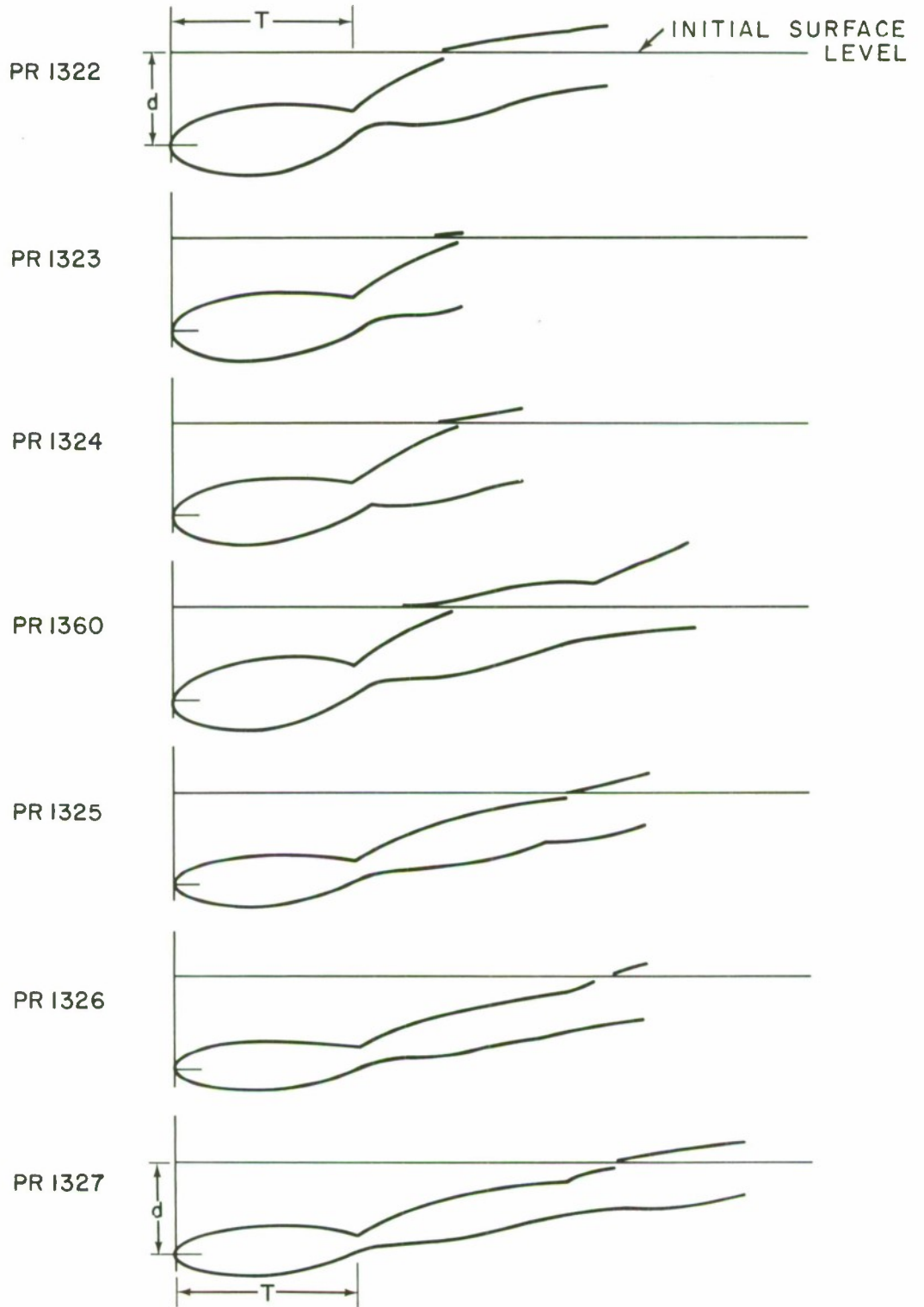


FIG.21 DISPLACEMENT HISTORIES OF DEEP WATER SHOTS

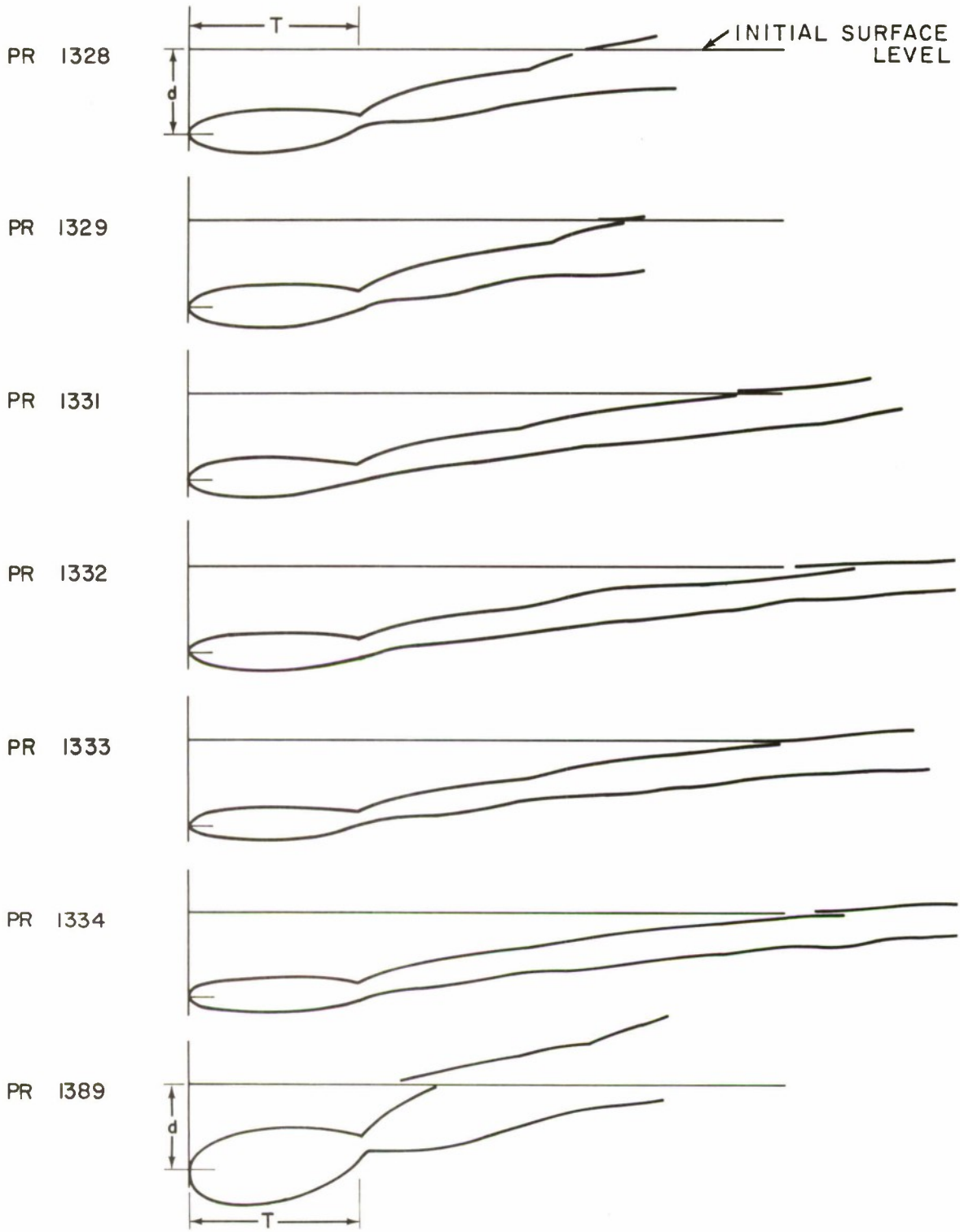


FIG.22 DISPLACEMENT HISTORIES OF DEEP WATER SHOTS

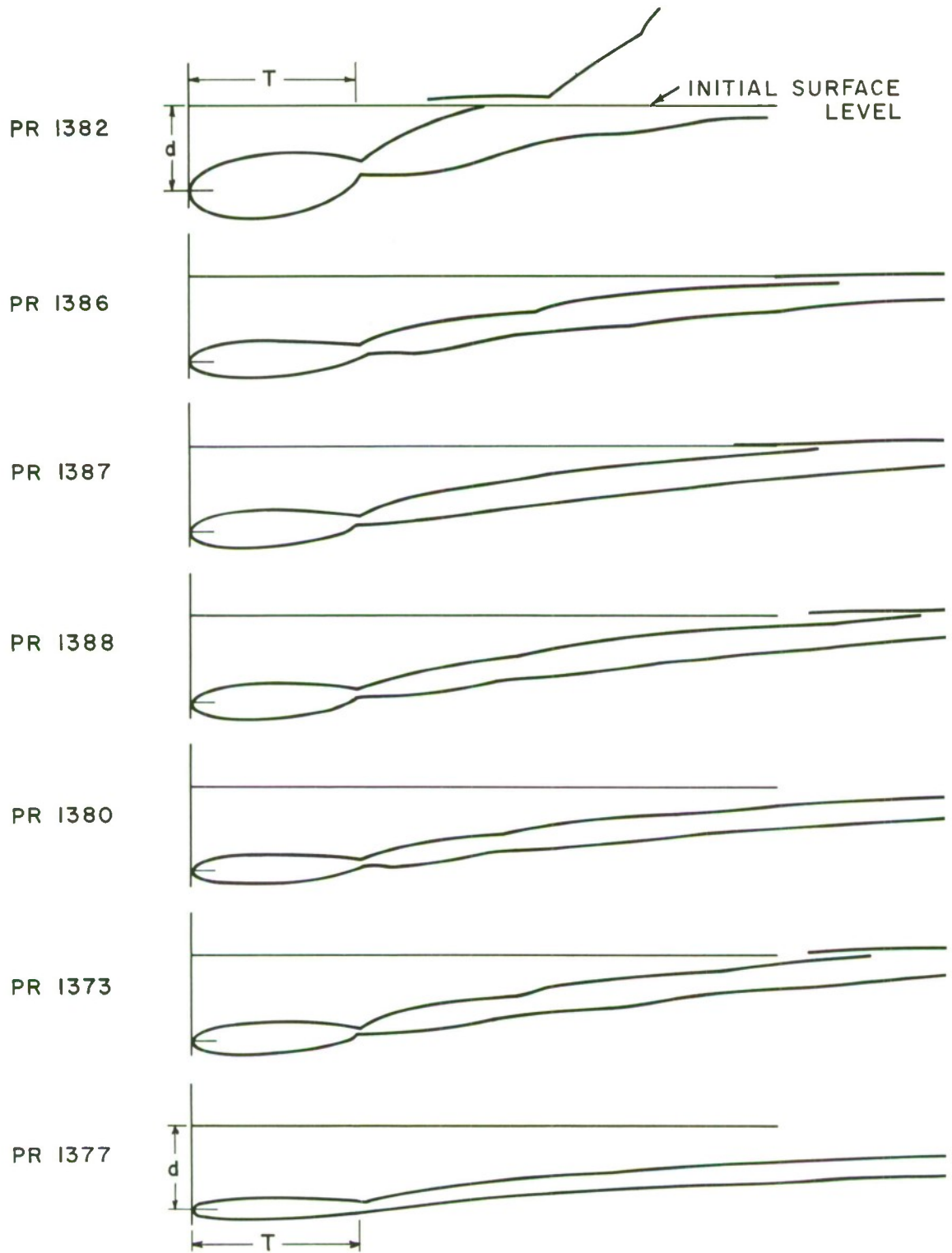


FIG.23 DISPLACEMENT HISTORIES OF DEEP WATER SHOTS

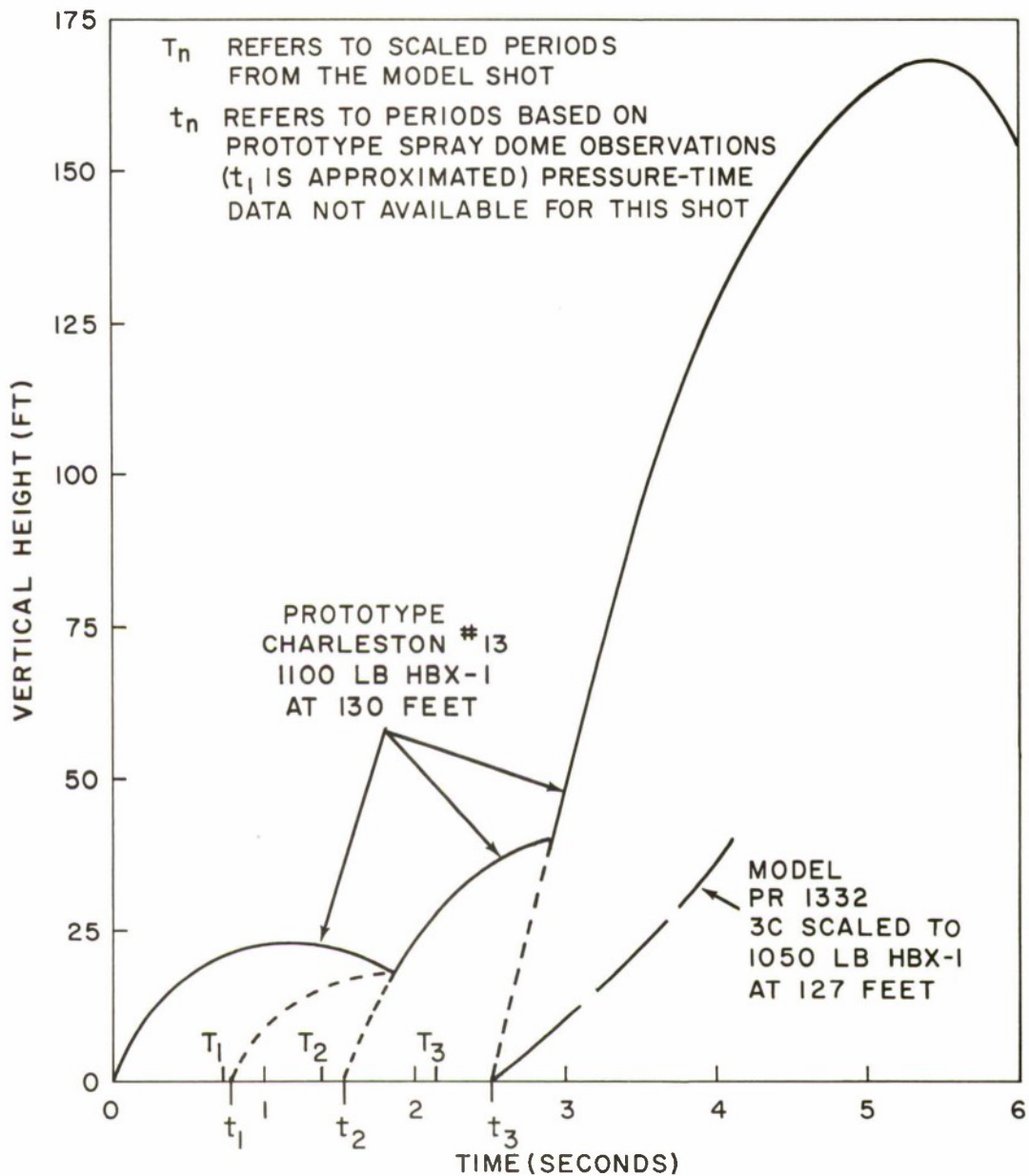


FIG.24 COMPARISON OF SURFACE DEVELOPMENT OF A THREE CRITERIA SCALED MODEL WITH ITS PROTOTYPE FOR A DEEP WATER SHOT

average difference between the scaled model and prototype predictions is small. The largest difference occurs at the first maximum. This difference may be attributed to the assumption for prototype predictions, that no migration occurs during the first part of the initial bubble oscillation. Statistically this difference of 3.0 ± 1.1 feet is significant, i. e., there is a clear disagreement between model and prototype predictions. The scaled and prototype positions of the bubble during the second and third bubble maxima are in excellent agreement, and the differences are statistically insignificant.

The scaled bubble maxima for the second oscillation are statistically different from the prototype predictions; the third maxima are not significantly different. The differences may be attributed to three causes. First, as was previously mentioned, measurements of A_{\max} 's in the model were crudely obtained. Secondly, the prototype predictions may be grossly in error. (Independent measurements of A_{\max} 's are rarely obtained in the field thus the prototypes of successive A_{\max} 's have not been empirically confirmed as have predictions of successive periods or bubble migration from pressure-time records.) Third, since different explosives are used in model and prototype, differences in behavior through several oscillations may be the result of differences in explosion gas characteristics.

The differences of the second period (52 milliseconds or about 6.7% on the prototype scale) and the third period (16 milliseconds or about 1.5%) are not statistically significant. In both cases, the scaled model period is less than the prototype predictions of reference 11. The time or period differences are cumulative, thus the third bubble minimum in the scaled model shot will occur, on the average, 68 milliseconds before that of its prototype. This difference is confirmed by the comparison of surface characteristics discussed below.

Of the five three-criteria-scaled prototypes shown in Table 6, only one is at a condition closely comparable with one of the prototypes; PR 1332 scales 1070 pounds of HBX-1 at 127 feet and Charleston shot number 13 was 1100 pounds of HBX-1 at 130 feet. For purposes of direct comparison this Charleston shot is considered the prototype of model shot PR 1332.

Figure 24 compares their vertical surface displacement histories. The height scale is taken from the scaled depth of the charge and the time scale from the scaled first period.

Surface phenomena are generally attributed to two factors; shock wave interaction with the water surface giving rise to spray dome development (consisting of multitudinous jets and drops of water in field shots) and the water displaced by the oscillating bubble giving rise to a mound of water or plumes (which contain larger masses of water) over the explosion.

A spray dome is initiated at the surface at each pressure wave impingement, i.e., by the shock wave and at each bubble minimum if the bubble pulse is of sufficient strength. The spray dome in small model tank shots is very rudimentary:

it consists of a few spikes of water which are often difficult to identify in photographic records. Fluid viscosity, surface tension and possibly other characteristics of the medium which are not considered in the scaling applied here, are probably the cause of this. As a result the water beneath the spray is readily observed in model shots.

On the other hand, the water mound is largely masked by the spray dome in prototype observations. Comparing observations of surface development of the model shot and its prototype as in Figure 24, some notion of the structure of surface development can be obtained. Thus, during the first three oscillations (as deduced from the model explosion) or two and a half seconds, the visible surface development is exclusively spray domes. Later when the bubble has migrated to a point near the surface, the surface development consists of a large mound of water capped with the large jets of water and spray which collectively are often referred to as plumes. Beneath these plumes rises a mound of water as indicated in the surface development late in the model explosion.

This analysis of surface development structure presumes the applicability of the scaling procedures used. In the preceding paragraphs it was shown that differences between predicted prototype and scaled model bubble characteristics were statistically insignificant for most points of comparison.

The prototype surface development history of Figure 24 provides one more comparison for the periods. If the spray dome growth curves are extrapolated back to the surface of origin the time indicated should approximately correspond to the bubble periods. Thus the start of the initial spray dome corresponds to detonation or zero time. The first bubble pulse apparently gives rise to a spray dome which does not rise above the first. Its path is approximated by the first dashed line. The second bubble pulse occurs at about 1.52 seconds, as indicated by the second dashed line. The third bubble pulse, as indicated by the third dashed extrapolated line, occurs at about 2.52 seconds. The periods measured on the scaled model are indicated along the time scale by T_1 , T_2 , and T_3 . This comparison shows the difference in model scaled periods from their prototypes based on surface observations.

Model shots on a bottom are considered next. The purpose for conducting shots on the bottom under the same tank conditions as deep water shots was to evaluate the effect of the bottom in the same range as prototype bottom shots for comparison purposes.

The indexes, I_A and I_T (Eq. 15 and 16) are the ratios of the measured bubble characteristic (of bottom shots in this case) to the predicted characteristic of an identical shot in free water. The values obtained are

$$I_A = 1.12$$

$$I_T = 1.14$$

These indexes may be used for prediction of bottom shot bubble characteristics. Ignoring the presence of a bottom, A_{\max} and T for free water may be estimated from Equations 9 and 10. The characteristics for a bottom shot may then be estimated from:

$$A_{\max} \text{ for a bottom explosion} = 1.12 A_{\max} \text{ predicted for a free water explosion}$$

$$T \text{ for a bottom explosion} = 1.14 T \text{ predicted for a free water explosion}$$

The denominators of these indexes contain predicted values of the free water explosion characteristics. Though these predictions were shown to be fairly accurate on the average, a better index may be defined by the ratio of the measured bottom shot bubble characteristic to the free water shot characteristic under the same firing conditions. Since the program of this section contains shots fired at nearly identical conditions with and without a bottom (the nominal 190 g shots listed in Table 1) improved bottom indexes may be defined by:

$$B_A = \frac{A_{\max m} \text{ (measured, bottom shots)}}{A_{\max m} \text{ (measured, deep water shots)}} = 1.147 \quad (17)$$

$$B_T = \frac{T_m \text{ (measured, bottom shots)}}{T_m \text{ (measured, deep water shots)}} = 1.165 \quad (18)$$

The index B_T determined from model shots (1.165) compares well with that obtained in comparable prototype shots (1.152).

Table 7 lists the prototype conditions which were calculated using the four kinds of bubble scaling. For three and two criteria scaling, measured $A_{\max m}$ and T_m were converted to the deep water equivalent by Equations (17) and (18), since these two scaling methods are applicable only for the deep water case. Simplified three and two criteria scaling do not require a measured $A_{\max m}$ or T_m and therefore did not require this conversion. Figures 25 and 26 show the displacement histories of these shots. The scales may be evaluated from the values of d_p and T_p of Table 7, depending on the type of bubble scaling considered.

Three of these bottom shots had three criteria prototype solutions and one of these was for conditions similar to an actual prototype shot; PR 1345 scaled 1040 pounds of HBX-1 at 80 feet and shot number 21 at Charleston was 1100 pounds of HBX-1 at 80 feet. The surface developments of these shots are

CONFIDENTIAL
 NOLTR 63-125

TABLE 7 CALCULATED PROTOTYPE CONDITIONS FOR HIGH EXPLOSIVE SHOTS FIRED ON A BOTTOM

Shot No.	Scaling	d _p (ft)	W _p (lb HBX-1)	T _p (sec)
PR 1342	3 C	-	-	-
	S 3 C	82.8	948	.882
	2 C	107	2680	1.07
	S 2 C	82.9	952	.883
PR 1344	3 C	-	-	-
	S 3 C	67.1	925	.967
	2 C	58.7	637	.914
	S 2 C	70.3	1070	.990
PR 1345	3 C	80	1040	.922
	S 3 C	80	942	.896
	2 C	86.4	1330	.959
	S 2 C	80.9	977	.901
PR 1346	3 C	-	-	-
	S 3 C	92.8	952	.833
	2 C	73.5	452	.744
	S 2 C	91.7	915	.828
PR 1347	3 C	-	-	-
	S 3 C	98.2	952	.808
	2 C	78.1	457	.724
	S 2 C	97	912	.803
PR 1348	3 C	-	-	-
	S 3 C	96.2	954	.818
	2 C	116.	2160	.951
	S 2 C	94.6	900	.811
PR 1349	3 C	-	-	-
	S 3 C	109	960	.767
	2 C	127	1770	.848
	S 2 C	105	849	.753
PR 1350	3 C	114	973	.748
	S 3 C	114	962	.746
	2 C	101	644	.704
	S 2 C	109	828	.729

CONFIDENTIAL
NOLTR 63-125

TABLE 7 CALCULATED PROTOTYPE CONDITIONS FOR HIGH EXPLOSIVE SHOTS FIRED ON A BOTTOM (Cont'd)

Shot No.	Scaling	d_p (ft)	W_p (lb HBX-1)	T_p (sec)
PR 1351	3 C	125	918	.697
	S 3 C	125	965	.708
	2 C	109	575	.651
	S 2 C	118	790	.688
PR 1352	3 C	-	-	-
	S 3 C	107	956	.773
	2 C	390	109,000	1.50
	S 2 C	104	876	.763
PR 1353	3 C	-	-	-
	S 3 C	108	959	.768
	2 C	147	2990	.917
	S 2 C	104	850	.754
PR 1358	3 C	-	-	-
	S 3 C	76.3	918	.909
	2 C	109	3500	1.14
	S 2 C	82.0	1160	.943

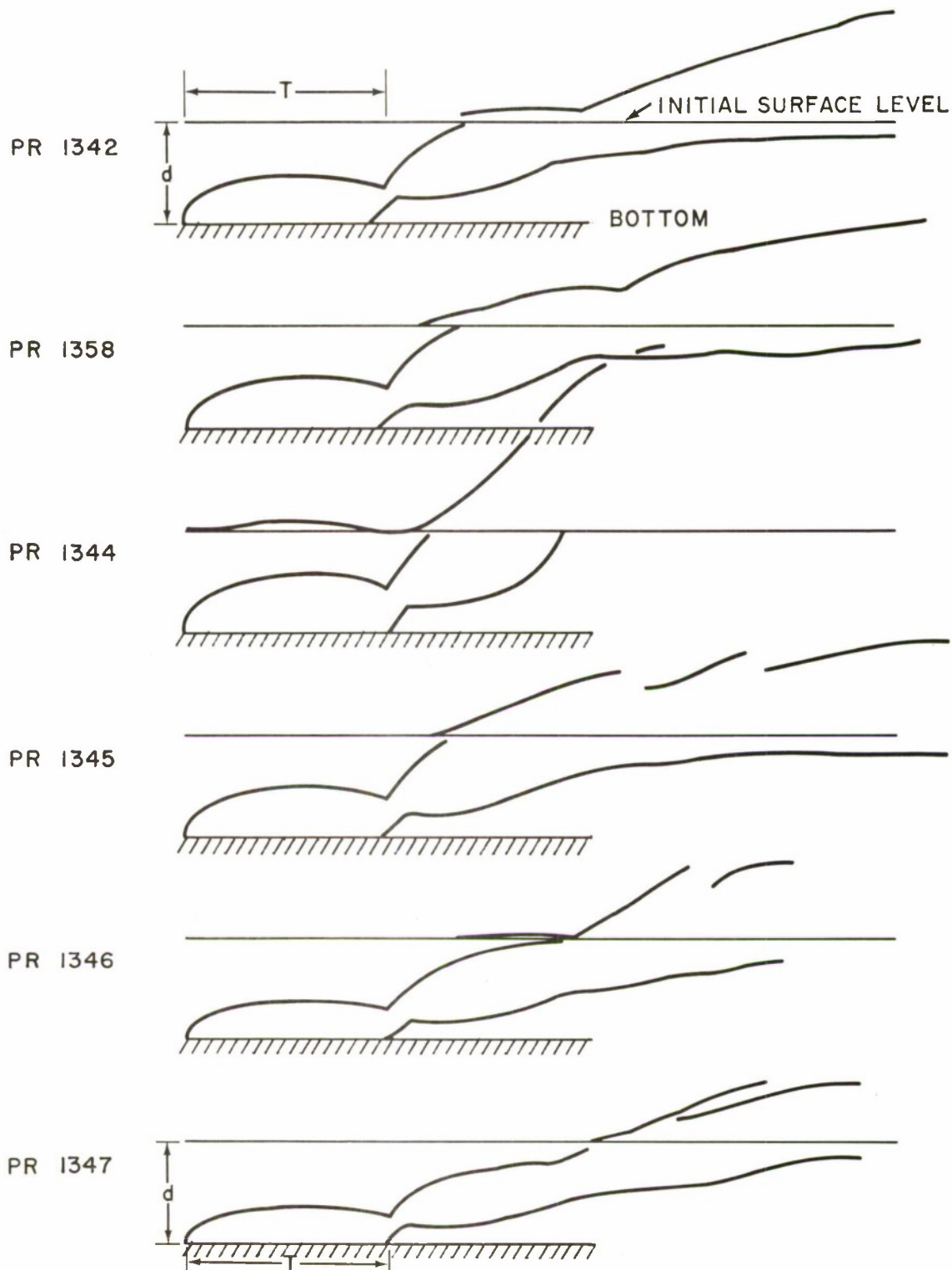


FIG.25 DISPLACEMENT HISTORIES OF BOTTOM SHOTS

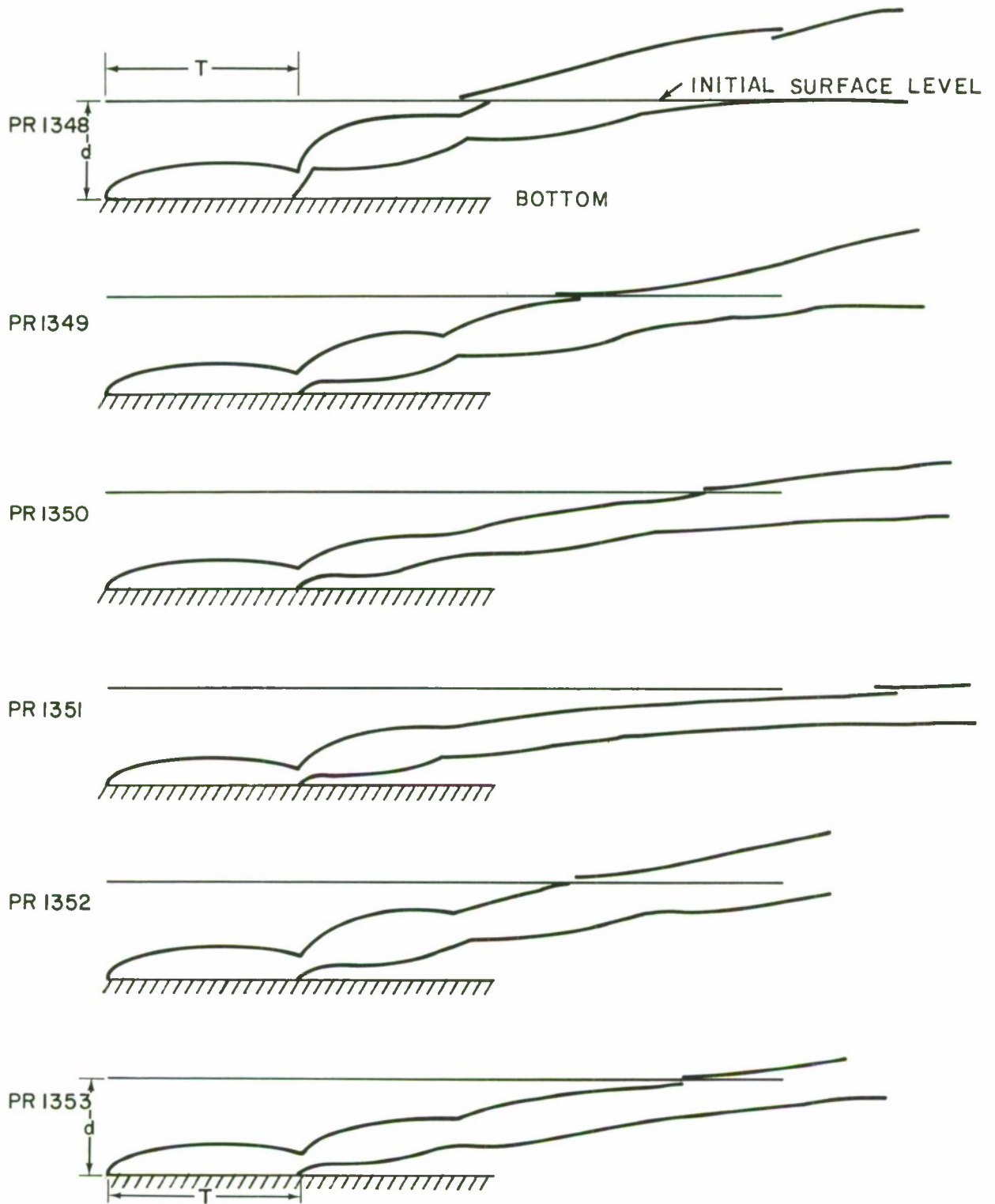


FIG. 26 DISPLACEMENT HISTORIES OF BOTTOM SHOTS

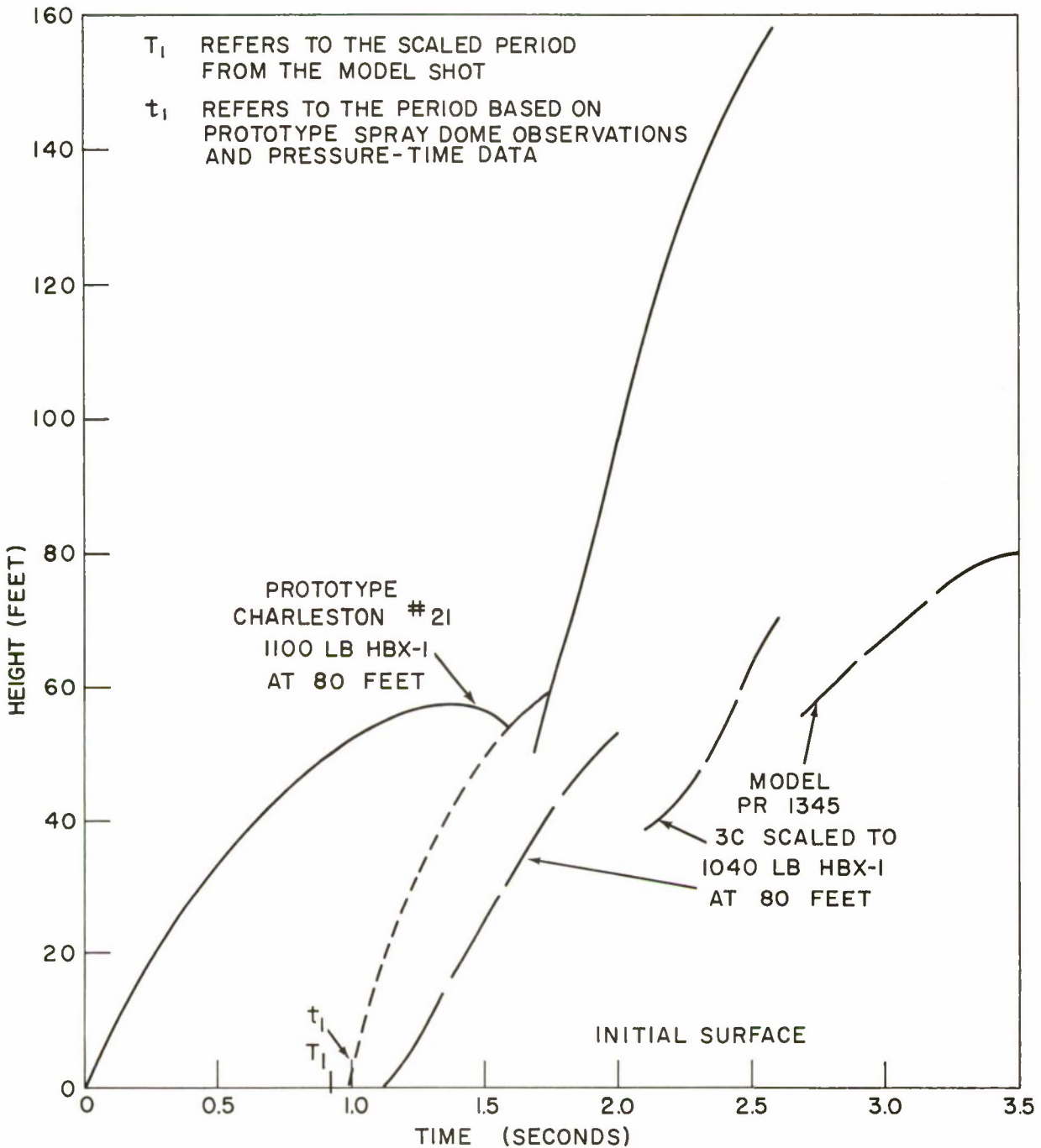


FIG. 27 COMPARISON OF SURFACE DEVELOPMENT OF A THREE CRITERIA SCALED MODEL WITH ITS PROTOTYPE FOR A BOTTOM SHOT

plotted in Figure 27. For this comparison shot 21 at Charleston is considered the prototype of shot PR 1345 in the tank.

The initial spray dome development of shot 21 at Charleston was quite large and apparently obscured the second spray dome. The dashed line in Figure 27 indicates its possible growth. It begins at 0.994 seconds which corresponds to the end of the first period as determined by pressure-time instrumentation. The period scaled from the model shot was 0.922 seconds. The growth of the water mound in the model results from the water displacement during the second and successive bubble oscillations.

To summarize the program of this section:

1. The application of three criteria bubble scaling resulted in scaled prototypes whose differences from actual prototypes was insignificant for most points of comparison under water.
2. Bottom effect indexes were evaluated so that A_{max} and T for bottom shots can be estimated from free water conditions. The bottom period index was in good agreement with prototype evaluations.
3. Direct comparisons of surface phenomena between scaled prototypes and real prototypes show marked differences with regard to spray domes and plumes. Real prototype periods estimated from surface development were generally greater than those of the scaled prototype.

4.3.3 Scaling Under-Ice Explosions. Setting up for an under-ice shot proved to be very difficult. Because of the small access ports, the simulated ice had to be formed in the tank. A sheet metal loop was formed inside the tank and held flush with the water. This loop formed the walls and the water formed the bottom of a mold into which melted paraffin was slowly poured. The paraffin disk which resulted was irregular in thickness; it formed in layers or striations with air and water pockets between. The resulting "ice floe" was most unsuitable but was used.

At the conditions fired, simplified two criteria scaling indicated a prototype of 65 pounds of HBX-1 at 3.18 feet beneath the ice. The model ice (paraffin) scaled to about 8 feet in thickness. This is close to a prototype of 60 pounds of HBX-3 (equivalent to 66 pounds of HBX-1) at 3.9 feet below ice which was from 6 to 14 feet thick. The prototype was fired under an ice floe in the Arctic Ocean (Ref.3). Figure 28 shows the scaled vertical displacement history of the model shot. Films of the prototype appear similar to the model at early times; however, the framing rate of the prototype films has not been resolved and no direct comparisons can be made.

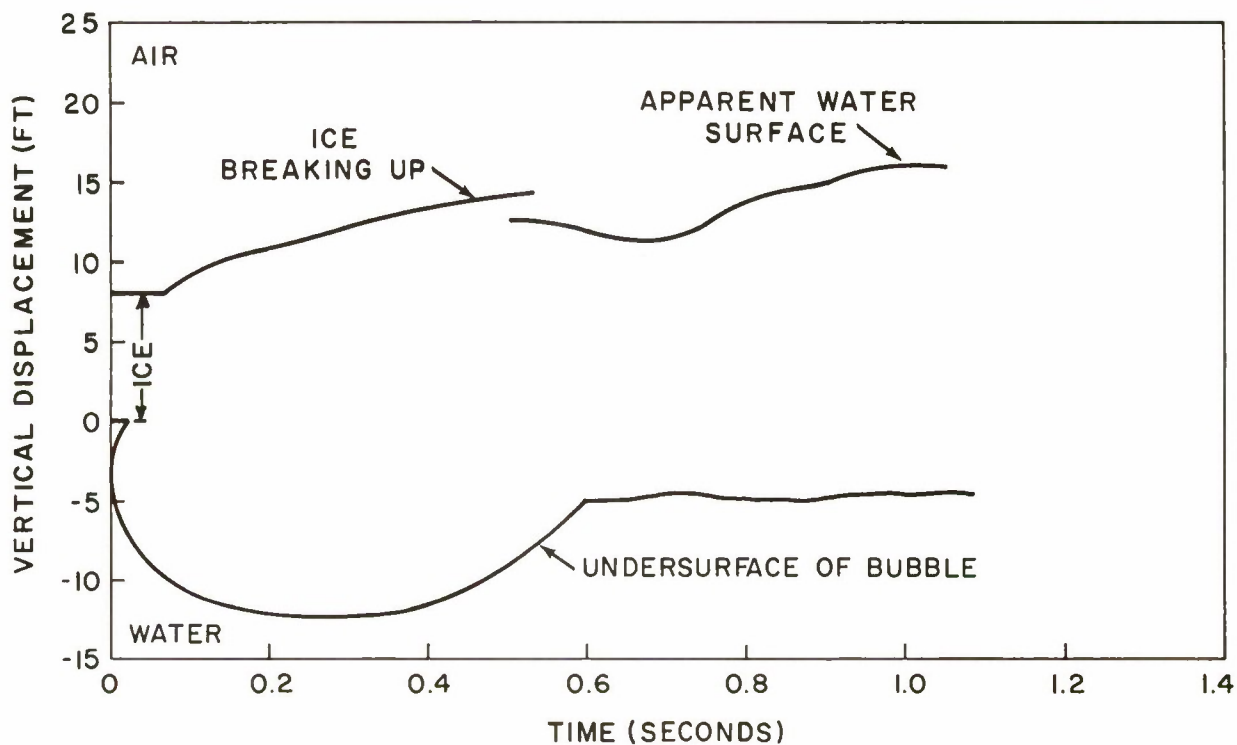


FIG. 28 BUBBLE AND SURFACE DEVELOPMENT OF A SIMPLIFIED TWO CRITERIA SCALED UNDER-ICE SHOT

After this shot, the test tank was contaminated with fragments of paraffin for the remainder of the 1960 shots. It is suspected the water cooling system did not operate efficiently thereafter because paraffin obstructed water circulation through the cooler. Because of the difficult set up and resulting paraffin contamination, only the one shot was fired.

In future under-ice experiments, it will be necessary to scale for ice thickness and to find ice-simulating materials which will be easier to work with.

4.3.4 Scaling Deep Nuclear Explosions. Nuclear explosions at such depths that one or more bubble oscillations can occur, are of particular interest to the Navy. Laboratory scaling of such nuclear shots is especially important because of the Nuclear Test Ban Treaty of 1963. Two criteria bubble scaling was developed specifically for this class of scaling problem (Ref. 16).

Experimental conditions for two criteria scaling of Wahoo (9 KT at 500 feet), Willow (10 KT at 1000 feet), and Wigwam (32 KT at 2000 feet) were determined. (The Willow shot was a planned nuclear shot that was cancelled.) The tank conditions specified are listed in Table 1.

Using the conditions actually obtained in the tank, the prototype conditions calculated are indicated in Table 8. None of these shots had a three criteria or simplified three criteria solution and several had no two criteria solution.

None of the solutions was close to the prototypes intended. Only four two-criteria prototypes were in a range of useful nuclear scaling. These were modeled by PR 1319, 1383, 1384, and 1385. (See Table 8.) Two criteria scaled vertical displacement histories of the bubble and surface development for these shots are shown in Figure 29.

Since there have been no nuclear prototypes fired with these conditions, no comparative evaluation of the scaling applied could be obtained.

4.3.5 Scaling Shallow Nuclear Shots. A final group of shots were fired shallow, i. e., at depths where the bubble characteristics, A_{\max} and T , cannot be identified because of blow-out or venting of explosion gases during the initial expansion of the explosion bubble. For this program geometric or λ scaling was used. This is essentially one criterion scaling in which the ratios λ_d and λ_t are the same in model and prototype:

$$\lambda_d = \frac{d_p}{W_p^{1/3}} = \frac{d_m}{W_m^{1/3}} \quad (19)$$

$$\lambda_t = \frac{t_p}{W_p^{1/3}} = \frac{t_m}{W_m^{1/3}} \quad (20)$$

CONFIDENTIAL
NOLTR 63-125

TABLE 8 PROTOTYPE CONDITIONS FOR DEEP NUCLEAR EXPLOSIONS

Shot No.	Scaling	d _p	Y _p	T _p
		(ft)	(kt)	(sec)
PR 1301	2 C	131	.0547	2.40
	S 2 C	83.7	.00862	1.73
PR 1303	2 C	-	-	-
	S 2 C	138	.00163	.812
PR 1319	2 C	1770	84.7	4.22
	S 2 C	250	.0381	1.51
PR 1372	2 C	-	-	-
	S 2 C	138	.00275	.959
PR 1374	2 C	-	-	-
	S 2 C	157	.00283	.894
PR 1375	2 C	-	-	-
	S 2 C	168	.00247	.822
PR 1376	2 C	-	-	-
	S 2 C	166	.00238	.815
PR 1378	2 C	-	-	-
	S 2 C	215	.00473	.858
PR 1379	2 C	-	-	-
	S 2 C	181	.00227	.760
PR 1381	2 C	108	.0393	2.37
	S 2 C	92.3	.0154	1.96
PR 1383	2 C	185	.188	2.87
	S 2 C	98.1	.0127	1.81
PR 1384	2 C	154	.124	2.79
	S 2 C	93.4	.0139	1.90
PR 1385	2 C	285	.797	3.45
	S 2 C	105	.0132	1.78
PR 1390	2 C	165	.0939	2.51
	S 2 C	101	.0117	1.75
PR 1391	2 C	124	.0377	2.22
	S 2 C	97.1	.0119	1.79

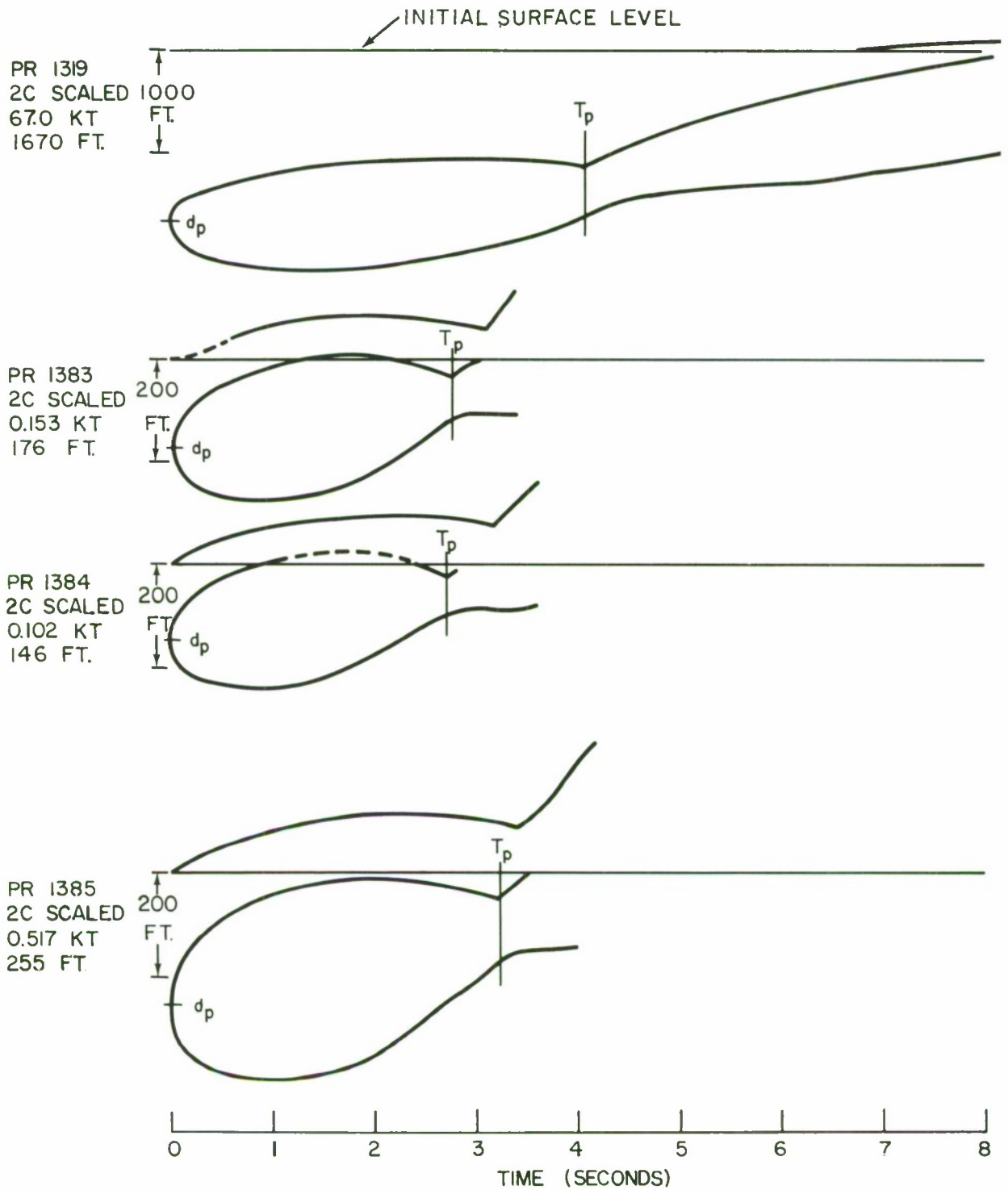


FIG. 29 BUBBLE AND SURFACE DEVELOPMENT OF TWO CRITERIA SCALED DEEP NUCLEAR EXPLOSIONS

CONFIDENTIAL
 NOLTR 63-125

Since this scaling is commonly applied in the field, the air pressure is presumed to be one atmosphere and the acceleration, one gravity. These factors may be introduced as variables in the gravity tank. Air pressure is known to have an effect on shallow explosions; the lower the air pressure the more divergent are the column walls. In these tests air pressure was held at about one atmosphere. The acceleration level would have little or no observable effect on the early explosion mechanisms since the total hydrostatic pressure would be changed by only a small amount at very shallow depths. There may be an effect on the surface development, however. To qualitatively evaluate this effect, two levels of acceleration were arbitrarily selected for each proposed shot condition.

Another purpose was to observe the effect of a bottom at or near the charge, thus some shallow shots were planned with and some without a bottom.

The prototypes selected for scaling were shots Umbrella (8 KT at 150 feet on the bottom) and Baker (23.5 KT at 90 feet in 180 feet of water). In addition, some hypothetical nuclear shots were included.

The scaling relationships, Equations 19 and 20, presume the same explosive in the model and prototype case. For a nuclear prototype, W_p is converted to radiochemical yield by the relationship (Refs. 9 and 16):

$$W_p = 4.04 \times 10^6 Y_p \quad (21)$$

For the Umbrella shot, λ_d , upon converting to equivalent lead azide charge weight, is 0.470; for the Baker shot, λ_d is 0.20. Table 9 lists the actual λ_d obtained for the model shots and indicates whether the shot was on the bottom or in deep water. Of the 1960 shots (through PR 1354) only one (PR 1310) is in the range intended. The others were too deep either because of gross errors in computing the nominal model depths or because of control difficulties. Five other shots are not shown in Table 9; the water level was so low that they were fired in air. Four additional shots were fired in 1961 with greater success; scaled depths were in the intended range.

TABLE 9 λ_d FOR SHALLOW SHOTS

PR	1310*	1311*	1321*	1335*	1336*	1339:	1354:	1368:	1369:	1370#	1371#
λ_d	.18	5.01	5.26	1.84	1.89	4.59	4.35	.26	.30	.37	.32

* In deep water.

: Fired on the bottom.

Fired at mid-depth

Mid-depth shots PR 1370 and 1371 best approximate the divergent Baker plume and bottom shots PR 1368 and 1369 best approximate the cylindrical Umbrella plumes. From the λ_d point of view this is opposite to what would be expected. The position of the charge with respect to the bottom seems to be the more important criterion in this comparison.

The first few frames of each shot are shown in Figures 30 (PR 1370 and 1371) and 31 (PR 1368 and 1369). For these shallow shots it would have been desirable to employ a higher speed camera to provide better resolution.

The pairs of shots in Figures 30 and 31 are at about the same tank conditions except for acceleration, therefore observed differences may be attributed to acceleration. The main difference noted is in the greater irregularity along the top of the plume in the higher acceleration shots (PR 1369 and PR 1371). This phenomenon probably results from a difference in the growth of surface irregularities which are dependent on accelerations acting at the water-air interface (Ref. 13). The column in both high acceleration shots is apparently more divergent than is the low acceleration shots; the high acceleration plume phenomena appear squatter than at low acceleration.

In a general way, the simulations of Baker and Umbrella show some of the differences apparent between the prototypes' surface phenomena. For example, the Baker simulations exhibit smoke crowns while the Umbrella simulations do not. More carefully controlled shots will be necessary before any definite conclusions can be drawn.

5. CONCLUSIONS

The underlying reasons for these experiments were to determine if a centrifugally accelerated test tank could reasonably be used for model explosion studies and to attempt a variety of programs. These generally have been satisfied; a variety of shots has been fired and except for the under-ice shot (Section 4.3.3), the difficulties have been minor. The control of tank conditions has been investigated; the control attained was satisfactory for an initial series of tests on a new facility (see Section 3.9). It is concluded that the use of a centrifugally accelerated test tank for model explosion studies is practical.

In general, the data obtained indicate that the systems of explosion scaling (especially three criteria scaling) may be applied over a wide range of conditions. Where comparisons between model and prototypes were possible, the underwater bubble characteristics were similar. Because of poor control and other difficulties specific prototypes of military interest were not scaled in these programs.

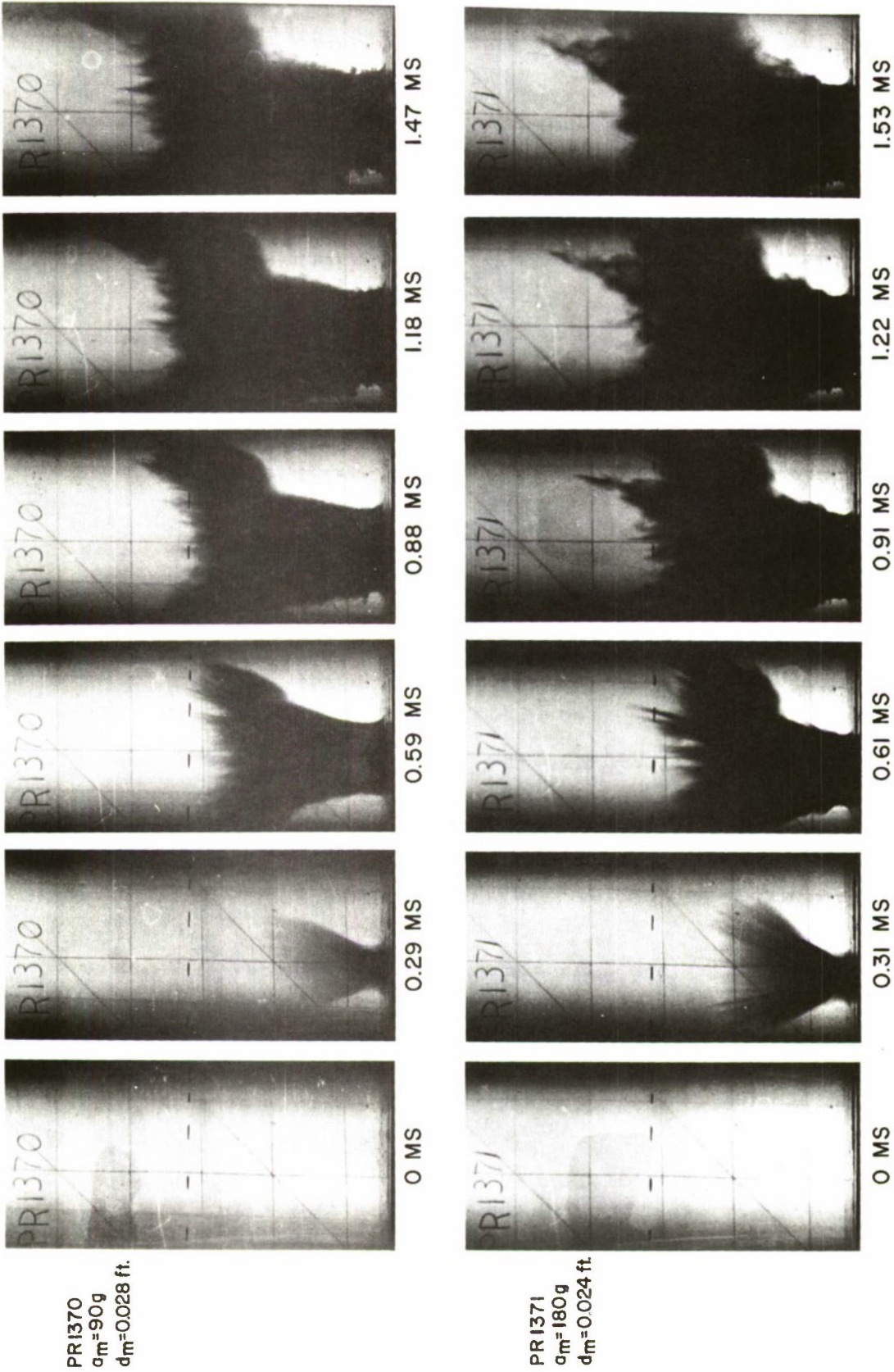


FIG.30 SELECTED FRAMES OF SHALLOW SHOTS APPROXIMATING BAKER PLUMES

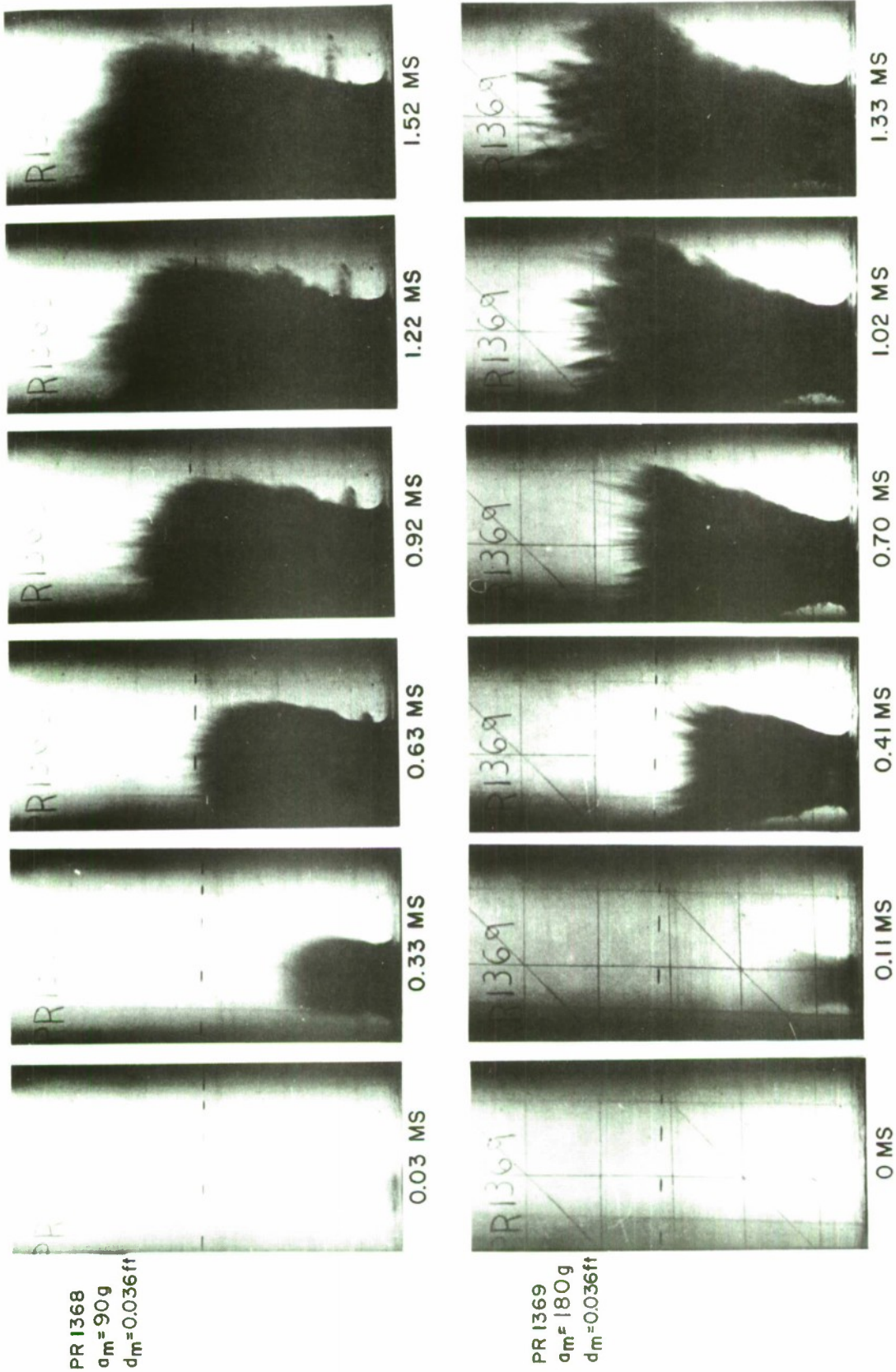


FIG. 31 SELECTED FRAMES OF SHALLOW SHOTS APPROXIMATING UMBRELLA PLUMES

CONFIDENTIAL

NOLTR 63-125

Some of the more specific goals relating to explosion scaling were only partially satisfied:

1. The experiment intended to yield a comparison of different forms of bubble scaling (Section 4.3.1) did not do so. Preliminary computational errors and poor control of tank conditions were the reasons.
2. A comparison of the characteristics of some three-criteria scaled model shots with predicted prototype results and with a few actual prototype measurements (Section 4.3.2) was obtained. The differences between the scaled model's and the predicted prototype's bubble characteristics were statistically insignificant except for the bubble depth at the first maximum and the size of the second bubble maximum (see Table 6). Period comparisons between the scaled model and actual prototype data show the scaled model periods to be consistently shorter.
3. Two criteria scaling of specific deep nuclear explosions (Section 4.3.4) was unsuccessful because of preliminary computational errors and poor control of tank conditions; however, several shots could be scaled to prototypes in the range of military interest.
4. One criterion scaling of shallow nuclear shots seemed more sensitive to positioning of the charge relative to the bottom rather than to the depth. (Section 4.3.5). Poor resolution and limited field of view hampered comparisons.
5. All shots that were measurable provided data about some prototype condition. The four kinds of bubble scaling and one criterion scaling were applied to measurements of all the shots; the prototypes scaled were computed (see Tables 4, 5, 7, 8, and 9). Several of the prototypes scaled were at conditions of military significance.

As a result of these experiments numerous improvements in instrumentation and capability are being incorporated into the NOL High Gravity Tank Centrifuge installation. Other desirable practices, which time limitations precluded here, such as shot replication and check computations of desired conditions, will derive from Laboratory operation.

CONFIDENTIAL

NOLTR 63-125

REFERENCES

1. Abbott, Ira H., and Von Doenhoff, Albert E.; "Theory of Wing Sections", McGraw-Hill Book Co., Inc., New York, 1949.
2. Aronson, C. J., et al, "Underwater Free-Field Pressures to Just Beyond Target Locations", Operation Wigwam, Project 1.2, WT-1005 (NOIR-1215), 27 May 1957, Confidential, Formerly Restricted Data.
3. Leslie, Donald M., and Nelson, Carl A.; "Explosion Tests Under Thick Polar Ice", NOLTR 61-146, 1 November 1961, Confidential.
4. Goertner, J. F.; "Vacuum Tank Studies of Gravity Migration of Underwater Explosion Bubbles", NAVORD Report 3902, 1 March 1956, Confidential.
5. Hoerner, Sigward F.; "Fluid-Dynamic Drag", Sigward F. Hoerner, Midland Park, New Jersey, 1958.
6. Levine, David, "A 30,000 FPS Rotating Mirror Framing Camera", NAVORD Report 4288, 1 August 1956, Unclassified.
7. Price, R. S.; "Underwater Explosion Tests in a Preliminary High-Gravity Tank Accelerated by a Centrifuge", NAVWEPS Report 7365, August 1961, Unclassified.
8. Slie, W. M. and Derwin, J. W., "Special Detonators for Underwater Explosive Studies", NAVORD Report 3575, 16 November 1953, Unclassified.
9. Snay, H. G., et al; "Predictions of Underwater Explosion Phenomena", Operation Wigwam, Project 1.1, WT-1004 (NOIR-1213), 24 January 1957, Confidential, Formerly Restricted Data.
10. Snay, H. G., et al; "Small Scale Experiments to Determine Migration of Explosion Gas Globes Towards Submarines", NAVORD Report 2280, 1 July 1952, Confidential.
11. Snay, H. G.; "The Hydrodynamic Background of the Radiological Effects of Underwater Nuclear Explosions", NAVWEPS Report 7323, 29 September 1960, Confidential.
12. Swift, E., Jr., et al; "Surface Phenomena from Underwater Bursts", Operation Hardtack, Project 1.3, ITR-1608, 19 January 1958, Confidential, Formerly Restricted Data.
13. Taylor, Sir Geoffrey, "The Instability of Liquid Surfaces when Accelerated in a Direction Perpendicular to their Planes", Proceedings of the Royal Society, Vol. A 201, 1950.
14. Washington Technological Associates, "Final Report; Feasibility Study and Design Investigation for a Scaled Underwater Explosion Test Facility", WTA 125, NORD 17605, March 1958, Confidential.
15. Zuke, W. G.; "Laboratory Scaling of Underwater Nuclear Explosion Bubbles", NAVWEPS Report 6707, 21 October 1960, Confidential.
16. Zuke, W. G.; "Underwater Explosion Scaling Predictions for an Accelerated Test Tank", NAVORD Report 6794, 4 January 1962, Confidential.
17. Zuke, W. G., Plentzas, S. G.; "Effects on Underwater Explosion Bubble Characteristics, Part I, Free Water Effects", (to be published).
18. Zuke, W. G.; "Underwater Explosion Bubble Scaling in an Accelerated Test Tank", NOLTR 63-135, to be published.

APPENDIX A

SIMPLIFIED BUBBLE SCALING

1. Simplified Three Criteria Bubble Scaling. The general relationships used in three criteria scaling are:

a. For geometric scaling at the bubble maximum:

$$\frac{d_m}{d_p} = \frac{A_{\max m}}{A_{\max p}} = \left[\frac{W_m}{W_p} \right]^{1/3} \left[\frac{Z_p}{Z_m} \right]^{1/3} \frac{J_m}{J_p} \quad (\text{A1})$$

where:

$$A_{\max} = J \left[W/Z \right]^{1/3} \quad (\text{A2})$$

and subscripts m refer to the model, p to the prototype. See page A-4 for definition of terms.

b. For Froude or gravitational scaling:

$$\frac{A_{\max m} T_p^2 a_p}{A_{\max p} T_m^2 a_m} = \frac{J_m a_p}{J_p a_m} \left[\frac{K_p}{K_m} \right]^2 \left[\frac{W_p}{W_m} \right]^{1/3} \left[\frac{Z_m}{Z_p} \right]^{4/3} = 1 \quad (\text{A3})$$

where:

$$T = KW^{1/3}/Z^{5/6} \quad (\text{A4})$$

c. For geometric scaling at the bubble minimum:

$$\frac{A_{\min m}}{A_{\max m}} = \frac{A_{\min p}}{A_{\max p}} \quad \text{or} \quad \frac{Z_m}{Z_p} = \left[\frac{N_p}{N_m} \right]^3 \quad (\text{A5})$$

where:

$$A_{\min} / A_{\max} = Z^{1/3} N \quad (A6)$$

For three criteria scaling the prototype bubble coefficients, K and J, are free field values and the model values are tank values, i.e., they include wall effects. Thus the ratios of A's and T's are of tank values and free field values and the scaling implied is from tank shots to free field prototypes. For simplified scaling, the bubble coefficients must all (model and prototype) either incorporate tank effects or not incorporate them. It is easiest to use free field values for all the bubble coefficients, thus J_m and K_m are the free field coefficients for the model explosive. Incorporating this change in coefficients into the above equations gives the relationships which are applied to the simplified three criteria scaling.

Substituting the defined relationships for Z_m and Z_p:

$$Z_m = d_m a_z + P_m \quad (A7)$$

$$Z_p = d_p + 34 \quad (A8)$$

into A5 and solving for d_p:

$$d_p = \left[d_m a_z + P_m \right] \left[N_m / N_p \right]^3 - 34 \quad (A9)$$

gives the prototype depth scaled as determined by the third scaling criteria.

Combining Equations A1 and A5 and solving for W'_p:

$$W'_p = W_m \left[\frac{d_p N_m J_m}{d_m N_p J_p} \right]^3 \quad (A10)$$

gives the prototype weight determined from the first and third criteria.

Combining Equations A3 and A5 and solving for W''_p:

$$W''_p = W_m \left[\frac{J_p a_m}{J_m a_p} \right]^3 \left[\frac{K_m}{K_p} \right]^6 \left[\frac{N_m}{N_p} \right]^{12} \quad (A11)$$

CONFIDENTIAL

NOLTR 63-125

gives the prototype weight determined from the second and third criteria, W'_p must equal W''_p . This would be a rare occurrence. To obtain a reasonable number of solutions an arbitrary 10% increment of error has been allowed, thus if W'_p and W''_p do not differ from each other by more than 10%, a three criteria solution is obtained. The prototype weight designated is an average of these two:

$$W_p = \frac{W'_p + W''_p}{2} \quad (A12)$$

Thus for any set of tank parameters and knowledge of the explosives used (therefore the J's, K's, and N's) the prototype depth may be evaluated from Equation A9, and the prototype weight from A10, A11, and A12.

2. Simplified Two Criteria Scaling. For simplified two criteria scaling only the first two criteria listed above are applied (Equations A1 and A3). The change in bubble coefficients is made, as above, to give simplified two criteria scaling relationships.

Equations A1 and A3 are solved for W'_p and W''_p respectively, thus:

$$W'_p = W_m \left[\frac{d_p J_m}{d_m J_p} \right]^3 \left[\frac{Z_p}{Z_m} \right] \quad (A13)$$

$$W''_p = W_m \left[\frac{Z_p}{Z_m} \right]^4 \left[\frac{a_m J_p}{a_p J_m} \right]^3 \left[\frac{K_m}{K_p} \right]^6 \quad (A14)$$

To satisfy the two criteria W'_p must equal W''_p . Equating Equations A13 and A14; substituting A8 for Z_p ; and solving for d_p gives:

$$d_p = \frac{34}{\left[\frac{Z_m a_p}{d_m a_m} \left(\frac{J_m K_p}{J_p K_m} \right)^2 - 1 \right]} \quad (A15)$$

Thus for any set of tank parameters and knowledge of the explosives used, the prototype depth may be evaluated from Equation A15. The prototype weight may then be evaluated from either Equation A13 or A14.

DEFINITION OF TERMS

The terms below may refer to either model or prototype depending on the subscript used.

- a Acceleration (a_p is always one gravity)
- d Charge depth
- J Bubble radius coefficient
- K Bubble period coefficient
- N Bubble minimum coefficient
- P Air pressure at water surface (P_p is 34 feet of fresh water or 33 feet of sea water)
- T First period of bubble oscillation
- W Charge weight
- Z Total hydrostatic pressure at the charge
- A_{max} First maximum bubble radius
- A_{min} Radius of first bubble minimum

DISTRIBUTION

	Copies
Chief Bureau of Naval Weapons Washington, D. C. 20360 Attn: Library DLI-3	2
RUME -4	1
RRRE -5	1
Chief of Naval Operations Washington, D. C. 20350 Attn: OP -75	1
Chief of Naval Research Washington, D. C. 20360 Attn: Code 418	1
Code 429	1
Code 466	1
Chief Bureau of Ships Washington, D. C. 20360 Attn: Code 423	2
Chief Bureau of Yards and Docks Washington, D. C. 20370	1
Commanding Officer & Director US Naval Radiological Defense Laboratory San Francisco, 24, California Attn: Code 222	1
Code 911	1
Code 934	1
Commander Naval Ordnance Test Station China Lake, California 93550 Attn: Technical Library	1
Commander Naval Ordnance Test Station 3202 E. Foothill Blvd Pasadena, California 91107	1
Director Naval Research Laboratory Washington, D. C. 20390	2

DISTRIBUTION Cont'd

Copies

Commanding Officer & Director David Taylor Model Basin Washington, D. C. 20007	2
Commanding Officer & Director David Taylor Model Basin Underwater Explosions Research Division Norfolk Naval Shipyard Portsmouth, Virginia Attn: Code 780	1
Superintendent US Naval Postgraduate School Monterey, California	1
Director US Navy Electronics Laboratory San Diego, California	2
Commanding Officer Naval Torpedo Station Keyport, Washington	1
Commanding Officer US Naval Air Development Center Johnsville, Pennsylvania	1
Commanding Officer Nuclear Defense Laboratory Edgewood, Maryland	1
Commander US Naval Oceanographic Office Washington, D. C. 20390	1
Commanding Officer US Navy Mine Defense Laboratory Panama City, Florida	1
Commanding Officer & Director Naval Civil Engineering Laboratory Port Hueneme, California	1
Commanding Officer US Naval Weapons Evaluation Facility Kirtland Air Force Base Albuquerque, New Mexico	1

CONFIDENTIAL

NOLTR 63-125

DISTRIBUTION Cont'd

	Copies
Chief of Research & Development Department of the Army Washington, D. C. 20350	1
Commanding General Army Material Command Headquarters US Army Washington, D. C. 20390	2
Chief of Engineers Department of the Army Washington, D. C. 20390 Attn: ENGNB	2
	1
Director Waterways Experiment Station Vicksburg, Mississippi Attn: F. R. Brown	1
	1
	1
Commanding General Ballistic Research Laboratories Aberdeen, Maryland 21005	1
Commanding Officer Engineer Research & Development Laboratory Fort Belvoir, Virginia Attn: Chief, Technical Support Branch	1
Commanding Officer USA Signal R&D Laboratory Fort Monmouth, New Jersey Attn: Technical Documents Center	1
Director of Research & Development Hq. US Air Force Washington, D. C. 20390	1
Commander, OOAMA Hill Air Force Base Utah Attn: AF Ammunition Services Office	1

CONFIDENTIAL
NOLTER 63-125

DISTRIBUTION Cont'd

Copies

Headquarters Air Proving Ground Center US Air Force, ABDC Eglin Air Force Base, Florida Attn: PGTRI, Technical Library	1
Commander AF Logistics Command Wright-Patterson AFB Dayton, Ohio	1
Aeronautical System Division Wright-Patterson AFB Dayton, Ohio	1
Director Lawrence Radiation Laboratory Livermore, California	1
Director University of California Los Alamos Scientific Laboratory PO Box 1663 Los Alamos, New Mexico 87544 Attn: Dr. D. P. MacDougall	2
NASA Scientific & Technical Information Facility PO Box 5700 Bethesda, Maryland	1
Sandia Corporation Sandia Base Albuquerque, New Mexico Attn: Classified Document Division	1
Defense Documentation Center Cameron Station Alexandria, Virginia ATTN: TIPDR	20
Amherst College Physics Department Amherst, Massachusetts Attn: Dr. Arnold Arons	1

DISTRIBUTION Cont'd

Copies

Commander AF Special Weapons Center Kirtland AFB Albuquerque, New Mexico Attn: Technical Library	1
Director Defense Research & Engineering Washington, D C 20350 Attn: Technical Library	1
Director Applied Physics Laboratory Johns Hopkins University Silver Spring, Maryland	1
Director Defense Atomic Support Agency Washington, D. C. 20301	3
Director Applied Physics Laboratory University of Washington Seattle, Washington	1
Research Analysis Corporation 6935 Arlington Rd Bethesda, Md Washington, D. C.	1
Director Ordnance Research Laboratory Pennsylvania State University University Park, Pennsylvania	1
Director Woods Hole Oceanographic Institution Woods Hole, Massachusetts	1
Director Scripps Institute of Oceanography La Jolla, California	2
Columbia University Hudson Laboratories 145 Palisade St Dobbs Ferry, New York	1

CONFIDENTIAL
NOLTR 63-125

DISTRIBUTION Cont'd

Copies

Michigan State University
E. Lansing, Michigan
C/o Gerald Knapp, Security Officer
Administration Bldg
Attn: Dr. T. Triffet
Department of Applied Mechanics

1

United Research Services, Inc
1811 Trousdale Drive
Burlingame, California
Attn: Kenneth Kaplan
Deputy Director

DA-49-146-XZ-122

1

CATALOGING INFORMATION FOR LIBRARY USE

BIBLIOGRAPHIC INFORMATION			
DESCRIPTORS	CODES	DESCRIPTORS	CODES
NOL technical report	NOLTR	Confidential - 34	C034
REPORT NUMBER 63-125	630125		
REPORT DATE 5 June 1964	0664		
		SECURITY CLASSIFICATION AND CODE COUNT	
		CIRCULATION LIMITATION	
		CIRCULATION LIMITATION OR BIBLIOGRAPHIC	
		BIBLIOGRAPHIC (SUPPL., VOL., ETC.)	

SUBJECT ANALYSIS OF REPORT

DESCRIPTORS	CODES	DESCRIPTORS	CODES
Underwater	UNDE	Phenomena	PHEO
Explosions	EXPS	Effects	EFFE
Gravity	GRAV	Size	SIZE
Tank	TANZ	Air	AIRE
Bubbles	BUBB	Pressure	PRES
Scaling	SCAL	Explosive	EXPL
Accelerated	ACCL	Charge	CHAR
Centrifuge	CENT	Depth	DEPT
Photography	PHOT	Methods	METH
Model	MODE	Comparison	CMRI
Small	SMAL	Prototypes	PRTY
Movies	MOVE	High	HIGH
		Tests	TEST
		High-speed	HIGS
		Firing	FTRI
		Oscillation	OSCA
		Migration	MIGR
		Equipment	EQUI
		Installation	INST
		Measurements	MEAU
		Experimental	EXPE
		Control	CONT

Naval Ordnance Laboratory, White Oak, Md.
(NOL technical report 63-125)
A STUDY OF UNDERWATER EXPLOSIONS IN A HIGH GRAVITY TANK (U), by R. S. Price and others.
5 June 1964. v.p. illus., diagrs., tables.
BuWeeps task RRRE-51001-003 and NOL task 440/DASA.

CONFIDENTIAL

Small explosions were fired in a tank accelerated up to 190 gravities. Movies were taken of the phenomena. The effects of tank size, air pressure, acceleration, and charge depth on the explosion characteristics were determined and several methods of using the scaling laws were compared. Specific prototypes were scaled.

1. Explosions, Underwater
2. Bubbles, Explosion
- I. Title
- II. Price, Robert S.
- III. Project
- IV. Project

Abstract card is unclassified.

Naval Ordnance Laboratory, White Oak, Md.
(NOL technical report 63-125)
A STUDY OF UNDERWATER EXPLOSIONS IN A HIGH GRAVITY TANK (U), by R. S. Price and others.
5 June 1964. v.p. illus., diagrs., tables.
BuWeeps task RRRE-51001-003 and NOL task 440/DASA.

CONFIDENTIAL

Small explosions were fired in a tank accelerated up to 190 gravities. Movies were taken of the phenomena. The effects of tank size, air pressure, acceleration, and charge depth on the explosion characteristics were determined and several methods of using the scaling laws were compared. Specific prototypes were scaled.

1. Explosions, Underwater
2. Bubbles, Explosion
- I. Title
- II. Price, Robert S.
- III. Project
- IV. Project

Abstract card is unclassified.

Naval Ordnance Laboratory, White Oak, Md.
(NOL technical report 63-125)
A STUDY OF UNDERWATER EXPLOSIONS IN A HIGH GRAVITY TANK (U), by R. S. Price and others.
5 June 1964. v.p. illus., diagrs., tables.
BuWeeps task RRRE-51001-003 and NOL task 440/DASA.

CONFIDENTIAL

Small explosions were fired in a tank accelerated up to 190 gravities. Movies were taken of the phenomena. The effects of tank size, air pressure, acceleration, and charge depth on the explosion characteristics were determined and several methods of using the scaling laws were compared. Specific prototypes were scaled.

1. Explosions, Underwater
2. Bubbles, Explosion
- I. Title
- II. Price, Robert S.
- III. Project
- IV. Project

Abstract card is unclassified.

Naval Ordnance Laboratory, White Oak, Md.
(NOL technical report 63-125)
A STUDY OF UNDERWATER EXPLOSIONS IN A HIGH GRAVITY TANK (U), by R. S. Price and others.
5 June 1964. v.p. illus., diagrs., tables.
BuWeeps task RRRE-51001-003 and NOL task 440/DASA.

CONFIDENTIAL

Small explosions were fired in a tank accelerated up to 190 gravities. Movies were taken of the phenomena. The effects of tank size, air pressure, acceleration, and charge depth on the explosion characteristics were determined and several methods of using the scaling laws were compared. Specific prototypes were scaled.

1. Explosions, Underwater
2. Bubbles, Explosion
- I. Title
- II. Price, Robert S.
- III. Project
- IV. Project

Abstract card is unclassified.

Naval Ordnance Laboratory, White Oak, Md.
(NOL technical report 63-125)
A STUDY OF UNDERWATER EXPLOSIONS IN A HIGH GRAVITY TANK (U), by R. S. Price and others.
5 June 1964. v.p. illus., diagrs., tables.
BuWeps task RRRE-51001-003 and NOL task 440/DASA.

CONFIDENTIAL

Small explosions were fired in a tank accelerated up to 190 gravities. Movies were taken of the phenomena. The effects of tank size, air pressure, acceleration, and charge depth on the explosion characteristics were determined and several methods of using the scaling laws were compared. Specific prototypes were scaled.

1. Explosions, Underwater
2. Bubbles, Explosion
- I. Title
- II. Price, Robert S.
- III. Project
- IV. Project

Abstract card is unclassified.

Naval Ordnance Laboratory, White Oak, Md.
(NOL technical report 63-125)
A STUDY OF UNDERWATER EXPLOSIONS IN A HIGH GRAVITY TANK (U), by R. S. Price and others.
5 June 1964. v.p. illus., diagrs., tables.
BuWeps task RRRE-51001-003 and NOL task 440/DASA.

CONFIDENTIAL

Small explosions were fired in a tank accelerated up to 190 gravities. Movies were taken of the phenomena. The effects of tank size, air pressure, acceleration, and charge depth on the explosion characteristics were determined and several methods of using the scaling laws were compared. Specific prototypes were scaled.

1. Explosions, Underwater
2. Bubbles, Explosion
- I. Title
- II. Price, Robert S.
- III. Project
- IV. Project

Abstract card is unclassified.

Naval Ordnance Laboratory, White Oak, Md.
(NOL technical report 63-125)
A STUDY OF UNDERWATER EXPLOSIONS IN A HIGH GRAVITY TANK (U), by R. S. Price and others.
5 June 1964. v.p. illus., diagrs., tables.
BuWeps task RRRE-51001-003 and NOL task 440/DASA.

CONFIDENTIAL

Small explosions were fired in a tank accelerated up to 190 gravities. Movies were taken of the phenomena. The effects of tank size, air pressure, acceleration, and charge depth on the explosion characteristics were determined and several methods of using the scaling laws were compared. Specific prototypes were scaled.

1. Explosions, Underwater
2. Bubbles, Explosion
- I. Title
- II. Price, Robert S.
- III. Project
- IV. Project

Abstract card is unclassified.

Naval Ordnance Laboratory, White Oak, Md.
(NOL technical report 63-125)
A STUDY OF UNDERWATER EXPLOSIONS IN A HIGH GRAVITY TANK (U), by R. S. Price and others.
5 June 1964. v.p. illus., diagrs., tables.
BuWeps task RRRE-51001-003 and NOL task 440/DASA.

CONFIDENTIAL

Small explosions were fired in a tank accelerated up to 190 gravities. Movies were taken of the phenomena. The effects of tank size, air pressure, acceleration, and charge depth on the explosion characteristics were determined and several methods of using the scaling laws were compared. Specific prototypes were scaled.

1. Explosions, Underwater
2. Bubbles, Explosion
- I. Title
- II. Price, Robert S.
- III. Project
- IV. Project

Abstract card is unclassified.